THE UNIVERSITY OF MICHIGAN

COLLEGE OF ENGINEERING

Department of Nuclear Engineering

Technical Report

SCINTILLATION ANISOTROPY IN CRYSTALLINE ANTHRACENE

Donald Bruce Oliver
Glenn F. Knoll

ORA Project 07357

June 1969

This report was also a dissertation submitted by the first author in partial fulfillment of the requirements for the degree of Doctor of Philosophy in The University of Michigan, 1969.

TABLE OF CONTENTS

LIST OF TABLES

LIST OF FIGURES

LIST OF FIGURES

CHAPTER 1

INTRODUCTION

The subject of this dissertation is the directional dependence in the scintillation light yield of crystalline anthracene. Original experimental results are presented which show the influence of the specific energy loss of excitation particles and the effects of permanent radiation damage. Interpretation of the results is based on three models of the scintillation process. In each model the directional variations in the light yield are assumed to result from different fundamental excitation or energy transfer mechanisms. Anisotropic exciton diffusion is concluded to be the most plausible source of the directional effects.

1.1. BACKGROUND

In 1958 Coon[1] first noted that the total scintillation light yield (response) of anthracene, stilbene, and p-terphenyl crystals depends on the direction of incidence of monoenergetic fast neutrons relative to the crystallographic axes of the scintillators. Measurements indicated a maximum variation in light yield of 15% for 14 MeV incident neutrons. Subsequently there have been numerous investigations of the phenomenon. eKeinzle and Flammersfeld[2] examined twelve crystalline organic compounds and found the scintillation response to 8.75 MeV alpha particles to be directionally dependent in all cases. There is no experimental evidence of anisotropic response to electrons.

1

Crystalline anthracene was selected for the investigation reported here because large crystals of adequate purity are easily obtained and many of the solid state phenomena in anthracene are reasonably well understood.

1.1.1. Properties of Crystalline Anthracene

Anthracene molecules ($C_{14}H_{10}$) in the condensed phase form monoclinic crystals belonging to the space group $P2_{1/a}$. There are two molecules per unit cell as illustrated in Figure 1.[3] The angle defined by the a and c axes is 124.7°. Shown in the figure with the true crystal axes (a,b, and c) is the artificial axis (c') which is normal to the ab plane. It is defined for future convenience. Dimensions of the unit cell are: a = 8.56 Å, b = 6.04 Å, and c = 11.16 Å. The ab plane is the only prominent cleavage plane.

Large anthracene crystals are grown from the melt by the Bridgman method. As a result the crystals are in the form of long cylinders with the ab cleavage plane perpendicular to the axis of the cylinder. Right circular cylindrical crystals of a desired length, such as those used in the present study, are obtained by cleaving the long crystal. Small crystals have often been used in response anisotropy measurements involving alpha particles. Such crystals are grown from solution or by vacuum deposition and have the form of lamella with the flat surfaces parallel to the ab crystal plane.

1.1.2. Previous Scintillation Experiments

Figure 2 illustrates the results of several room temperature scintillation experiments involving anthracene crystals.[4,5,6] Specific scintillation light yield (dL/dx) is plotted as a function of specific energy loss (dE/dx)
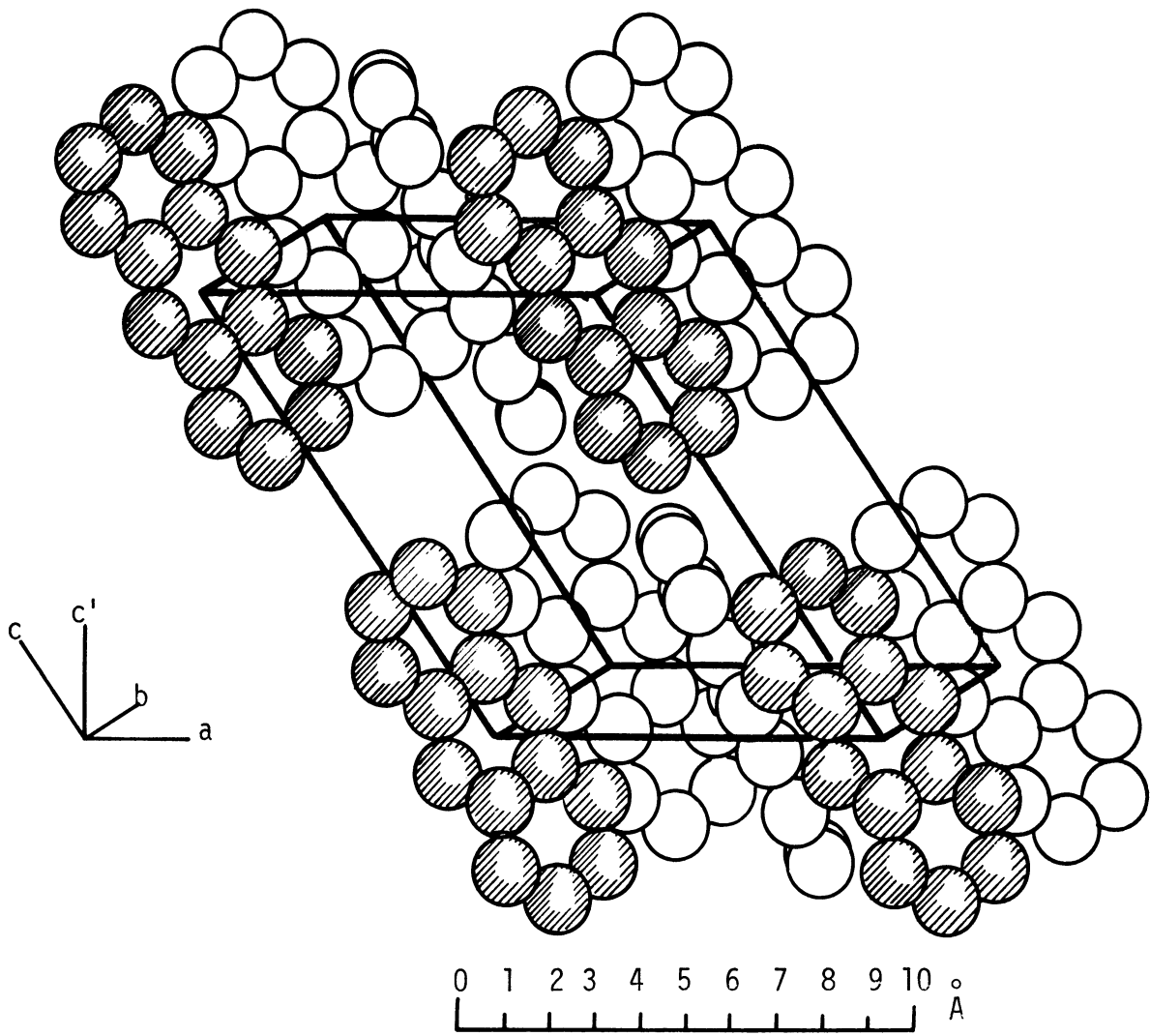
FIGURE 1

Positions of the anthracene molecules in the unit cell.

FIGURE 2

Scintillation response of anthracene crystals-I.
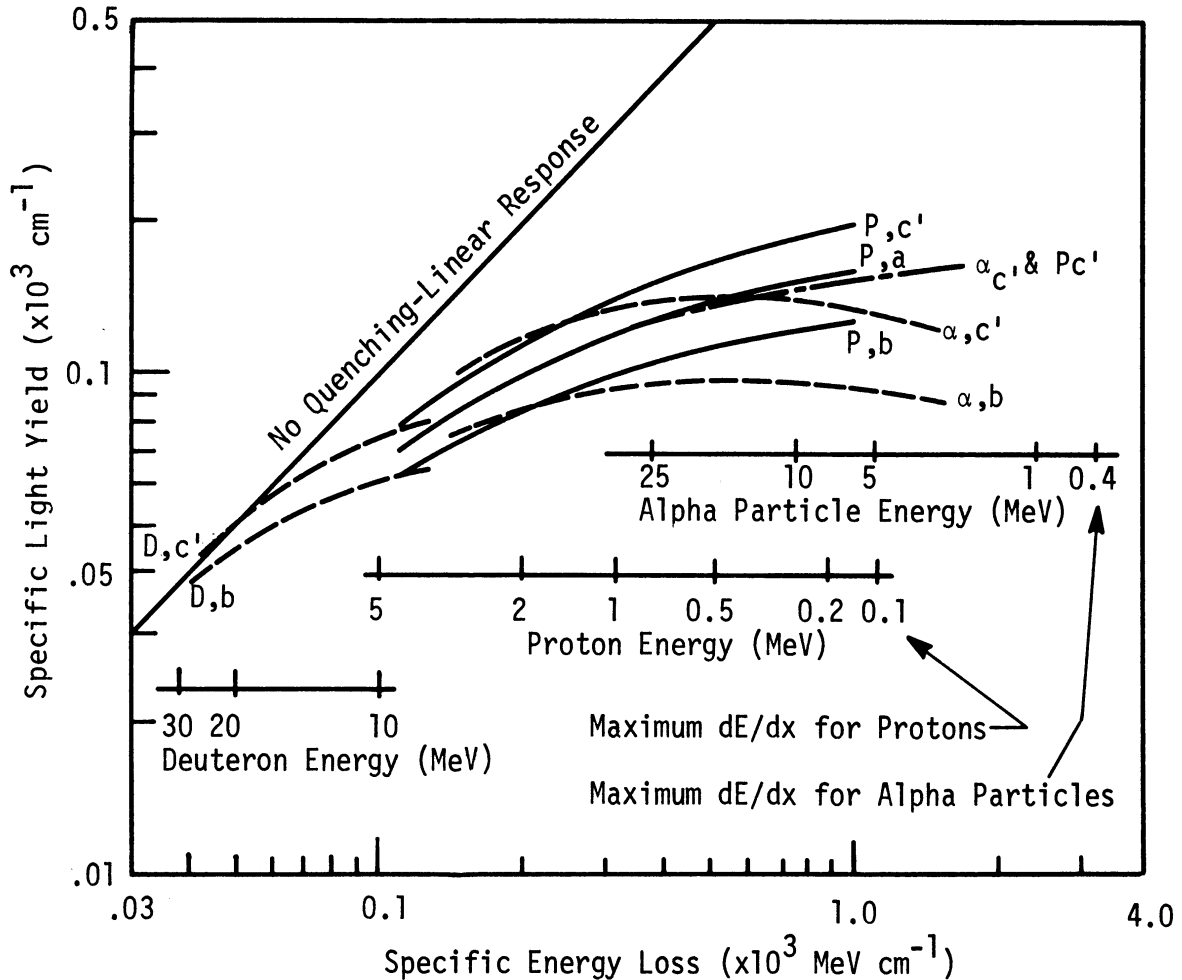
Curve labels (P, D, and α) and (a, b, and c') indicate respectively the type of exciting particle (protons, deuterons, and alpha particles) and which crystal axis (a, b, or c') is parallel to the direction of incidence.

------ are curves fitting the alpha particle and deuteron results of Schott.[5]

— - — is a curve generated by Birks' formula[4] which describes Brook's compilation of anthracene response data to 1956.[7] In most cases the data was obtained for particles incident parallel to the c' axis. The normalized form of Birk's formula is $dL/dx = (dE/dx)(1 + KBdE/dx)^{-1}$ where $KB = 5.28 \times 10^{-3}$ cm MeV^{-1} for agreement with Brook's results.

———— are curves generated by Birk's formula with KB adjusted to fit the results of Tsukada et al.[6]

The relation between proton energy and dE/dx was obtained from direct measurements[8] and by the calculational method of Whaling.[9] The relation between alpha particle energy and dE/dx is that given by Brooks.[7] The similar relation for deuterons is that given by Schött.[5]

and the direction of the exciting particle relative to the set of orthogonal
crystal axes (a,b, and c'). The light yield is normalized to that produced
in the same crystal by a 1 MeV electron.

It is clear that dL/dx for heavy charged particles varies nonlinearly
with dE/dx and is directionally dependent for dE/dx values greater than about
40 MeV cm^{-1}. The nonlinearity in specific light yield is commonly attributed
to a process called "ionization quenching."

The specific response to alpha particles begins to limit (saturate) at
approximately 500 MeV cm^{-1}, and the response to protons and deuterons appears
to approach saturation in a similar manner. Consequently, the ratio of the
specific light yield for particles incident in one direction to the yield
for particles incident in another direction (the specific response anisotropy
ratio) tends toward a limiting value. The limiting value is apparently about
the same for both alpha particle and proton excitation.

There is some uncertainty about the behavior of dL/dx for different types
of heavy charged particles which are incident in the same direction. Birks[4]
assumes that dL/dx is the same for protons and alpha particles with the same
dE/dx; whereas Schött's deuteron and alpha particle experiments imply a dif-
ference. Schött's alpha particle results also show a decrease in dL/dx as
dE/dx becomes greater than about 500 MeV cm^{-1}. Voltz et al.[10] have performed
relevant experiments with thin films of Ne 102 plastic scintillator. dL/dx
and dE/dx were measured directly. The results indicate that the maximum value
of dL/dx differs for alpha particle and proton excitation, and dL/dx decreases
as dE/dx increases beyond the value corresponding to the maximum dL/dx.

During measurements of the directional response of a thin (70 micron) anthracene crystal to alpha particles, Wick and Flammersfeld[11] observed an effect which they attribute to "channeling." A plot of the response for directions of incidence parallel to the ac plane is illustrated in Figure 3. It is noted that small decreases in the response for narrowly resolved directions are superimposed upon the slowly varying portion of the directional light yield. Alpha particles incident in the directions corresponding to the small decreases in the yield are assumed to have easily penetrated the very thin crystals along channels. As a result, the total light yield was less than for other directions of incidence. The stopping power measurements of Brandt et al.[12] corroborate the existence of such channeling in anthracene. Since dL/dx and dE/dx were measured directly in the case of the anisotropic response to deuterons shown in Figure 2, it seems clear that the slowly varying response is not a result of channeling.

The time behavior of the scintillation light emission can be described in terms of several distinct components. Most of the light appears as a prompt emission component which decays exponentially. The time constant varies between 10 and 30 nanoseconds depending on the purity of the crystal and reabsorption effects.[4] Recently, evidence of a small short lived component with an exponential decay constant of about 6 nanoseconds has been noted.[13,14] Some of the light is emitted nonexponentially over a much longer period on the order of microseconds. The relative fraction of the total yield which is contained in this delayed component increases with increasing dE/dx.[15] Apparently, the light in all the emission components arises from similar
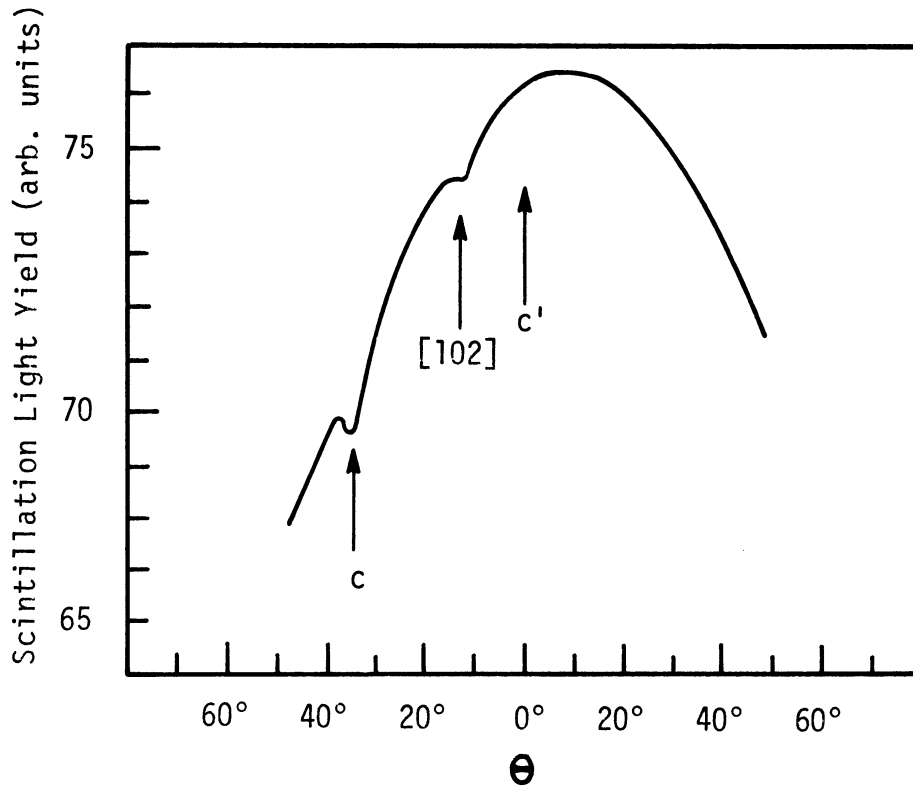
Scintillation yield of a 70 micron thick anthracene crystal as a function of direction for 6.75 MeV alpha particles incident in the ac crystallographic plane.[11]

The angle in the ac plane between the c' crystal axis and the direction of incidence is θ.

FIGURE 3

Channeling effects in anthracene.

electronic transitions since the emission spectrum is not a function of time.[16] It has been shown[17,18] that the response anisotropy is much greater for the prompt component than the delayed. Since most of the light is emitted as the prompt component, the total response anisotropy is essentially the same as that of the prompt component; therefore, no distinction is made in Figure 2 between the prompt and the total emission.

1.2. THE PRESENT INVESTIGATION

Although luminescence phenomena in organic crystals have been intensively investigated, the origin of ionization quenching and the directional anisotropy in the scintillation response remain unclear. A prominent feature of both effects is the strong dependence on the specific energy loss of the incident particles.

The purpose of the experimental study reported here was a better understanding of the nature of the response anisotropy. Two separate investigations comprised the study.

In the first investigation the response anisotropy in large anthracene crystals was measured with exciting particles having a significantly wider range of average specific energy loss than any employed in previous experiments. A novel method based on Hofstadter's Compton spectrometer technique[19] was used for the measurements. Recoil protons and carbon ions with a continuous spectrum of energies were produced in the crystal of interest by fast neutron scattering. A two detector coincidence system allowed analysis of selected scintillation events corresponding to monoenergetic particles recoil-

ing in a unique direction.

Recoil directions in the ac plane near the c' axis and inclined toward the a axis resulted in maximum scintillation yields for both proton and carbon ion excitation. Minimum yields were noted for recoils parallel to the b crystal axis. The directional response was measured for protons with energies ranging from 0.92 to 7.3 MeV. For 7.3 MeV protons the maximum directional variation in the response was 20%. As the energy was decreased to 0.92 MeV, the variation increased to 35%. Response measurements were made for recoil carbon ions with energies between 2 and 3.5 MeV. The results provide the first accurate values for the magnitude and the anisotropy of the response of anthracene to carbon ions in this energy range. For recoil directions giving maximum response the light yield per MeV was 1.9% of that produced by a 1 MeV electron. Over the energy range considered, the maximum directional variation of the yield for carbon ions remained constant at 40%.

It is significant that the maximum variation in the directional light yield for 0.92 MeV protons and 2 to 3.5 MeV carbon ions differs by only 10%, whereas the average specific energy loss differs by a factor of 10.

The object of the second investigation was the determination of the effects of permanent radiation damage on the anisotropy of both the prompt and the delayed emission components. Excitation was provided by 5.3 MeV alpha particles. The response was measured for various directions of incidence parallel to the ab crystal plane. With no radiation damage the maximum variation in the prompt component was 26.5%. The percentage variation remained essentially unchanged as the crystal was subjected to 1000 kilorad of CO-60

gamma radiation. However, the maximum percentage variation in the delayed scintillation yield gradually increased from 5.6% for the case of no damage to 14.5% when the cumulative gamma ray dose reached 500 kilorad.

Interpretation of the experimental results is necessarily based on a detailed description of the scintillation process since the directional dependence of the scintillation yield is a consequence of one or more of the many processes which follow in the wake of an energetic heavy charged particle. In Chapters 2 and 3 of this dissertation three models are formulated each emphasizing different processes. Four possibilities are examined: (1) anisotropic initial yield of the excited states which lead to fluorescence, (2) anisotropic quenching of the initial excited states by transient quenchers, (3) anisotropic exciton diffusion resulting in a directionally dependent rate of biexcitonic annihilation (quenching) of excitons, (4) anisotropic exciton diffusion out of the original excitation column where quenching results from damaged molecules.

The features of model (3) are concluded to be the most consistent with published results and the experimental results of the present studies.

CHAPTER 2

CHARGED PARTICLE INTERACTIONS IN CRYSTALLINE ANTHRACENE

2.1. INTRODUCTION

In this chapter a basis is established for subsequent formulations of

the scintillation process in anthracene crystals. A qualitative descrip-

tion is given of the sequence of events which occur on a microscopic scale

in a crystal along the track of an energetic charged particle. Pertinent

terminology is also clarified. The description is founded on several dis-

cussions[7,20,21,22] of charged particle interactions in condensed media.

Anthracene, in particular, is considered where appropriate.

The two following figures serve as a prelude to the discussion. Fig-

ure 4 summarizes the order of magnitude estimates by Hart and Platzman[21]

for the duration of relevant processes or events in liquids or solids. For

convenience these and other processes will be categorized as primary and

secondary processes. In general the primary processes are involved in the

initial deposition of energy by an incident particle; whereas the secondary

processes are involved in the evolution of the initial excitation and ioniza-

tion. Figure 5 shows an energy level diagram for various states in crystal-

line anthracene.[23,24]

2.2. PRIMARY PROCESSES

When an energetic charged particle traverses a solid it loses energy

predominantly in direct molecular excitation and ionization events. These
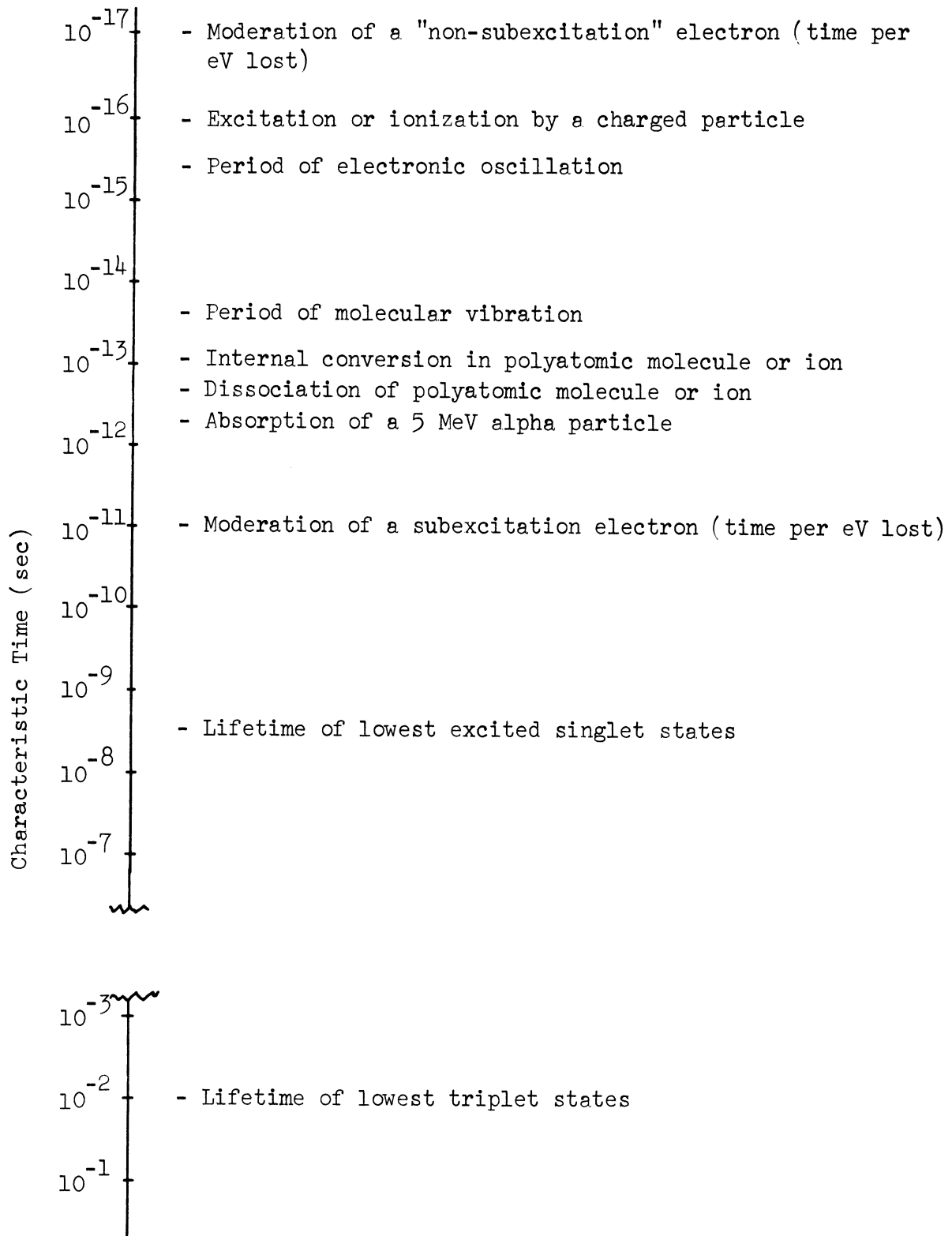
FIGURE 4

Characteristic times of selected processes.
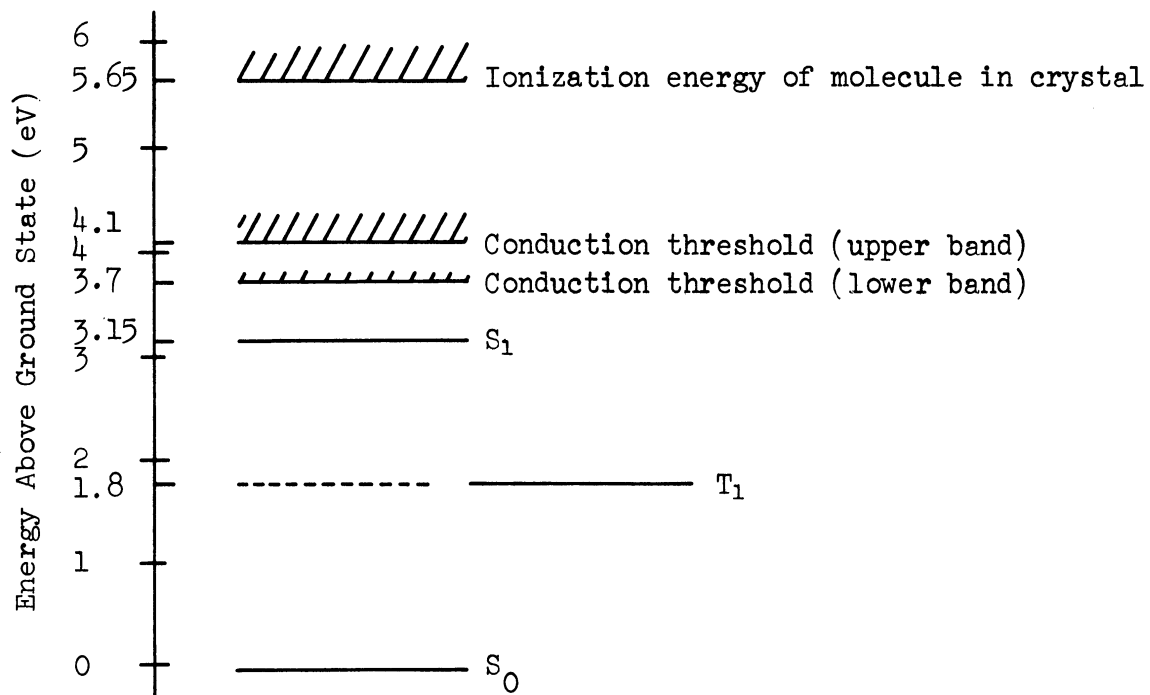
Singlet and triplet exciton bands are labeled by S_i and T_i respectively. The subscript identifies the band level.

FIGURE 5

Energy level diagram for crystalline anthracene.

are called "primary events," and they necessarily occur near the path of the particle. Ensuing events are termed "secondary events."

Electrons ejected during ionization have a spectrum of energies which is peaked at the low energy end. These electrons produce further electronic excitation and ionization when energetically allowed. Once the energy of an ejected electron is below that necessary for electronic excitation, the electron is termed a "subexcitation electron" and loses energy more slowly by exciting only vibrational states. Since the elastic scattering probability for ejected electrons is roughly proportional to the inverse square of electron energy,[25] the majority of the electrons are reduced to subexcitation electrons in the vicinity of the initial ionization. However, a few ejected electrons have enough energy (more than 75 to 100 eV) to travel relatively large distances while losing energy much as the original particle. These higher energy electrons are called "delta rays" and in the case of electron, proton, and alpha particle excitation they produce approximately half the total ionization and excitation. Electron-hole pairs produced directly by the original particle or resultant delta rays are referred to as "clusters." A cluster also includes any excitation or ionization produced in the vicinity by the moderation of the ejected electron.

Energy loss due to elastic nuclear scattering is a second order effect considering the particles and energies of interest here. Yet, such collisions do result in atomic displacements which contribute to cumulative radiation damage. According to Snyder and Neufeld,[26] the energy dissipated in elastic nuclear collisions by an energetic carbon ion (our most extreme case)

does not become equal to that resulting from inelastic electron collisions until the energy of the ion is less than 95 keV. Conservative calculations based on the results of Linhard and Thomsen[27,28] indicate that, at most, 15% of the energy of a 2 MeV carbon ion is expended in elastic nuclear scattering.

Other primary events involving energy loss are: direct multiple excitation and ionization of a single molecule, charge pickup and loss by the exciting particle, excitation of pure molecular vibrations, and in the case of fast electrons, bremsstrahlung. These mechanisms are at least an order of magnitude less significant than nuclear scattering in the cases considered here.[21,29]

Thus, the tracks of the incident particle and the delta rays consist essentially of random linear distributions of directly excited molecules and clusters of excited and ionized molecules. In an organic crystal such as anthracene, excited π-orbital singlet states are among those produced directly or during electron moderation. However, it is doubtful whether many π-electron triplet states are formed in this manner since optical transitions from ground π-electron singlet states to excited π-electron triplet states are forbidden. The initially excited π-singlet states are considered the origin of the prompt scintillation emission; whereas the delayed emission is thought to arise indirectly from the triplet states produced predominantly by electron-hole recombination.

The primary processes are considered terminated once the ejected electrons have become subexcitation electrons. Since ejected electrons lose energy in a solid by electronic excitation and ionization at a typical rate of 10^{17} eV per second,[21] the primary processes usually end less than 10^{-13} seconds

after the primary events.

2.3. SECONDARY PROCESSES

As the primary processes subside new (secondary) processes become impor-
tant. Molecular excitation is dissipated by "internal quenching."* In this
way directly formed highly excited π-electron singlet states decay quickly
(10^{-13} to 10^{-11} seconds) to the lowest excited states. Excited π-triplet
states may decay a bit more slowly. Possibly, some excited π-states result
from the deexcitation of σ and K- electron states. Electron-hole recombina-
tions yield additional highly excited singlet and triplet states with subse-
quent internal quenching. Statistically, it has been calculated[30] that as
many as 75% of the recombinations result in triplet states. Subexcitation
electrons also contribute to the vibrational energy of the system as they are
thermalized at a rate of 10^{11} to 10^{13} eV per second.[21]

Temporary and permanent molecular dissociation occurs. Direct dissocia-
tion occurs in approximately one-half a molecular vibrational period (about
10^{-13} seconds),[21] and it probably results from excitation and ionization of
σ-electrons.[4] Indirect dissociation results from certain statistical con-
centrations of the vibrational energy of the system.

Eventually, the spatial distribution of excitation and ionization begins
to change significantly because of energy and charge migration through the

---

*Internal quenching consists of "internal conversion" which is the conversion
of electronic excitation to molecular vibrational energy and "internal de-
gredation" which is the transfer of molecular vibrational energy to adjacent
molecules of the crystal lattice.

crystal lattice. The theory which properly describes the migration of the excited π-electron energy is included in an area of scientific endeavor recently termed "excitonics." While there is disagreement about which of the various exciton models is most appropriate, it suffices here to consider excitons as wave packets which describe the migration of π-electron singlet and triplet state excitation.

Excitation and charge migration result in a variety of interactions. Even though the concept of simple isotropic diffusion is limited, a convenient phenomenological description of the migration and interactions is provided by the following set of coupled equations.

$$\left\{ \frac{\partial n_i}{\partial t} = D_i \nabla^2 n_i - \sum_j K_{ij} n_i + \sum_j K_{ji} n_j - \sum_{jkl} K_{ijkl} n_i n_j + \sum_{jkl} K_{jkli} n_j n_k \right\} \qquad (2.1)$$

where:

$n_i = n_i(r_i, t)$, the space and time dependent concentration (number cm^{-3}) of excitons or charges in crystal quantum states of level or type i. (E.g., concentration of singlet or triplet excitons in the lowest excited level.)

D_i = isotropic diffusion coefficient ($cm^2 sec^{-1}$) for members of concentration i.

K_{ij} = rate constant (sec^{-1}) for the transition of a member of concentration i to concentration j (first order loss process for the concentration i).

K_{ji} = rate constant (sec^{-1}) for the transition of a member of concentration j to concentration i (first order process which increases concentration i).

K_{ijkl} = rate constant (cm^3sec^{-1}) for the annihilation interaction between a member of concentration i and a member of concentration j yielding a new member in both concentrations k and l (second order process which decreases the concentration i).

K_{jkli} = rate constant (cm^3sec^{-1}) for the annihilation interaction between a member of concentration j and a member of concentration k yielding a new member in both concentrations l and i (second order process which increases the concentration i).

Examples of experimentally established first order processes relevant to the case of anthracene are:

(1) Radiative decay of excitons in the lowest excited π-states to ground states,

(2) Internal conversion from a higher excited state to a lower one of the same multiplicity,

(3) Intersystem crossing between singlet and triplet states,

(4) Capture of an exciton by an impurity, damaged molecule, or lattice discontinuity.

Examples of second order processes relevant to the case of anthracene are:

(1) Biexcitonic annihilation of two singlet excitons producing a ground state singlet and an electron-hole pair,

(2) Biexcitonic annihilation of two triplet excitons producing a ground state singlet and an excited singlet or triplet exciton,

(3) Electron-hole recombination producing a highly excited singlet or triplet exciton.

Recent evidence indicates that additional processes of significance occur in crystalline anthracene. One such process is the annihilation of triplet excitons by free electrons.[31] Another process is the conjectured intermediate role of charge-transfer excitons during the conversion of a recombined electron-hole pair to a singlet or triplet exciton.[32] Because the knowledge about these processes is incomplete, they are not included in the formulations which follow.

CHAPTER 3

ANALYSIS OF THE SCINTILLATION PROCESS IN CRYSTALLINE ANTHRACENE

3.1. INTRODUCTION

Considering the primary and secondary processes enumerated in the previous chapter, a variety of mechanisms may be conceived as the source of scintillation response anisotropy and ionization quenching in crystalline anthracene. Since more than one mechanism may be involved, it is an idealization to formulate them separately. However, because of the complexity of the problem, analysis is possible only if one mechanism predominates; and the others produce second order effects.

Three models which emphasize different mechanisms are analyzed in this chapter. Numerical estimates are presented, when possible, which allow an evaluation of the models and the corresponding formulations.

In the first model (Static Quenching Model) quenching is assumed to take place before any significant migration of excitons. Two alternate mechanisms are proposed in order to explain the observed anisotropy of the prompt scintillation emission. One mechanism is a directionally dependent initial yield of excited π-electron states; whereas the other is directionally dependent quenching.

In the second and third models (Dynamic Quenching Models) the quenching is assumed to arise from the migration of excitons. Anisotropic migration is demonstrated to result in directionally dependent quenching and hence anisotropic scintillation response. The predominant process in the second model

is presumed to be the biexcitonic annihilation of singlet and triplet excitons. In the third model, quenching of diffusing excitons by temporarily damaged molecules is considered to predominate.

3.2. STATIC QUENCHING MODEL

The basis for this model is the assumption that the prompt response anisotropy and ionization quenching result from mechanisms which act before the migration of excitons becomes a significant process. Along the tracks of an incident particle and the associated delta rays,,the nonradiative de-excitation of highly excited π-electron states to ground states is presumed to be enhanced by temporarily disturbed molecules or the high local electric fields resulting from ionization. By the time the π-electron excitation energy begins to migrate, all quenching has subsided; and the excitons diffuse and decay just as if they had been formed by the absorbtion of optical photons.

Voltz et al.[10] have formulated a description of the luminescence phenomena in organic materials utilizing the static quenching model. Subsequent analysis of this model is based on their description. The expression they obtained for the prompt specific scintillation component produced by a heavy charged particle is given below.

$$dL/dx = \eta_s \left\{ (F_T/w_s)(dE/dx)\exp[-BF_T dE/dx] + (F_S/w_s)dE/dx \right\} \tag{3.1}$$

where: dL/dx and dE/dx have been previously defined.

η_s = quantum efficiency of fluorescence.*

---

*The probability a transition from the lowest excited π-singlet state to the
 ground state will result in a photon escaping the crystal.

F_δ = the fraction of dE/dx appearing as delta ray energy.

F_T = the fraction of dE/dx deposited in the track of the incident particle (F_T = 1-F_δ).

w_s = the average energy dissipated by the incident particle per excited singlet state after internal conversion of higher states to the lowest excited level.

B = a quenching parameter related to the effectiveness of the quenching centers.

3.2.1. Partition of the Specific Energy Loss

A singificant feature of the formulation of Voltz et al. is the separation of the excitation and ionization produced by delta rays from that produced directly in the track of the incident particle. They suggest the following method of estimating the partition of the specific energy loss by use of the Rutherford scattering law and Bethe's stopping power formula.[25]

The energy transferred in the production of a delta ray is assumed to be large compared to the binding energy of the ejected electron. This assumption allows the scattering collision to be treated as an elastic collision between the incident particle and an initially stationary free electron. The specific energy loss of a heavy charged particle due to elastic collision with free electrons in which at least a minimum amount of energy (T_o) is imparted to the electron is

$$(dE/dx)_{T \geq T_o} = \int_{T_o}^{T_{max}} \frac{2\pi e^4 z^2}{m_e V^2} n_e \frac{dT}{T} ; \quad Zc/137 \ll V \ll c \qquad (3.2)$$

where:

m_e = the rest mass of an electron.

e = the charge of an electron.

z = the charge of the incident particle.

V = the velocity of the incident particle.

n_e = the density of the free electrons.

T = the energy transferred to the electron.

T_{max} = the maximum energy that can be imparted to an electron. (T_{max} = = $4m_e E/M$ where E and M are the energy and mass of the incident particle respectively.)

T_o = the minimum initial energy of a delta ray assumed hence to be 100 eV.

c = the velocity of light.

Z = the charge number of the atoms actually comprising the medium.

According to Bethe the specific energy loss of a heavy charged particle due to electronic interactions is

$$dE/dx = \frac{4\pi e^4 z^2}{m_e V^2} n_e \ln\left(\frac{4m_e E}{MI}\right) ; \quad Zc/137 \ll V \ll c \qquad (3.3)$$

where I for a particular medium can be deduced from experimental results. Voltz et al. used the method of Sternheimer[33] to calculate I for NE 102. Similar calculations give a value of I for anthracene of 64.5 eV.

The partition F_δ is now given by the ratio $(dE/dx)_{T \geq T_o} / (dE/dx)$ or

$$F_\delta = \frac{1}{2} \frac{\ln\left(\frac{4m_e E}{MT_o}\right)}{\ln\left(\frac{4m_e E}{MI}\right)} ; \quad E \geq MT_o/4m_e ; \quad Zc/137 \ll V \ll c . \qquad (3.4)$$

The validity of Equations (3.2), (3.3), and (3.4) becomes questionable

outside the velocity range indicated. The lower limit is of concern here.

When the velocity of the incident particle decreases to about that of the

orbital electrons of the atoms in the medium $(Zc/137)$, the charge of the par-

ticle begins to fluctuate due to charge pick-up and loss. Also, the faster

orbital electrons in the medium (K-shell) cease participation in the energy

loss process. Thus, there is a decrease in both the effective charge of the

incident particle and the effective electron density of the medium. However,

if the form of the Equations (3.2) and (3.3) remain valid with appropriately

compensated values for z and n_e, then F_δ is affected only through a change in

I due to the lack of participation by the inner electrons. Since the logarithm

of I is involved, the velocity effect should be much less pronounced in Equa-

tion (3.4) than in either Equation (3.2) or (3.3) considered alone. The par-

tition F_δ has been calculated by use of Equation (3.4) for the cases of ener-

getic alpha particles, protons, and carbon ions slowing down in an anthracene

crystal. It was assumed that I remained constant even though the velocity re-

quirements were not met for all energies considered. Figure 6 shows the re-

sults as a plot of F_δ versus specific energy loss. Also the value of dE/dx

for which the velocity of the particle (V) equals $(6c/137)$ is shown to indi-

cate the more reliable values of F_δ.

3.2.2. <u>Extension of the Model to Anisotropic Media</u>

The exponential quenching factor in Equation (3.1) arises from consid-

ering a one dimensional Poisson distribution of quenching centers along the
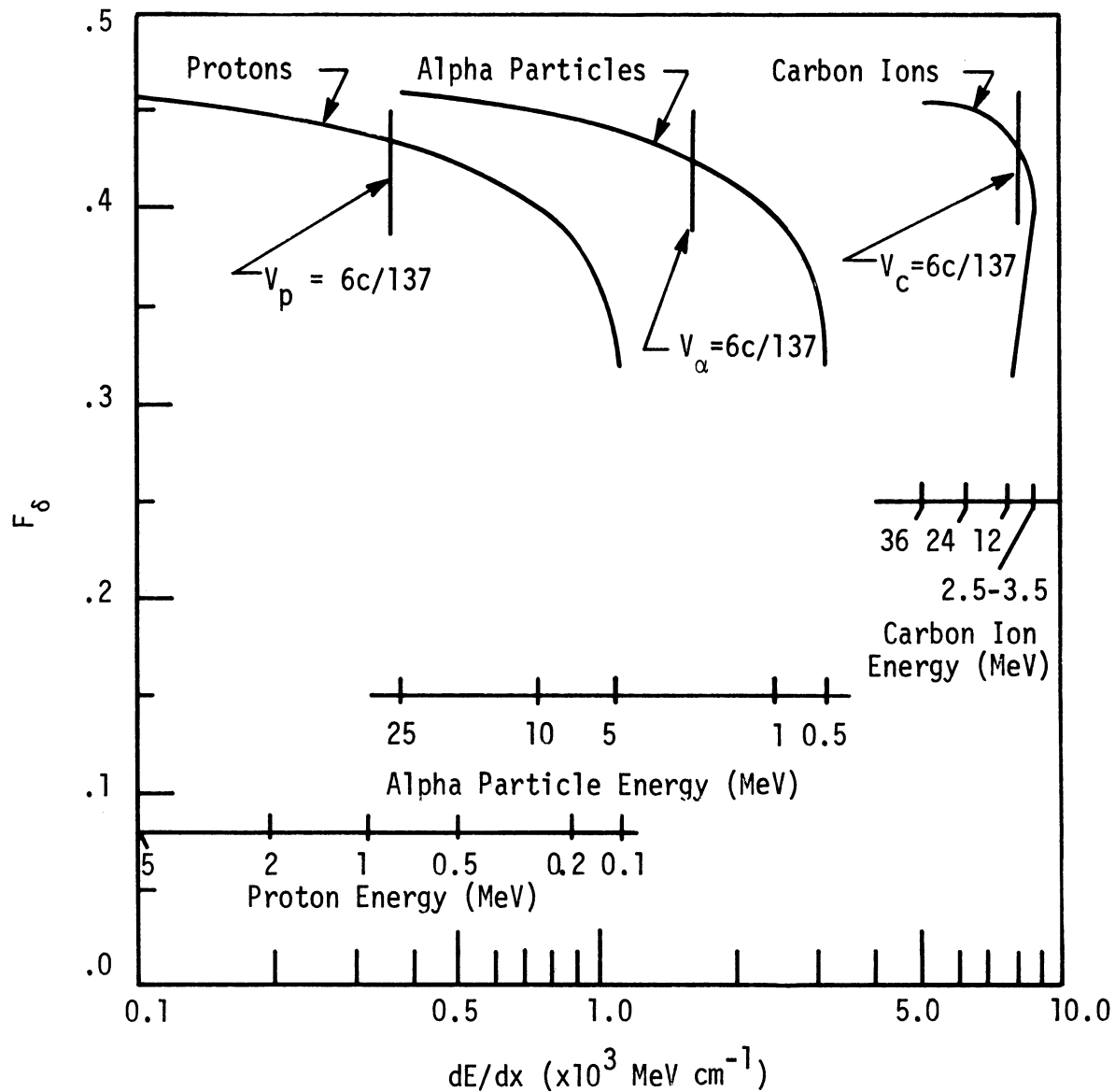
F_δ is the fraction of dE/dx appearing as delta ray energy.

Alpha particle and proton dE/dx versus energy relation is the same as in Figure 2. Carbon ion dE/dx versus energy relation was obtained from the data of Northcliff[28] for the stopping power of carbon for energetic carbon ions. The stopping power of anthracene was deduced from that of carbon by use of the Bragg-Kleeman Rule.[4]

FIGURE 6

Partition of specific energy loss.

path of the incident particle. All excited π-electron states which are

formed within a critical distance from these centers are assumed to be

quenched. The absence of a corresponding quenching factor in the delta ray

term is a simplification by Voltz et al.; therefore, an unspecified quench-

ing factor (Q_δ) will be included subsequently.

Voltz et al. imply that their model, qualitatively at least, describes

the type of response variation with dE/dx that both they and Schött[5] ob-

served for NE 102 and crystalline anthracene respectively. However, for

this model to adequately encompass the crystalline organic scintillators it

must predict a directional dependence. Two alternate modifications are pro-

posed below in cases (1) and (2).

(1) In this case it is proposed that the efficiency of producing ex-
cited π-singlet states directly is different for heavy charged
particles and low energy electrons than for delta rays. Likewise,
the efficiency for direct excitation in anisotropic media is as-
sumed to be anisotropic as well. These effects could result in
different directionally dependent values for w_s in both terms of
Equation (3.1). However, because of the multiple scattering of
the delta ray electrons, it is assumed that the yield of excited
π-singlet states resulting from delta rays is isotropic.

(2) As an alternative it is proposed that only the quenching parameter
B is dependent on the orientation of the track of the incident
particle relative to the crystal axes. Hence the scintillation
light yield resulting from excited π-electrons in the track is
directionally dependent. In contrast to the quenching in the track,
Q_δ is presumed to be isotropic because of delta ray scattering.

If Q_δ and w_δ are isotropic, the appropriate form of Equation (3.1) for

both cases is

$$dL_i/dx = \eta_s(dE/dx)\left\{(F_T/w_{si})\exp[-B_iF_T dE/dx] + (F_\delta/w_\delta)Q_\delta\right\} . \qquad (3.5)$$

The subscript (i) indicates that either w_s or B and therefore dL/dx are functions of the direction of incidence of the exciting particle relative to the crystal axes. Both w_s and B are assumed to be independent of dE/dx.

It is possible to quantitatively test Equation (3.5) for the case of anisotropic response. For example, the difference in the specific light yield for monoenergetic particles incident parallel to the c' and b crystallographic axes can now be expressed as

$$\left(\frac{w_e}{\eta_s}\right)\left(\frac{dL_{c'}}{dx} - \frac{dL_b}{dx}\right)\left(F_T \frac{dE}{dx}\right)^{-1} = \left(\frac{w_e}{w_{sc'}}\right)\exp\left[-B_{c'}F_T \frac{dE}{dx}\right] - \left(\frac{w_e}{w_{sb}}\right)\exp\left[-B_b F_T \frac{dE}{dx}\right]$$

$$(3.6)$$

where the subscript i in Equation (3.5) has been replaced by c' and b for the two directions of incidence, and w_e equals the average energy expended per lowest excited π-singlet state by the recoil electrons used for normalization of the light yield.

For case (1) $B_{c'} = B_b$ and Equation (3.6) can be rewritten as

$$\left(\frac{w_e}{\eta_s}\right)\left(\frac{dL_{c'}}{dx} - \frac{dL_b}{dx}\right)\left(F_T \frac{dE}{dx}\right)^{-1}\exp\left[B_{c'}F_T \frac{dE}{dx}\right] = \frac{w_e}{w_{sc'}} - \frac{w_e}{w_{sb}} = const. \quad (3.7)$$

It is clear that $(dL_{c'}/dx - dL_b/dx)(F_T \, dE/dx)^{-1}$ must vary with dE/dx as the inverse of the exponential term for this expression to be valid.

In case (2) it is assumed that $w_{sc'}$ and $w_{sb} = w_e$. Then Equation (3.6) can be written as

$$\left(\frac{w_e}{\eta_s}\right)\left(\frac{dL_c{}'}{dx} - \frac{dL_b}{dx}\right)\left(F_T \frac{dE}{dx}\right)^{-1} = \exp\left[-B_c{}'F_T \frac{dE}{dx}\right] - \exp\left[-B_b F_T \frac{dE}{dx}\right] \quad . \quad (3.8)$$

The absolute value of the difference of two exponential terms such as

$|e^{-ax} - e^{-bx}|$, (a and b are constants) increases with increasing values of x

to a maximum and then decreases. Eventually the value approaches the abso-

lute value of the most slowly decaying term. Considering Equation (3.8) it

is noted that $(dL_c{}'/dx - dL_b/dx)$ $(F_T dE/dx)^{-1}$ should vary with dE/dx in a sim-

ilar manner.

Both cases may be evaluated by referring to Figure 7. In this figure

$(w_e/\eta_s)(dL_c{}'/dx - dL_b/dx)(F_T dE/dx)^{-1}$ is plotted as a function of dE/dx. The

difference in specific light yield was obtained from the alpha particle re-

sults of Schött[5] and the proton results of Tsukada et al.[6] Corresponding

values for F_T were obtained from Figure 6. Neither of the curves in Figure

7 has the linear appearance of a logarithmic plot of a single exponential

function or the proper curvature of a logarithmic plot of the difference of

two exponential functions. The curve corresponding to Schött's data varies

by at least 20% from a judicious linear fit of the curve over the dE/dx range

of 200 to 1500 MeV cm^{-1}. A similar variation is noted in the curve calculated

from the results of Tsukada et al.; however, this curve extends over a much

smaller dE/dx range. Allowance for the calculated variation of F_T with dE/dx

in the exponents appearing in Equations (3.7) and (3.8) does not improve the

agreement. Likewise, it is doubtful that the approximate nature of the cal-

culated values for F_T is the reason for the non-exponential form of the
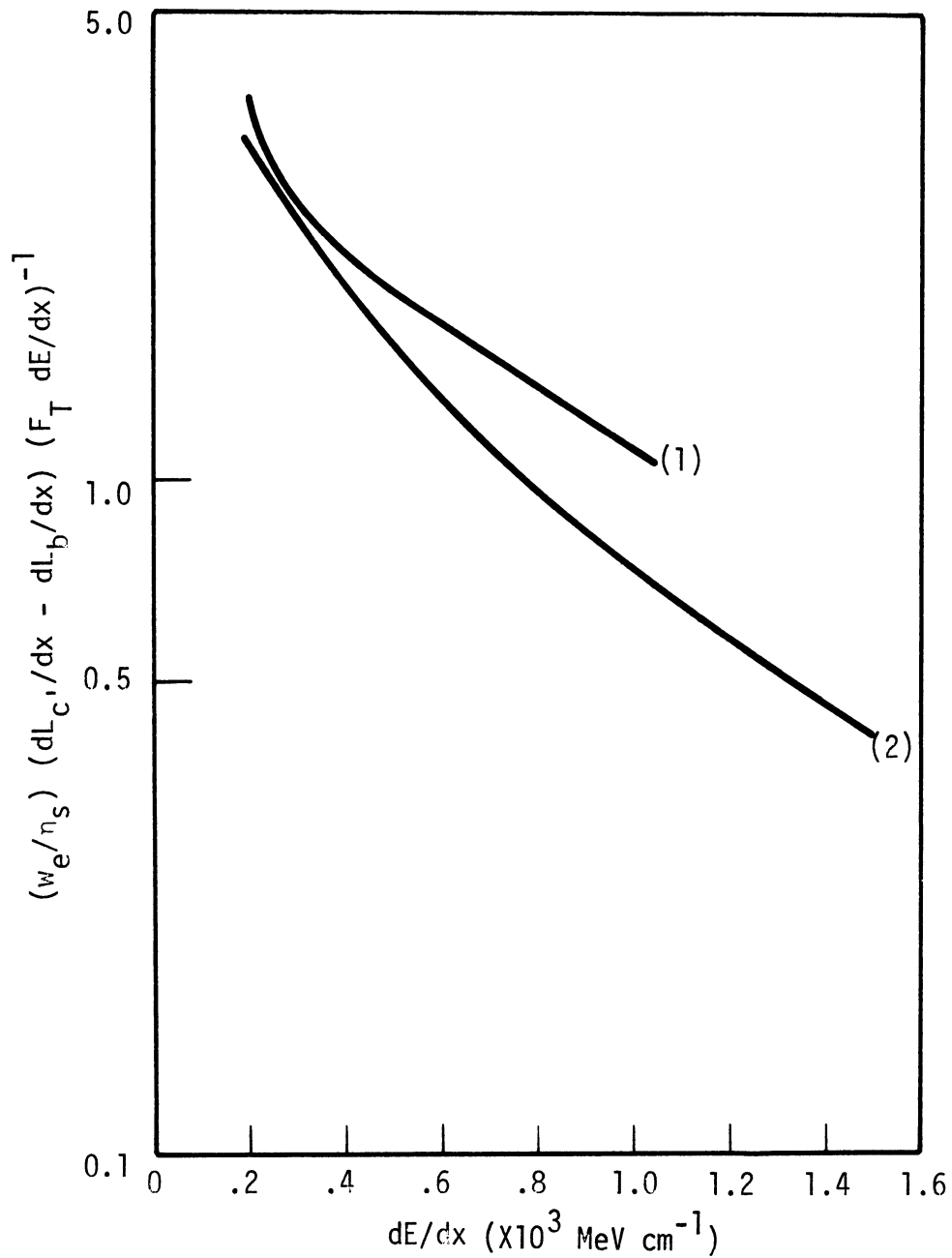
FIGURE 7

Weighted difference in specific light yield as a
function of specific energy loss-I.

experiment-related curves in Figure 7. The assumption that $w_{sc'}$, w_{sb}, and B are independent of dE/dx is certainly an approximation; however, it would be surprising if any variation of these quantities with dE/dx is great enough to linearize or reverse the curvature of the relevant curves.

In conclusion, it appears there is difficulty in interpreting the phenomenon of directional scintillation response anisotropy by use of the formulation of Voltz et al.

3.3. DYNAMIC QUENCHING MODELS

Quenching and response anisotropy may be consequences of the secondary processes. Since the prompt scintillation decay constant is apparently unaffected by the mechanisms, the processes responsible would be significant during the time interval between 10^{-13} to 10^{-9} seconds after the passage of the exciting particle. Equations from the set (2.1) are used in this section for the analysis of the secondary processes in anthracene.

Unfortunately, most of the experimentally determined rate constants correspond to the lowest singlet and triplet exciton states. Nevertheless, a description of these states is a good first order approximation. They are the longest lived of those of their respective multiplicities; thus they are probably the most affected if quenching and anisotropy arise from migration.

Due to the complexity of the equations describing these states, general solutions are not available. However, with adequate approximations solutions have been obtained. Discussed in order below are: the general equations, initial simplifications, simplified geometry, initial yields, and solutions

corresponding to special cases.

3.3.1. General Equations

Once internal conversion from higher levels becomes negligible, the appropriate equations for the exciton concentrations in the lowest excited singlet (s) and triplet (t) levels are:

$$\frac{\partial n_s}{\partial t} = D_s \nabla^2 n_s - (K_{sf} + K_{sic} + K_{sq}^D + K_{sq}^t + K_{st})n_s - K_{ss}n_s^2 + K_{tts}n_t^2 + K_{ts}n_t \quad , \quad (3.9)$$

$$\frac{\partial n_t}{\partial t} = D_t \nabla^2 n_t - (K_{tp} + K_{tic} + K_{tq}^D + K_{tq}^t + K_{ts})n_t - K_{tt}n_t^2 + K_{st}n_s \quad (3.10)$$

where:

K_{sf}, K_{sp} = fluorescent or phosphorescent decay to the ground state respectively.

K_{sic}, K_{tic} = decay to the ground state by internal conversion.

K_{sq}^D, K_{tq}^D = quenching due to permanent radiation damage.

K_{sq}^t, K_{tq}^t = quenching due to transient quenching centers.

K_{st}, K_{ts} = intersystem crossing, singlet to triplet or triplet to singlet states respectively.

K_{ss}, K_{tt} = biexcitonic annihilation.

K_{tts} = biexcitonic annihilation of two triplet excitons leading directly to a singlet exciton ($K_{tts} \leq 1/2 \, K_{tt}$).

Simple expressions for several of the constants have been used recently by various authors[34,35,36,37] in their discussions of exciton migration in organic crystals. The pertinent expressions arise from considering the band

model (weak scattering) or the hopping model (strong scattering) of exciton

migration. Neither model has been demonstrated experimentally to be pre-

cisely correct and the actual case probably lies somewhere between the two.

The following expressions are valid in form for both singlet and triplet

excitons even though the singlet subscripts are used.

<div align="center">

Band Model   **Hopping Model**

</div>

$$D_s = \frac{1}{3} \lambda_s v \qquad\qquad D_s = \frac{1}{6} N_h d^2$$

$$K_{ss} = \frac{1}{2} \sigma_{ss} v \qquad\qquad K_{ss} = \frac{1}{2} \frac{\epsilon_a N_h}{N_m}$$

$$K_{sq} = \sigma_{sq} v N_q \qquad\qquad K_{sq} = \frac{\epsilon_q N_h N_q}{N_m}$$

where:

λ_s = mean free path between exciton-phonon scattering events.

v = exciton velocity.

σ_{ss} = cross section (cm^2) for exciton-exciton annihilation interaction. A simple expression is $\sigma_{ss} = \pi r_m^2$ where r_m is the effective radius of an anthracene molecule.

σ_{sq} = cross section (cm^2) of a quenching site for exciton capture and subsequent quenching (similar form for both transient and permanent damage quenches).

N_q = concentration (number cm^{-3}) of quenching sites (transient or permanent damage quenchers).

N_h = number of randomly directed hops a hopping exciton makes per second.

d^2 = mean square displacement of a hopping exciton per hop.

ϵ_a = efficiency of annihilation process.

N_m = number of anthracene molecules per cm^3 (4.2×10^{21} at room temperature).

ϵ_q = efficiency of quenching once the exciton is adjacent to the quenching center.

The expressions for K_{ss} and K_{sq} are appropriate for a uniform exciton distribution in an infinite medium. Such is not the case in the wake of a charged particle so the expressions are, at best, only approximate.

3.3.1.1. Initial simplifications

For the case of crystalline anthracene typical published experimental values for the coefficients appearing in Equations (3.9) and (3.10) are listed in Table 1.

TABLE 1

DIFFUSION AND INTERACTION CONSTANTS

$D_s = 2 \times 10^{-3}(cm^2 sec^{-1})$.[35]	$D_t = 2 \times 10^{-4}(cm^w sec^{-1})$.[37]
$K_{sf} = 9 \times 10^7(sec^{-1})$.[4]	$K_{tp} \ll 10^2(sec^{-1})$.[41]
$K_{sic} = 10^7(sec^{-1})$.[4]	$K_{tic} = 10^2(sec^{-1})$.[41]
$K_{st} = 1.6 - 2.4 \times 10^6(sec^{-1})$.[38]	K_{ts} is very small.
$K_{ss} = .5 - 1.3 \times 10^{-8}(cm^3 sec^{-1})$.[39]	$K_{tt} = 5 \times 10^{-11}(cm^3 sec^{-1})$.[41]
$K_{sq} = 68 (sec^{-1} rad^{-1})$.[40]	$K_{tq}^D = (0.33 \ sec^{-1} rad^{-1})$.[40]

The measurement of these constants involved the excitation of pertinent electronic states with optical photons. As a result of the techniques employed,

the values correspond to averages for all crystal directions. A notable exception is the experiment of Levine and Jortner.[37] They determined the triplet exciton diffusion coefficient for the a, b, and c' crystal directions and found it to be isotropic within 20%.

The transient quenching coefficients K^t_{sq} and K^t_{tq} have been proposed to explain ionization quenching. Since some of the effects of charged particle excitation are virtually impossible to produce with optical photons, these coefficients have not been measured and their significance remains conjectural.

The importance of various terms in Equations (3.9) and (3.10) can be estimated by use of the experimental values tabulated above. A comparison of the terms allows immediate simplification of the equations for most purposes. Considering Equation (3.9) it is clear that intersystem crossing from the singlet states to the triplet states is a negligible singlet exciton loss process compared to internal conversion or fluorescent decay to the ground state. The radiation damage term is only significant after the crystal has absorbed an appreciable dose of damaging radiation. Intersystem crossing from triplet states to singlet states is negligible since it is a thermally activated process which proceeds very slowly at room temperature. When only the prompt scintillation component is considered, the contribution of the triplet biexcitonic annihilation term may be neglected in comparison to the singlet biexcitonic loss term. Since the ratio K_{ss}/K_{tts} is greater than ~10^3, the ratio n^2_s/n^2_t would have to be less than 10^{-3} for the two terms to compete. Such competition in the wake of a charged particle is unlikely because the yield and spatial distributions of ionized and excited π-electron

states should be about the same.[22]   Also, electron-hole pairs which produce

most of the triplet excitons do not necessarily recombine immediately. Some

ejected electrons become trapped and never recombine. The biexcitonic anni-

hilation of triplet excitons is considered partially responsible for the de-

layed scintillation; thus this process is quite important when the delayed

component, rather than the prompt component, is of interest.

An examination of the coefficients which appear in Equation (3.10) shows

that, at least at room temperature, the loss of triplet excitons due to phos-

phorescent decay and intersystem crossing to the singlet levels is negligi-

ble compared to internal conversion to the ground state. Biexcitonic anni-

hilation competes with internal conversion only in the case of reasonably

high concentrations such as exist initially in the track of a heavy charged

particle. However, if the singlet exciton concentration is great enough

relative to the triplet concentration, as in "flash spectroscopy," intersys-

tem crossing from the singlet population can become important. The radia-

tion damage quenching term becomes significant at a lower accumulated dose

than the comparable singlet exciton term, but it is negligible in most in-

stances.

3.3.1.2. Simplified geometry

When the specific energy loss is great enough along the track of an in-

cident particle, the clusters and direct excitations overlap to the extent

that the initial distribution becomes cylindrical. Once cylindrical geom-

etry is established, axial variations in the excitation and ionization dens-

ities are negligible along the track compared to the radial variations.

Therefore, the concentrations in Equations (3.9) and (3.10) can be considered

functions of time and the radial distance from the path of the incident par-

ticle only, with the initial conditions being constant for relatively large

increments of the track.

An expression for the minimum value of specific energy loss $(dE/dx)_{min}$

which results in cylindrical geometry may be obtained as follows. If w_c is

the average energy dissipated per cluster and F_T is the fraction of dE/dx

deposited in the track of the incident particle (i.e. not carried off by delta

rays) then the average distance (d) between clusters in the track is given by

$$d = \left(F_T \frac{1}{w_c} \frac{dE}{dx} \right)^{-1} \tag{3.11}$$

Within the clusters it is reasonable to assume that the probability distribu-

tion of the various ions and excited molecules is a three dimensional Gaussian

centered at some point near the path of the incident particle.[30,42] Samuel

and Magee[42] proposed the following initial distribution for the clusters of

radicals produced by the electrons ejected in the radiolysis of water.

$$\phi(r) = \phi_o \exp[-r^2/r_o^2] , \quad r_o = 5N_o^{1/3} \text{ Å (Characteristic radius)}$$

where $\phi(r)$ is the radical distribution function, ϕ_o is a constant, and N_o is

the total number of radicals in a cluster. It is believed that the cluster

size in water is the minimum possible size.[30] Kuppermann and Belford[43] con-

sidered the superposition of an infinite number of equivalent spherical

Gaussian distributions with colinear centers. When the centers are separated by twice the characteristic Gaussian radius, the resultant columnar distribution varies less than 3% axially. Thus a simple criterion for the establishment of cylindrical geometry is that value of dE/dx for which $d = 2r_o$. This criterion, Equation (3.11) and the expression for r_o in water yield the desired relation

$$dE/dx = w_c (10F_T N_o^{1/3} \overset{o}{A})^{-1} \qquad (3.12)$$

where N_o in the case of a solid is the number of electronically excited molecules and electron-hole pairs.

Two independent estimates of w_c are obtained as follows. Whyte[44] recently reviewed many of the published experimental values for the specific energy expended by charged particles in the ionization of gases. He concluded that for a wide variety of gases the specific energy expended by electrons, protons and alpha particles is 32 ± 6 eV per ion pair. This value is essentially independent of particle type and specific energy loss. The frequency distribution for the number of ion-pairs per cluster produced in a cloud chamber[45] shows the average to be 1.62. Thus, the average energy loss per cluster in a gas is 52 ± 9.7 eV. A comparable value for solids can be extracted from the experiment of Rauth and Hutchinson.[46] They deduced from the energy loss spectra of a beam of fast electrons (5-20 KeV) which were transmitted through thin plastic and metal foils that the average electron energy loss per primary event (w_p) is 60 eV. Assuming that the efficiency of cluster production is the same for the incident electrons and ensuing delta rays, the

average energy expended per cluster (w_c) is given by

$$w_c = w_p(1-F_\delta^e)/(1-f_\delta) \qquad (3.13)$$

where F_δ^e is the fraction of the energy loss carried off by delta rays, and

f_δ is the fraction of the primary events resulting in delta rays.* The

partition F_δ^e for electrons can be calculated in a manner similar to that used

for heavy charged particles. A simplified form of Bethe's stopping power

formula for electrons is applicable since the velocity of the incident elec-

trons was relatively low $(v^2/c^2 \leq .079)$. In an electron-electron collision

the most energetic electron after the collision is considered the incident

particle for subsequent events; thus the maximum delta ray energy is half the

energy (E) of the incident electron. With these considerations and the appro-

priate electron-electron scattering cross section[25]

$$F_\delta^e = \frac{1}{2} \frac{\ln(E/2T_o) + 2\ln(E/2(E-T_o)) + 2 - E/(E-T_o)}{\ln(\sqrt{e/2}\ E/I)} \ .$$

When the value of I for NE 102 scintillating plastic is substituted, F_δ^e is

found to range between .314 and .356 for 5 to 20 KeV electrons respectively.

The fraction f_δ is simply the ratio of the specific yield of delta rays

(dN_δ/dx) to the specific yield of primary events (dN_p/dx). An expression for

dN_δ/dx obtained from the electron-electron scattering cross section is

$$dN_\delta/dx = \int_{T_o}^{E/2} \frac{2\pi e^4}{m_e v^2} n_e \ [\frac{1}{T^2} + \frac{1}{(E-T)^2} - \frac{1}{T(E-T)}]dT \ .$$

---

*The energy loss spectra indicate that practically all primary events are
 ionizations.

By definition dN_p/dx is $(dE/dx)/w_p$. Introduction of Bethe's simplified expression for dE/dx yields

$$f_\delta = \frac{w_p[1/T_0 - 1/(E-T_0) - (1/E)\ln((E-T_0)/T_0)}{2\ln(\sqrt{e/2}\ E/I)} \ .$$

After substitution of the appropriate quantities this ratio is found to vary

between 0.0594 and 0.049 for 5 to 20 KeV electrons respectively. Thus, Equa-

tion (3.13) can be evaluated. The average energy expended per cluster is found

to be about 40 eV. Since this value was deduced for materials similar to an-

thracene it will be used in the calculation to follow.

Newton[47] estimates that there are two excited molecules per electron-

hole pair. Assuming that there are 1.68 pairs per cluster, a reasonable value

for N_0 is ~ 5. In Figure 6 it is seen that F_T for a 5 MeV alpha particle is

about 0.56. Substitution of these values into Equation (3.12) gives the fol-

lowing result.

$$(dE/dx)_{min} \sim 420 \text{ MeV cm}^{-1}$$

Even though the assumption of columnar geometry makes Equations (3.9)

and (3.10) more tractable, there remains the problem of properly describing

the initial radial distribution. The radius of the column of overlapping

spheres considered above represents a lower limit for several reasons. One

is the conservative estimate of the radius of a cluster. Another is the as-

sumption that cluster centers are linearly distributed. Finally, the pos-

sibility is neglected that some of the clusters produced by delta rays lie

near or in the track of the incident particle.

3.3.1.3. Initial yields

The yield of singlet excitons in the lowest excited level can be obtained from the absolute scintillation efficiency (S_x) and related quantities. Birks[4] defines S_x for pure crystal scintillators as that fraction of the energy deposited in the bulk of a thick crystal by an energetic electron which later escapes from the surface as visible light. Ionization quenching is assumed to be negligible. A useful relation between S_x and other pertinent quantities is

$$S_x = (\hbar\omega)\eta_s\left(\frac{1}{w_s}\right) \tag{3.14}$$

where $\hbar\omega$ is the average energy of photons escaping from a thick crystal, η_s is the quantum efficiency of fluorescence, and w_s is the average energy expended by a charged particle for each singlet exciton eventually appearing in the lowest excited level. After a survey of published values for anthracene crystals, Birks proposes 0.04 and 0.68 as the most reliable values for S_x and η_s respectively. $(\hbar\omega)$ was found from spectroscopic data to be 2.63 eV for thick crystals ($\geq$ 1mm). By use of these values and Equation (3.14), w_s is found to be 44.7 eV per exciton corresponding to a yield of 2.24 x 10^4 excitons per MeV. Since the delayed scintillation emission contributes only a few per cent in the case of electron excitation, these values can be considered to correspond to the singlets produced during the primary processes. They will also be assumed valid for excitation by heavy charged particles.

An upper limit for the yield of σ-electron excitations and ionizations can be obtained by considering the experiments of Swanson and Powell.[48] They

investigated the energy loss spectra of 20 KeV electrons incident normally

on very thin films of polystyrene and similar polymers. Two loss peaks were

noted for electrons scattered at zero angle. One at approximately 7 eV and

one at 21.3 eV. The 7 eV peak was attributed to excitation of π-electrons

in the benzene rings and the 21.3 eV peak to excitation and ionization of σ-

electrons. Assuming that the latter value is also valid for anthracene and

that all energy loss is due to σ-electron events, the average energy loss

per σ-electron excitation or ionization is 21.3 eV. This is equivalent to a

yield of 4.7×10^4 σ-electron events per MeV.

3.3.2. Biexcitonic Quenching Model

In this model the transient quenching due to the temporary disturbances

in the wake of the incident particle is neglected. Also, the initial sim-

plifications of subsection 3.3.2 and cylindrical geometry are assumed valid.

With these assumptions Equations (3.9) and (3.10)

$$\frac{\partial n_s(r,t)}{\partial t} = D_s \frac{1}{r} \frac{\partial}{\partial r} \left(r \frac{\partial}{\partial r} \right) n_s(r,t) - \frac{1}{\tau_s} n_s(r,t) - K_{ss} n_s^2(r,t) \quad (3.15)$$

$$\frac{\partial n_t(r,t)}{\partial t} = D_t \frac{1}{r} \frac{\partial}{\partial r} \left(r \frac{\partial}{\partial r} \right) n_t(r,t) - \frac{1}{\tau_t} n_t(r,t) - K_{tt} n_t^2(r,t) \quad (3.16)$$

where in the absence of quenching by permanent radiation damage τ_s and τ_t are

the natural lifetimes of the lowest singlet and triplet states respectively.

In the case of damage quenching, $\tau_s = (K_{sf} + K_{sic} + K_{tq}^D)^{-1}$. Since these equa-

tions have the same form, an exact analytic solution would satisfy both of

them. Such a solution is nonexistent; however, numerical solutions and an approximate analytical solution do exist. The solutions result from various studies of equations of the same form which describe the recombination of ions or the reaction of radicals after an alpha particle passes through a gas or solution. The scintillation problem is discussed in terms of these solutions below.

3.3.2.1. Numerical solutions

Two sets of numerical solutions to the radical reaction problem were obtained independently by Fricke and Phillips,[49] and Kuppermann and Belford[50] with the aid of fast digital computers. Both sets of results correspond to a similar range of parameters. The solutions have an estimated accuracy of better than 2% and corresponding solutions agree between the two sets within 1%. Figure 8 shows a plot of the results of Fricke and Phillips which are pertinent to the scintillator problem. The solutions and input parameters have been rephrased in terms related to Equation (3.15). Unfortunately, the range of input parameters is not appropriate for the triplet exciton concentration described by Equation (3.16). The solutions give the light emission integrated from time zero to infinity. The yield (dL/dE) is normalized to that of a 1 MeV electron. Unique solutions are given for each pair of input parameters B and E. The initial radial exciton distribution $n_s(r,o)$ is assumed to be Gaussian. Thus,
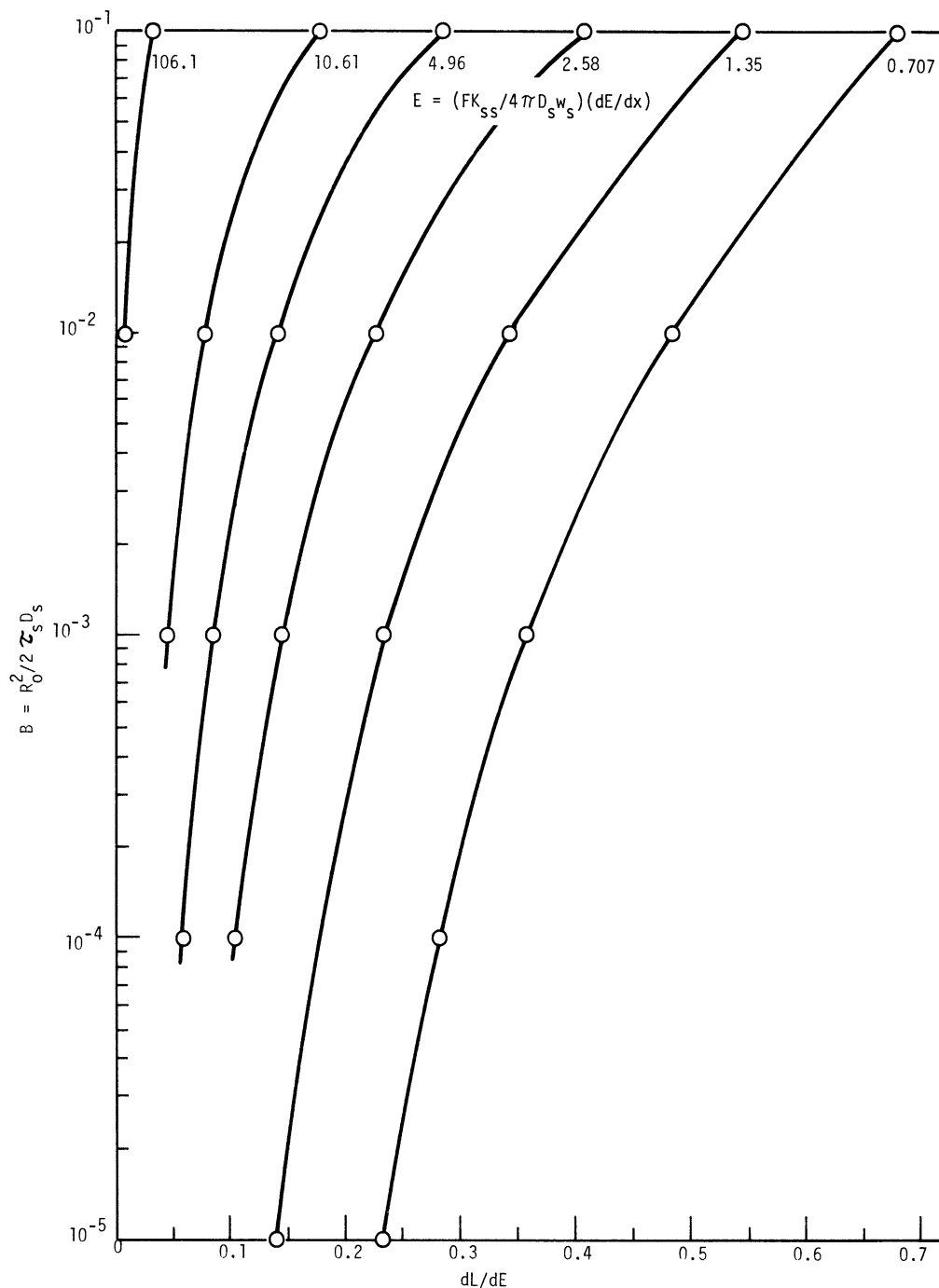
⊙ represents the computer solutions of $\frac{\partial n}{\partial t} s = D_s \frac{1}{r} \frac{\partial}{\partial r} \left(r \frac{\partial}{\partial r} \right) n_s - \frac{1}{\tau_s} n_s - k_{ss} n_s^2$ for B and E values shown.

$$dL/dE = \frac{1/\tau_s \int_o^\infty \int_o^\infty n(r,t)d^2r dt}{\int_o^\infty n(r,o)d^2r}$$

FIGURE 8

Computer solutions of the diffusion kinetics equation.

$$B = R_o^2/2\tau_s D_s \; ;$$

$$E = (FK_{ss}/4\pi D_s w_s)dE/dx, \quad F_T \leq F \leq 1 \; ;$$

$$n_s(r,o) = (F/w_s \pi R_o^2)dE/dx \; \exp[-r^2/R_o^2] \; , \quad r_o \leq R_o$$

where (dE/dx), w_s, F_T and r_o have been previously defined, F is the effective fraction of the energy loss contributing to the exciton concentration in the column, and R_o is the characteristic Gaussian radius. There is some uncertainty in the proper values for R_o and F because they must account for the delta ray effects in a nonrigorous manner.

Since $dL/dx = (dL/dE)(dE/dx)$, it is simple to generate theoretical scintillation response curves from the results shown in Figure 8. The simplest case is when the effective Gaussian radius R_o is considered constant over the dE/dx range of interest. Then B is a constant since τ_s and D_s are presumably not functions of dE/dx. Assuming that K_{ss} and w_s are constants as well, E varies linearly with dE/dx. Figure 9 shows four dL/dx versus dE/dx response curves generated under these conditions. Parameters B and E were selected so that the theoretical response would correspond approximately to the experimental results which are also shown in the figure. The relationship between the parameter variations and the variation of the constants for the four theoretical cases is shown below:

Case	B	$E(cm\ MeV^{-1})$	D_s	Ro	FK_{ss}/w_s
(1)	4×10^{-4}	$3.5 \times 10^{-3}(dE/dx)$	$D_s(1)$	$R(1)$	$(FK_{ss}/w_s)(1)$
(2)	2×10^{-4}	$1.75 \times 10^{-3}(dE/dx)$	$2D_s(1)$	$R(1)$	$(FK_{ss}/w_s)(1)$
(3)	4×10^{-4}	$1.75 \times 10^{-3}(dE/dx)$	$D_s(1)$	$R(1)$	$1/2(FK_{ss}/w_s)(1)$
(4)	16×10^{-4}	$3.5 \times 10^{-3}(dE/dx)$	$D_s(1)$	$2R(1)$	$(FK_{ss}/w_s)(1)$

X-axis: Specific Energy Loss ($\times 10^3$ MeV cm^{-1})

Y-axis: Specific Light Yield ($\times 10^3$ cm^{-1})
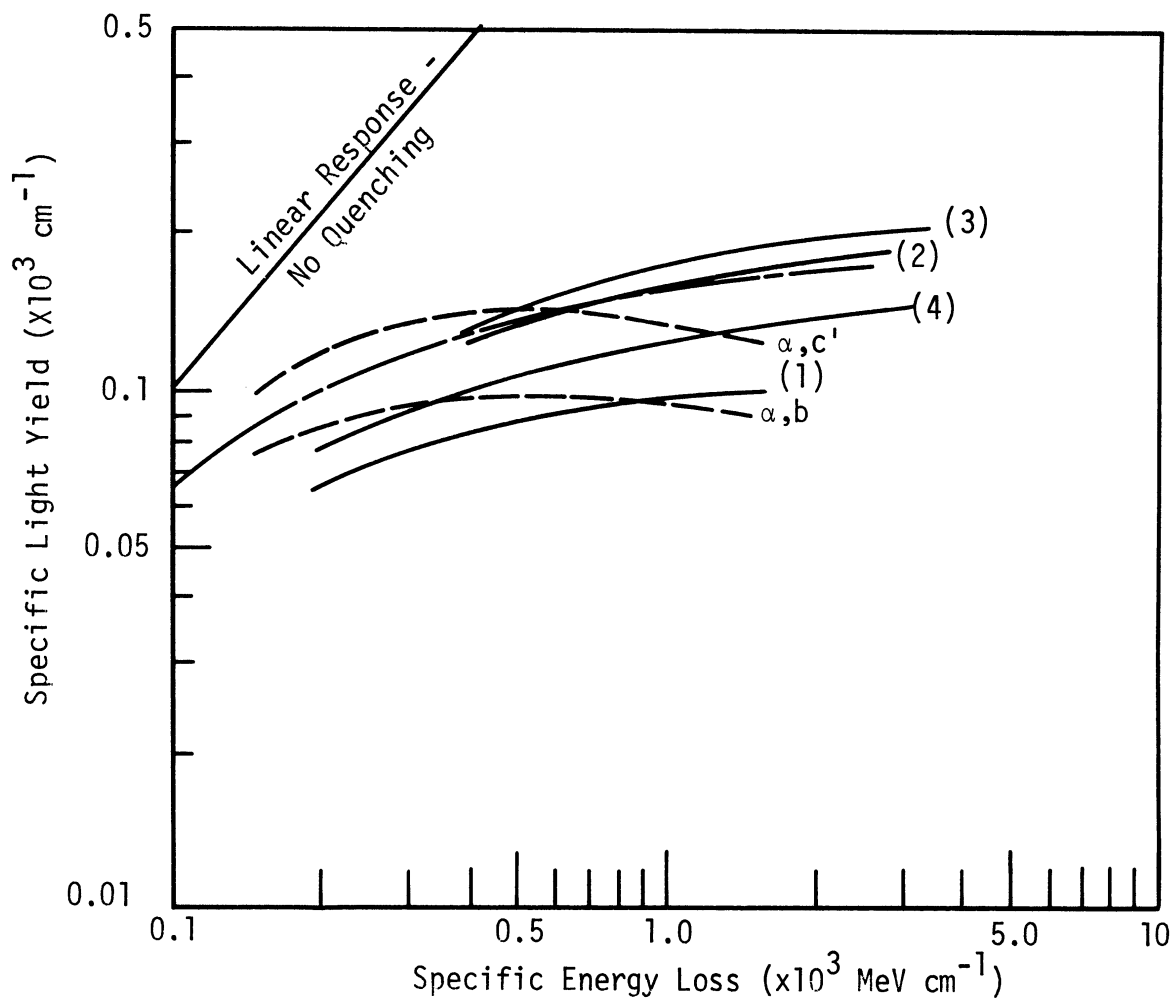
——— are curves generated from computer solutions to the diffusion-kinetics equation.

(1) B = 4x10^{-4},   E = 3.5x10^{-3} cm MeV^{-1} dE/dx
(2) B = 2x10^{-4},   E = 1.75x10^{-3} cm MeV^{-1} dE/dx
(3) B = 4x10^{-4},   E = 1.75x10^{-3} cm MeV^{-1} dE/dx
(4) B = 16x10^{-4},   E = 3.5x10^{-3} cm MeV^{-1} dE/dx

— · —is the curve generated by Birks' formula (KB = 5.28x10^{-3} cm MeV^{-1}).

— — — are curves fitting Schött's alpha particle results[5] (Curve labels are the same as in Figure 2.)

FIGURE 9

Scintillation response of anthracene crystals-II.

Here the term labels (1), (2), (3), and (4) correspond to the appropriate case numbers.

There are several interesting features about the curves in Figure 9. First, the differential response anisotropy ratio determined from response curves (2) or (3) relative to curve (1) is about the same as that determined experimentally in the same dE/dx range for alpha particles incident in directions parallel to the crystallographic c' and b axes. Therefore, a factor of two variation in D_s or FK_{ss} with direction appears adequate to explain the magnitude of the measured response anisotropy. A factor of two variation in R_o, curves (1) and (4), produces a much smaller effect. Next, it is noted that for certain values of the parameters B and E the absolute magnitude of dL/dx is close to the experimental curves. Also, the variation of dL/dx with dE/dx appears to agree with the general response curve of Birks. However, this type of variation is clearly different from that which Schött observed.

The plausibility of the model may be tested by examining the self-consistency of the values for the constants corresponding to the values of B and E which result in approximate agreement between theoretical and experimental response curves. If there is negligible radiation damage τ_s is about 10^{-8} seconds. Reliable values for D_s and w_s are 2×10^{-3} $cm^2 sec^{-1}$ and 44.7×10^{-6} MeV per singlet exciton respectively. Thus in case (1) where $B = 4 \times 10^{-4}$, R_o is uniquely determined and equals 12.6 Å. Similarly, $E/(dE/dx) = 3.5 \times 10^{-3}$ cm MeV^{-1} which requires that $FK_{ss} = 0.4 \times 10^{-8} cm^3 sec^{-1}$.

The value of R_o from above is surprisingly close to the estimated radius of a cluster, r_o. Since $1/2 \leq F_T \leq F \leq 1$, K_{ss} is very near the value deter-

mined experimentally.[34] Considering the accuracy with which τ_s, D_s and K_{ss} are known along with the estimate of w_s, it seems that the constants form a self-consistent set. It is noted that the theoretical results of this model represent only the prompt emission; whereas the experimental curves in Figure 4 include the delayed emission as well as the prompt. While the exact correction necessary in the experimental curves is not known, in general the prompt response would be a fraction of the total light yield shown which decreases slowly with increasing dE/dx. The minimum value of the fraction would not be less than 80% for the dE/dx range considered.[4] This correction would improve the agreement between the experimental and theoretical values of K_{ss} as deduced above.

The excessive quenching shown by the theoretical response curves at lower dE/dx values could easily be due to the violation of the cylindrical geometry assumption. Likewise, the possibly insufficient quenching at higher values of dE/dx could be corrected if R_o decreases with increasing dE/dx. Thus, it is concluded that the model considered here provides a reasonable description of the dynamics of the exciton system which explains both quenching and response anisotropy.

3.3.2.2. Approximate analytical solution

When the second order term in either Equations (3.15) or (3.16) is not the dominant loss term, a reasonably accurate approximate analytical solution can be obtained by the method of "forced diffusion." This method was first employed by Jaffé.[51] Essentially the method consists of first neglecting

the second order term in an equation such as (3.15) or (3.16). The resulting

equation is linear, and if the initial distribution is in the form of a

Gaussian and the medium is infinite, the solution has the form of a Gaussian

which spreads spatially and is exponentially damped with time. Finally, the

second order term is introduced as a perturbation which is only allowed to

provide further damping with time of the Gaussian solution.

Recently Blanc et al.[52] applied the technique to the scintillation re-

sponse problem. They found an expression for the magnitude and time behavior

of the prompt scintillation component by solving an equation equivalent to

Equation (3.15) using the forced diffusion technique. However, because of the

magnitude of the biexcitonic annihilation term required for adequate quenching

the approximate solution for this case is probably inaccurate.

Fortunately, the second order term is much smaller in the triplet exci-

ton problem. The description of the transient triplet population in the wake

of a heavy charged particle as given by a forced diffusion solution of Equation

(3.16) has been demonstrated to be appropriate in several cases.[53,54,55] Bi-

excitonic annihilation of triplet excitons resulting in the direct formation of

singlet excitons which promptly decay was assumed the origin of the delayed

emission. In particular, the solutions were deemed appropriate for a time

greater than 1 microsecond after the primary events; thus any questions about

electron-hole recombination and ionization quenching were avoided.

For the purpose of analyzing our experimental results it is desirable to

have a description of the triplet population during the evolution of the com-

plete scintillation process so as to include quenching and possible aniso-

tropic effects. Therefore, it is assumed that the forced diffusion solution

is valid at any time after the formation of the triplet population which is

presumed to occur in a short time compared to the time necessary for appreci-

able triplet diffusion ($\sim$ 40 nanoseconds).[53] A general expression for the

instantaneous specific light yield ($dL(T)/dx$) of the delayed component as

given by Voltz and Laustriat[54] is

$$\frac{dL(t)}{dx} \simeq \frac{\eta_s K_{tt} s}{2\pi R_o} \frac{(1/w_t)^2 (dE/dx)^2 \exp[-2t/\tau_t]}{\left\{1 + E \exp\left(\frac{t_a}{\tau_t}\right)\left[E_i\left(-\frac{t+t_a}{\tau_t}\right) - E_i\left(-\frac{t_a}{\tau_t}\right)\right]\right\}^2 \left(1 + \frac{t}{t_a}\right)} \quad (3.17)$$

where $(1/w_t)$ is the number of triplet excitons eventually formed in the low-

est excited level per MeV of energy loss,

$$E = K_{tt}(dE/dx)/8\pi D_t w_t \ ,$$

$$t_a = R_o^2/4D_t \ ,$$

$$E_i(-x) = -\int_x^\infty \frac{e^{-\alpha}}{\alpha} \, d\alpha$$

and the other constants are the same as defined previously. King and Voltz[53]

deduced that Equation (3.17) describes the published delayed emission decay

curves for undamaged anthracene crystals if values for E and t_a of 0.25 and

40 nanoseconds are used. If $dE/dx = 10^3$ MeV cm^{-1}, $w_t = w_s$, and the values of

K_{tt} and D_t are taken from Table 1, calculations show E to be equal to 0.22

which is surprisingly close to the value above. However, for t_a to be equal

to 40 nanoseconds, if D_t is taken from Table 1, R_o must be equal to 560 Å.

It is conceivable that the subexcitation electrons migrate a substantial distance from the clusters before being finally thermalized. Also, the holes are quite mobile and could diffuse outward from the initial distribution; however, a radial distribution of this magnitude initially upon recombination seems unreasonable.

For practical purposes, $t_a \ll \tau_t$. Likewise, considering the ambiguity of the initial conditions it is best to use Equation (3.17) to describe relative light yields with time or other parameters as variables. Therefore, a more usable form is

$$\frac{dL(t)}{dt} \propto \frac{(dE/dx)^2 \exp[-2t/\tau_t]}{\left\{1 + E\left[E_i\left(-\frac{t+t_a}{\tau_t}\right) - E_i\left(-\frac{t_a}{\tau_t}\right)\right]\right\}^2 \left(1 + \frac{t}{t_a}\right)} \tag{3.18}$$

Clearly, the directional anisotropy of the observed delayed emission could arise from a variation of D_t which would affect E and t_a in Equation (3.18). Similarly, radiation damage effects would decrease τ_t.

3.3.3. Linear Quenching Model

If biexcitonic annihilation in the wake of a heavy charged particle is less significant than was assumed in the previous model, it is possible that temporary quenchers such as dissociated molecules account for the observed quenching and response anisotropy. Presumably the quenching occurs during a time which is short compared to the natural lifetimes of the lowest exciton states; thus it is convenient to investigate both Equations (3.9) and (3.10) during two separate time intervals. The appropriate simplifications of sub-

section 3.3.1.1 and the assumption of cylindrical geometry are considered valid for both intervals.

3.3.3.1. Short time interval (10^{-13} sec $< t < 10^{-9}$ sec)

During this time period quenching by the transient quenching agents is assumed to dominate all other exciton removal processes. Both Equations (3.9) and (3.10) reduce to the form shown below for the singlet exciton concentration.

$$\frac{\partial n_s(r,t)}{\partial t} = D_s \frac{1}{r} \frac{\partial}{\partial r} \left(r \frac{\partial}{\partial r} \right) n_s(r,t) - K_{sq}^t(r,t) n_s(r,t) \qquad (3.19)$$

Here the time and spatial dependence of the transient quenching coefficient have been indicated. The quantitative estimates involved in the analysis of Equation (3.19) are significantly different in the case of singlet excitons from the case of triplet excitons; therefore, the discussion immediately following pertains only to singlet excitons. Relevant comments about the triplet exciton concentration are deferred to the end of the discussion.

Even though Equation (3.19) represents a considerable simplification of the original equation, further simplification is necessary before an analytic solution can be obtained. Initially the spatial distributions of the excitons and quenching agents are quite similar; however, during the time interval specified the exciton distribution spreads considerably while the quenching centers remain fixed. This evolution suggests that Equation (3.19) be solved separately for the fixed column defined by the quenchers and for the surrounding region which is free of quenchers.

A simple solution to the equation can be obtained with the assumptions:

(1)   A column of effective radius (R_e) is defined by the initial distributions of quenching centers and excitons $(r_o \leq R_o \leq R_e)$.

(2)   Once an exciton migrates out of the column $(r = R_e)$ it does not return. This corresponds to the condition that $n(r,t)$ vanishes at $r = R_e + \lambda$.

(3). The quenching centers are uniformly distributed within the column $(r \leq R_e)$. They are not destroyed upon quenching an exciton and persist until the excitons within the column have escaped or have been quenched.

(4)   Initially the radial exciton distribution can be represented by the zeroth order regular Bessel function of the first kind. The first zero of the Bessel function is required to occur when $r = R_e + \lambda$ so that assumption (2) above is fulfilled.

The solution to Equation (3.19) under these conditions is

$$n_s(r,t) = (\text{const.})(\exp[-(K_{sq}^t + \frac{2.405}{R_e+\lambda} D_s)t]) \; J_o(\frac{2.405}{R_e+\lambda} r), \quad r \leq R_e \quad (3.20)$$

where $J_o(\frac{2.405}{R_e+\lambda} r)$ is the zeroth order Bessel function of the first kind of

parameter $(2.405/(R_e+\lambda))$.

The singlet excitons which escape from the column are free to migrate

and decay naturally just as those formed by a fast electron. Therefore, the

prompt components of dL/dx for a heavy charged particle is proportional to

that fraction (f_e) of the initial exciton yield $((dE/dx)/w_s)$ which escapes

from the column. Since the quenching rate K_{sq}^t is necessarily large, 10^{-9} sec-

onds is essentially infinite when considering the decay of $n_s(r,t)$ within the

column. If f_e is the fraction of the exciton yield which is quenched, then

$f_e = (1+f_q/f_e)^{-1}$ since $f_e + f_q = 1$. Application of Fick's law at the surface

of the column $(r = R_e)$ results in

$$f_e = \left(\int_0^\infty dt \int_{\text{surface } r = R_e} (-D_s \nabla_r n(r,t)) dS \right) \left(\frac{1}{w_s} \frac{dE}{dx} \right)^{-1}$$

where dS is an element of area on the surface of the column, and ∇_r is the radial part of the gradient operator. Similarly

$$f_q = \left(\int_0^\infty dt \int_{\text{column } o \leq r \leq R_e} K_{sq}^t n(r,t) d^3r \right) \left(\frac{1}{w_s} \frac{dE}{dx} \right)^{-1}$$

where d^3r is a volume element within the column. By the use of Green's theorem and the explicit expression for $n_s(r,t)$

$$f_e = \left(\int_0^\infty dt \int_{\text{column } o \leq r \leq R_e} \left(\frac{2.405}{R + \lambda} \right)^2 D_s n(r,t) d^3r \right) \left(\frac{1}{w_s} \frac{dE}{dx} \right)^{-1}$$

Now

$$\frac{f_e}{f_q} = \frac{K_{sq}^t}{\left(\dfrac{2.405}{R + \lambda} \right)^2 D_s} \quad ,$$

and

$$\frac{dL}{dx} = \frac{dE/dx}{1 + \dfrac{K_{sq}^t}{\left(\dfrac{2.405}{R_e + \lambda} \right)^2 D_s}}$$

Where $(1/w_s)$ has been removed by normalization of the light yield to that of a 1 MeV electron. For both the band and hopping model expressions given in subsection 3.3.1 for K_{sq}^t it is noted that K_{sq}^t can be considered the product

of a constant (K) and the concentration of quenching centers N_q. Assuming

that w^t_{sq} is the energy expended per transient quenching center,

$$K^t_{sq} = K\left(\frac{1}{w^t_{sq}}\right)\left(\frac{dE}{dx}\right).$$

Now

$$\frac{dL}{dx} = \frac{dE/dx}{1 + \dfrac{K}{\left(w^t_{sq}\left(\dfrac{2.405}{R+\lambda}\right)^2 D_s\right)}\dfrac{dE}{dx}} \qquad (3.21)$$

where $K = \sigma_{sq} V$ for the band model, and $K = \epsilon_q N_h/N_m$ for the hopping model.

This expression has the same form as Birks' semiempirical formula[4] which has

been found to describe most experimental results quite well. Kallmann and

Brucker[56] as well as Birks himself[4] have made qualitative comments about the

origin of the quenching term (KBdE/dx) in Birks' formula. However, to the

knowledge of this author Equation (3.21) above is the first form of the

equation in which all terms are expressed as functions of clearly defined

parameters.

The conditions which are necessary for simple diffusion theory to be

valid must be added to the previous list of assumptions. In terms of exciton

migration they are:

(5) The probability of exciton scattering per unit time (K_s) must be
significantly greater than the probability of quenching per unit
time. Subsequently the requirement $K^t_{sq}/K_s \leq 0.2$ will be invoked.

(6) Diffusion theory is not accurate within several scattering mean
free paths of a boundary in the media.

(7) Exciton scattering is assumed isotropic.

However, the assumption of isotropic scattering must be violated since of

all the factors appearing in Equation (3.21) D_s is the only one that could

vary enough with direction to produce the observed response anisotropy.

Neglecting the ~ 15% difference between prompt and total light yield, it

can be shown that Equation (3.21) approximately describes the results of

Tsukada et al.[6] for protons incident in the c' and b crystallographic direc-

tions if the coefficient of dE/dx in second term in the denominator equals

4×10^{-3} and 7×10^{-3} cm MeV^{-1} respectively. This relation is equivalent to

the following requirement.

$$4 \times 10^{-3} \text{ cm MeV}^{-1} \frac{dE}{dx} \leq \frac{K^t_{sq}}{\left(\frac{2.405}{R_e}+\lambda\right)^2 D_s} \leq 7 \times 10^{-3} \text{ cm MeV}^{-1}\left(\frac{dE}{dx}\right) \qquad (3.22)$$

Another constraint arises from the assumption that quenching within the

column is complete well before fluorescent decay becomes significant. This

requirement is met if

$$K^t_{sq} \geq 10^{10} \text{ sec}^{-1} \quad . \qquad (3.23)$$

Elimination of K^t_{sq} between requirements (5) and (3.22) results in

$$\frac{dE}{dx} \leq \left(0.2K_s \Big/ \left(\frac{2.405}{R_e}+\lambda\right)^2 D_s\right)(4 \times 10^{-3})^{-1} \quad . \qquad (3.24)$$

Similarly, combination of requirements (3.22) and (3.23) leads to

(7) Exciton scattering is assumed isotropic.

However, the assumption of isotropic scattering must be violated since of all the factors appearing in Equation (3.21) D_s is the only one that could vary enough with direction to produce the observed response anisotropy. Neglecting the ~ 15% difference between prompt and total light yield, it can be shown that Equation (3.21) approximately describes the results of Tsukada et al.[6] for protons incident in the c' and b crystallographic directions if the coefficient of dE/dx in second term in the denominator equals 4×10^{-3} and 7×10^{-3} cm MeV^{-1} respectively. This relation is equivalent to the following requirement.

$$4 \times 10^{-3} \text{ cm MeV}^{-1} \frac{dE}{dx} \leq \frac{K_{sq}^{t}}{\left(\frac{2.405}{R_e + \lambda}\right)^2 D_s} \leq 7 \times 10^{-3} \text{ cm MeV}^{-1}\left(\frac{dE}{dx}\right) \quad (3.22)$$

Another constraint arises from the assumption that quenching within the column is complete well before fluorescent decay becomes significant. This requirement is met if

$$K_{sq}^{t} \geq 10^{10} \text{ sec}^{-1} \quad . \quad (3.23)$$

Elimination of K_{sq}^{t} between requirements (5) and (3.22) results in

$$\frac{dE}{dx} \leq \left(0.2K_s \middle/ \left(\frac{2.405}{R_e + \lambda}\right)^2 D_s\right)(4 \times 10^{-3})^{-1} \quad . \quad (3.24)$$

Similarly, combination of requirements (3.22) and (3.23) leads to

$$10^{10}/(7 \times 10^{-3})\left(\frac{2.405}{R_e + \lambda}\right)^2 D_s \leq \frac{dE}{dx} \quad . \tag{3.25}$$

Unless the radial extent of the original column in the wake of a heavy charged particle has been badly underestimated, assumption (6) above implies that the exciton scattering mean free path must be of the order of the intermolecular spacing (~ 5 Å) for the method of this section to be applicable. Assuming that the scattering mean free path is approximately 5 Å, the band model of exciton migration should become equivalent to the hopping model.[36] Therefore, further analysis of the inequalities requires the introduction of only the hopping model expressions for D_s, K_s and K_{sq}^t. Combination of inequalities (3.24) and (3.25) and use of the appropriate expressions results in

$$\frac{1.4 \times 10^{12}}{N_h}\left(\frac{R_e + \lambda}{d}\right)^2 \leq \frac{dE}{dx} \leq 50 \left(\frac{R_e + \lambda}{d}\right)^2 \tag{3.26}$$

where d is the root mean square hopping distance which is essentially the scattering mean free path. The number of exciton hops per second N_h is equivalent to the number of scattering events per second. Results of two independent measurements are compatible with a value for N_h of $4 \times 10^{+12}$ sec^{-1}.[4,57] Considering assumption (6) and the fact that λ is probably negligible compared to R_e, a reasonable value for $(R_e + \lambda)/d$ is 5. Substitution of these values into relation (3.26) results in the following inequality. 9 MeV cm$^{-1} \leq dE/dx \leq 1250$ MeV cm^{-1}. Since as shown in subsection 3.3.1.2 the assumption of cylindrical geometry is not valid for dE/dx values less

than about 400 MeV cm^{-1}, it is clear that the lower limit on dE/dx is greater

than the inequality above shows. Nevertheless, this range of dE/dx values

corresponds to protons with energies of $\sim$ 1 MeV or less and alpha particles

in the energy range of $\sim$ 4 to $\sim$ 25 MeV.

The constraints applied above can also be used to determine the magni-

tude of the number of quenching centers necessary to provide an adequate

amount of quenching. From requirement (3.23) and the hopping model expres-

sion for K^t_{sq} it is noted that

$$10^{10} \leq \frac{\epsilon_q N_h \left(\dfrac{1}{w^t_{sq}}\right) \dfrac{dE}{dx}}{N_m \pi R^2_e} \quad . \tag{3.27}$$

If ϵ_q = 1, dE/dx = 400 MeV cm^{-1}, λ is negligible and R_e = 25 Å, and N_h = 10^{12}

sec^{-1} it is found that $1/w^t_{sq}$ = 2.06 x 10^4 quenchers per MeV. Similarly, from

requirement (5)

$$\frac{\epsilon_q N_h \left(\dfrac{1}{w^t_{sq}}\right) \dfrac{dE}{dx}}{N_m \pi R^2_e N_h} \leq 0.2 \quad .$$

Considering that dE/dx = 1250 MeV cm^{-1} and the same values for the other con-

stants as before, it is found that $1/w^t_{sq} \leq$ 1.32 x 10^5 quenchers per MeV. It

is noted that the order of magnitude suggested for $(1/w^t_{sq})$ by the calculations

above is the same as that deduced for the upper limit of σ-electron excita-

tions per MeV of energy loss.

Allowing for the approximate nature of the assumed solution of Equation

(3.19) and the numerical estimates employed, it appears that this model gives a plausible description of ionization quenching and response anisotropy for a limited range of dE/dx values.

The diffusion kinetics of the triplet population can be treated in a manner analogous to that exploited above, and if assumptions (1) through (4) are met, an expression identical in form to Equation (3.21) is obtained. However, in attempting to relate such a result to the delayed emission observed, it is necessary to introduce the result into the biexcitonic model discussed in subsection 3.3.2. At least it is necessary if the ultimate role of triplet-triplet exciton annihilation in the delayed component is accepted. This additional complication seems unwarranted for our purposes.

3.3.3.2. Long time interval (10^{-9} sec $< t < \infty$)

It was assumed in subsection 3.3.3 that the transient quenchers become ineffective before 10^{-9} seconds has elapsed after the primary events. Thus, after 10^{-9} seconds, the remaining singlet exciton population is free to migrate and decay by the natural processes of internal conversion and fluorescence assuming that accumulated radiation damage has not resulted in an appreciable number of lurking permanent quenchers. In any case, the prompt decay and light emission will follow a single exponential as observed experimentally. We will assume that the delayed emission is adequately described in the discussion of subsection 3.3.2.

CHAPTER 4

THE SCINTILLATION RESPONSE TO PROTONS AND CARBON IONS

4.1. INTRODUCTION

In this chapter an investigation of the directional scintillation response
of large anthracene crystals to energetic heavy charged particles is elaborated.
The experimental method was based on the internal generation of recoil protons
and carbon ions with energies in the MeV range by the scattering of fast mono-
energetic neutrons from the nuclei within the crystal. A two detector fast-
slow coincidence system with variable detector geometry and a variety of dis-
crimination capabilities was employed to select scintillations for analysis
arising from monoenergetic protons or carbon ions recoiling in a particular
direction relative to the crystal axes. The energy and direction of the se-
lected recoils were continuously variable within certain ranges. In addition,
this method of excitation avoided surface effects which can arise when using
externally incident particles having a short range in anthracene.

The neutron source and detector geometry is illustrated in Figure 10. A
photograph of the actual system is shown in Figure 11. Fast neutrons with
nearly the same energy were produced at the point labeled "source." Detectors
I and II consisted of scintillators I and II directly coupled to photomultiplier
(PM) tubes with scintillator I being the anthracene crystal under investigation.
The centroids of the neutron source and the scintillators defined a horizontal
scattering plane.

A small fraction of the source neutrons were scattered from scintillator
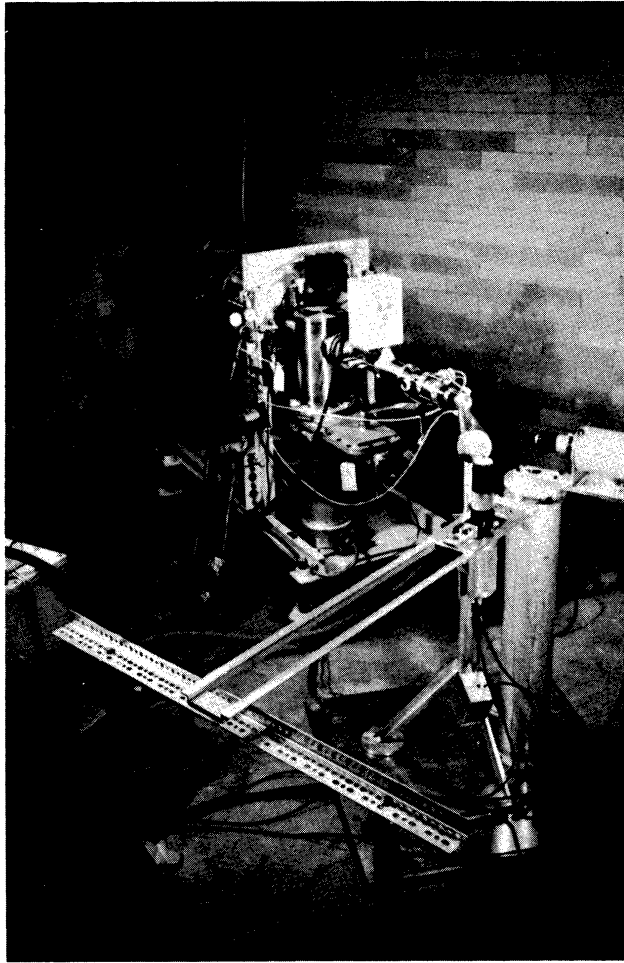
FIGURE 11

Pictorial view of experimental apparatus.

I into the solid angle subtended by scintillator II and subsequently interacted in the second detector. For these events, when the corresponding signal from detector I was delayed by approximately the flight time of the neutrons from scintillator I to scintillator II, the signals from the two detectors were in coincidence.

A schematic of the electronic system used to select and analyze linear signals from either detector is shown in Figure 12. Before a linear signal corresponding to a scintillation event was analyzed, it was required to pass a fast linear gate and the slow linear gate of the multichannel analyzer (MCA). In the coincidence mode of operation the opening of the fast gate required the proper time relationship between the timing pulses from detectors I and II. The fast signal from detector II was also subjected to amplitude requirements. By use of the pulse shape discrimination (PSD) circuit, the gate of the MCA could be restricted to open only when the signal from detector II corresponded to the detection of a neutron.

In the ideal case, the energy and direction of the selected recoiling nuclei in scintillator I were uniquely defined by the energy of the incident neutrons, type of scattering, and the scattering angle (α). However, the finite dimensions of the neutron source and the scintillators introduced a spread in both the energy and direction of the recoils. Also, there was a spread in the source neutron energies. Other deviations from the ideal case arose from chance coincidences and inelastic scattering events. Therefore, the limited resolution of the method prevented the observation of any effects well resolved in direction such as channeling in the crystal.

Linear Signal

Linear Signal

Detector I

Detector II

Fast
Signal

Space
Charge
Limited
Signal
(PSD)

One or Two
Linear Amplifiers
EG&G AN101/N

Discriminator-Trigger
EG&G TD101/N

Variable
delay

Discriminator-Trigger I
1/2 EG&G TR104S/N

Scaler-Ortec
Model 430

Emitter
Follower

Variable
Attenuator

Scaler-Ortec
Model 430

Discriminator-Trigger
Tektronix 531A CRO

Fast Linear Amplifier
EG&G-AN101/N

Fast Coincidence Circuit
EG&G C102B/N

Fast Linear Gate
EG&G LG101/N

Limiter
EG&G L102/N

Gate Generator
1/2 EG&G TR104S/N

Gate Generator
Tektronix Model
114 Pulser

2 µsec

Stretcher Amplifier
EG&G AN105/N

Coincidence
Input

Gate
Input

ND-120
512 Channel
MCA

Delay line

Polarity and approximate pulse shape
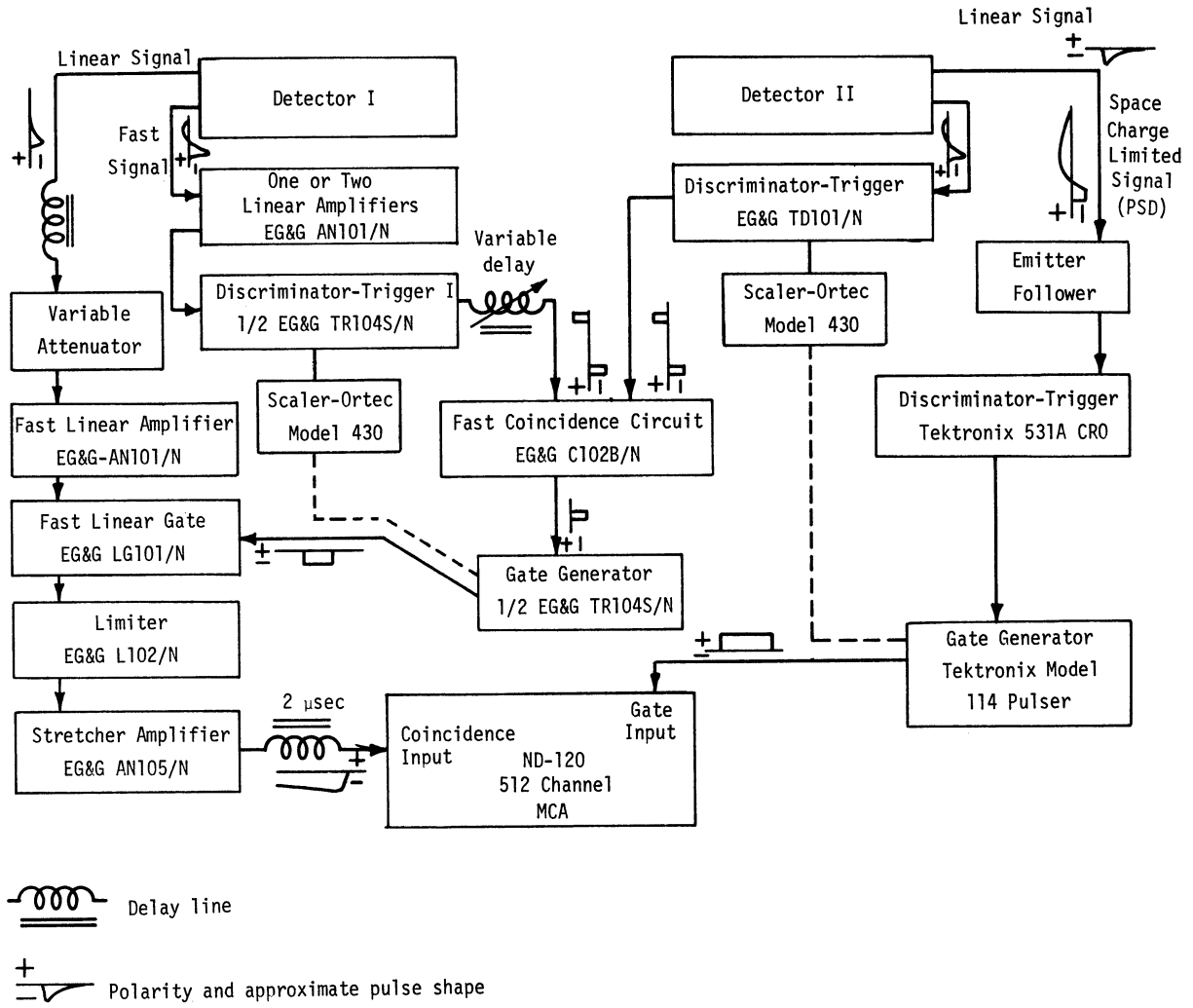
FIGURE 12

Electronic system-I.

4.2. EXPERIMENTAL ARRANGEMENT

4.2.1. Scattering System

The nuclear reactions, $_1H^2(H^2,n)_2 He^3$ and $_1H^3(H^2,n)_2He^4$ which served as the fast neutron sources were produced in the target assembly of the Texas Nuclear Corporation neutron generator shown in Figure 11. The generator is of the Cockroft-Walton design, and was operated at a deuteron accelerating potential of 140 kilovolts. Effectively "thick" deuterium and tritium impregnated titanium targets were utilized. The average energies of the neutrons which were emitted in the forward direction were 2.8 and 14.6 MeV respectively.

The mechanical support arrangement used to align and adjust the scattering geometry is evident in Figure 11. The cylindrical axis of the anthracene crystal was oriented to coincide with the horizontal scattering plane. The cylindrical axis of detector II was vertical. Freedom of motion was provided as follows:

(1) Rotation of the anthracene crystal about its horizontal cylindrical axis.

(2) Rotation of the anthracene crystal about a vertical axis through its center.

(3) Movement of detector II about the anthracene crystal in the horizontal scattering plane.

A cathetometer was used for the initial alignment of the source and detectors and also for periodic checks thereafter.

Calculations indicated that the brass shadow shield reduced the number of unscattered source neutrons which reached detector II by a factor of $\sim 10^2$.

Structural components were made principally of aluminum and as light in weight

as possible in order to reduce the scattering probability for neutrons in the vicinity of the detectors.

4.2.2. Detection and Analysis Systems

An RCA 8575 (bialkali photocathode) PM tube was employed in detector I. This tube was selected because of a favorable dark noise spectrum, fast response, and a high quantum efficiency in the wavelength range of the fluorescence of anthracene (4000 - 5000 Å). A fast timing signal was taken from dynode 12 of the tube, and a linear signal from the anode. The anthracene crystal of interest constituted the remainder of detector I. A 1" high by 1" diameter cylindrical crystal was used in the measurements reported in this chapter. It was convenient to attach one of the polished ab cleavage surfaces of the crystal to the flat face of the PM tube; optical coupling was provided by Dow Corning 20-057 compound. The remaining surfaces of the crystal were packed with 1/16" of MgO which served as a reflector and then covered with a 1/32" thick aluminum cap for mechanical support.

Detector II consisted of a 2" high by 2" diameter encapsulated NE 213 liquid scintillator coupled to an RCA 6810A (S-11 response) PM tube. The NE 213 liquid scintillator had the desirable features of high scintillation efficiency, fast light emission, and excellent pulse shape discrimination (PSD) characteristics. When PSD was required for rejection of gamma ray scintillations, the standard heavy duty voltage divider was replaced by one of Owen's design.[58] A linear signal was taken from dynode 12 and a fast timing signal from dynode 13 or the anode of the PM tube depending on whether or not PSD was employed.

As illustrated in Figure 12, timing pulses from detectors I and II were introduced into discriminator-trigger circuits I and II. These circuits provided low level and, in the case of trigger II, simultaneous high level leading edge triggering. Low level triggering provided accurate timing information while the high level allowed a veto of the timing signal if pulse amplitude requirements were not met. If, after appropriate delays, the fast timing signals arrived in coincidence within the resolution time of the coincidence circuit, a gate generator was actuated which opened the fast linear gate. Distortion of the linear signals resulting from pulse pile-up was minimized by the fast linear gate, limiter, and stretcher amplifer sequence since the majority of the pulses were rejected before significant integration. A frequency-compensated variable attenuator was inserted preceeding the fast linear amplifier to make the amplitudes of the pulses from detector I or II compatible with the requirements of subsequent components.

The PSD circuit, amplitude discriminator, gate generator, and the internal gate of the multichannel analyzer comprised the "slow" portion of the coincidence system. Pulses from the PSD circuit were subjected to amplitude discrimination by the input trigger level of a cathode ray oscilloscope (CRO). Upon triggering, the subsequent "gate pulse out" signal from the CRO actuated a pulser which served as the gate generator for the MCA gate.

4.3. EXPERIMENTAL TECHNIQUES

4.3.1. Practical Considerations

4.3.1.1. Scattering relations

Figure 13 illustrates the relationship between an ion recoil direction ($\hat{\beta}$) and the crystal axes (a,b,c, and c'). Angles θ and ϕ are polar coordinates with the polar angle θ measured from the crystal (cylindrical) axis c'. The azimuthal angle ϕ is measured in the ab plane counterclockwise from the a axis.

Energy and direction calculations were based on the following simple relations in the laboratory system of coordinates.

$$E_\beta = \frac{4E_o M}{(M+1)^2} \cos^2\beta \tag{4.1}$$

$$ME_\beta \sin^2\beta = E_\alpha \sin^2\alpha \tag{4.2}$$

$$\sqrt{E_\alpha} = \frac{\sqrt{E_o}}{(M+1)} (\cos\alpha)(1 \pm \{1 + \frac{1+M}{\cos^2\alpha}(M-1)\}^{1/2}) \tag{4.3}$$

where: E_o = energy of an incident neutron.

E_α = energy of the neutron after scattering.

α = angle through which the neutron is scattered.

E_β = energy of the recoil ion.

β = angle between the ion recoil direction and the incident direction of the source neutron.

M = mass of the recoil ion relative to that of the proton.

$\alpha+\beta = \pi/2$ (for recoil protons).
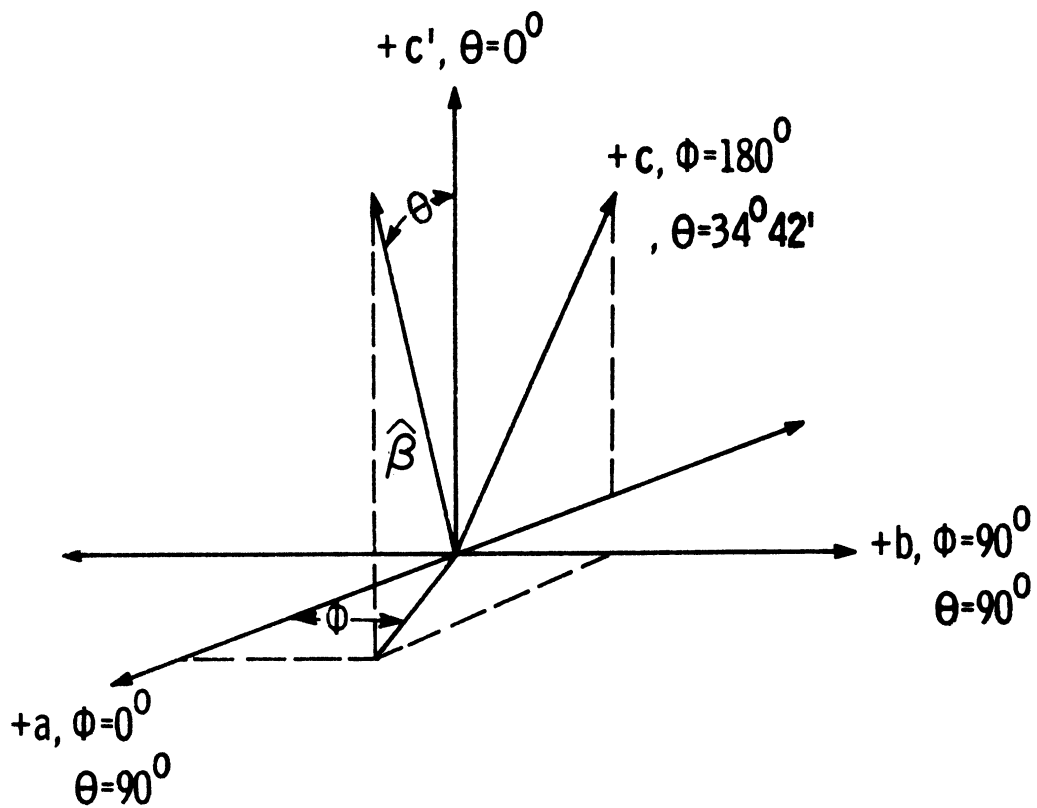
Crystallographic axes are a, b, c and c'. The ion recoil direction is $\hat{\beta}$.

FIGURE 13

Relationship between ion recoil direction and crystallographic axes,

4.3.1.2. Experimental limitations

Experimental conditions imposed stringent limitations on the usefulness

of the recoil ion excitation technique. The minimum practical recoil energy

was dictated by the geometry of the system which introduced a spread in recoil

energies (ΔE) and directions ($\Delta \beta$). These variations were directly related to

a spread in neutron scattering angles ($\Delta \alpha$) which resulted from the finite di-

mensions of the target and scintillators I and II. An indication of the energy

spread ΔE is given by the energy resolution ($R_E(\alpha)$).*

In the case of recoil protons an explicit expression for $R_E(\alpha)$ obtained

from Equation (4.1) is $R_E(\alpha) = 2(\text{ctn } \alpha)\Delta \alpha$. From this expression it is clear

that the resolution increases rapidly with a decrease in α when α is small.

To find the energy resolution for the carbon ion recoils, it was nec-

essary to solve Equations (4.1), (4.2), and (4.3) for each particular set of

scattering conditions. Since the maximum carbon recoil energy was less than

1 MeV for 2.8 MeV source neutrons, carbon recoil scintillations were analyzed

only for 14.6 MeV source neutrons.

The angular spread decreased when the source to detector I and the inter-

detector spacing was increased; hence, the energy resolution improved. How-

ever, these distances were ultimately limited by the interaction rates in de-

tectors I and II. The optimum detector spacing based on reasonable data ac-

quisition times and an acceptable angular spread was determined empirically in

preliminary experiments using recoil protons. It was noted that a significant

---

*Defined as the ratio of ΔE to the recoil energy for a particular neutron scat-
tering angle α.

increase in the spacing beyond that selected as optimum resulted in a negligible change in the measured anisotropy. The directional response results presented in this chapter were obtained with a source to detector I distance of 50 cm. Interdetector spacings of 70 cm and 30 cm were used for proton and carbon ion measurements respectively. The smaller separation in the case if recoil carbon ions was possible because of the neutron scattering dynamics.

The minimum practical neutron scattering angle for recoil proton measurements was 35° which resulted in 0.92 MeV protons for 2.8 MeV source neutrons and 4.8 MeV protons for 14.6 MeV source neutrons. Similarly, the minimum scattering angle used in the recoil carbon ion measurements was 83° which resulted in 2 MeV carbon ions. Approximate calculations for these cases indicate an energy resolution of 33% for recoil protons and 27% for recoil carbon ions. The corresponding angular spreads are 6° and 7.5°. The pulse height resolutions* of the peaks in the measured spectra corresponding to .92 MeV and 4.8 MeV recoil protons and 2 MeV recoil carbon ions were approximately 43%, 35% and 47% respectively. However, it is noted that the measured pulse height resolutions were increased by the statistical effects of scintillation light emission, detection, and subsequent electronic amplification and analysis. Also the peaks were broadened by any nonlinearity in the energy response of the scintillator.

The maximum scattering angle was also restricted. Whereas the energy resolution was greatly improved, the differential elastic scattering cross sections of the hydrogen and carbon nuclei decreased for large scattering

---

*Defined as the full width of the pulse height peak at half the maximum value (FWHM) divided by the mean pulse height of the peak.

angles. The resultant decrease in the intensity of the scattered neutrons was

accompanied by a decrease in the detection efficiency of detector II. Since

the scattered neutrons were less energetic at large scattering angles, fewer

of the corresponding pulses in detector II were above the discrimination thresh-

old of trigger II. Primarily because of these effects, the maximum practical

recoil energy in scintillator I was 1.88 MeV (α=55°) for protons when 2.8 MeV

source neutrons were used and 3.5 MeV (α=128°) for carbon ions with 14.6 MeV

source neutrons. The upper limit for recoil protons with 14.6 MeV source neu-

trons was not determined.

4.3.1.3. Empirical investigation of perturbations

Approximate calculations indicate that in the case of 2.8 MeV source neu-

trons (the most extreme case) approximately half the neutrons which reached

scintillator II after scattering in scintillator I had been scattered twice in

scintillator I with at least one of the two events resulting in a recoil pro-

ton. The effects of multiple scattering were examined in a preliminary exper-

iment in which the responses of two 1/2" high by 1/2" diameter cylindrical

anthracene crystals were scanned using 2.8 MeV source neutrons and the method

discussed in this chapter. The probability of multiple scattering was appre-

ciably less in the small crystals than in the larger crystal used in the final

measurements. Therefore, any significant effects of multiple scattering should

have been apparent when comparing the scintillation pulse height spectra for

similar proton recoils in the crystals. No noticeable difference in the rel-

evant peaks in the spectra was observed. It was concluded that the scintilla-

tion pulses produced in scintillator I by multiple scattering must have had a broad slowly varying spectrum in the range of the peak corresponding to single scattering events.

To demonstrate that the mechanical system was not contributing to the measured anisotropy, the large anthracene crystal was replaced after a series of proton recoil response scans by a cylinder of Pilot B plastic scintillator of the same size. The results of a response scan identical to one made with the anthracene crystal showed no anisotropy to within ± 1.5%, about the same as the uncertainty of all the scans.

4.3.2. Timing and Discrimination

The coincident events of interest were a small fraction ($\sim$10^{-4}) of the total number of scintillations occurring in either scintillator I or II. A list of the interactions in scintillator I of significance in the experiment is shown in Table 2. A proper balance of the source intensity, hence the count rate in each detector, and the time resolution of the fast coincidence system allowed the rejection of most of the uncorrelated events in both scintillators. However, as can be seen in Table 2 additional selectivity was required to eliminate the correlated but undesired events. The pulse height and pulse shape discrimination associated with detector II and time of flight discrimination of the fast coincidence system provided the required selectivity. It is convenient to discuss the features of the fast coincidence timing and the discrimination requirements arising with the two different source neutron energies separately.

TABLE 2

SIGNIFICANT INTERACTIONS IN SCINTILLATOR I

Radiation	Interaction in Scint. I	Consequences
2.8 MeV Source Neutrons	Elastic Scattering	(1) High rate of uncorrelated scintillations in scintillator I
		(2) Occasional true coincidence event of interest
Capture Gamma Rays	Compton Scattering	(1) High rate of uncorrelated scintillations in scintillator I
		(2) Occasional correlated Compton events in both scintillators
Scattered Source Neutrons	Elastic Scattering	(1) High rate of uncorrelated scintillations in scintillator I
		(2) Occasional production of a true coincidence event

(In Addition to the above the following events occur with
14.6 MeV source neutrons.)

14.6 MeV Source Neutrons	Inelastic Scattering $C^{12}(n,n'\gamma)C^{12}$	(1) ~6.8-9.55 MeV scattered neutrons produce occasional true coincidence events
		(2) 4.33 MeV gamma rays produce occasional correlated events
Inelastic Scattering Gamma Rays	Compton Scattering	(1) High rate of uncorrelated scintillations in scintillator I
		(2) Occasionally correlated Compton events in both scintillators

4.3.2.1. Fast timing

Several factors influenced the timing uncertainty of the fast coincidence timing system. One was the variation in the time of flight of neutrons which were scattered from scintillator I to scintillator II resulting from the spread in neutron energies and the difference in flight paths because of the finite size of the detectors. Another factor was the "slewing" of the timing pulse from the fast trigger circuits resulting from the shape and amplitude nonuniformities of the fast timing pulses from the detectors. In the most extreme case (recoil carbon ions) the timing uncertainty was measured using a time to amplitude converter. The resolution* of the true coincidence peak in the resultant pulse height spectrum or "coincidence curve"** was 4.55 nanoseconds. During the response measurements, the coincidence system was operated with relatively large timing resolutions*** of 30 and 40 nanoseconds for recoil proton and carbon ion cases respectively so that a minimum number of the desired true coincidences would be missed. The optimum delay of the timing pulse from trigger I for a coincidence with a corresponding true coincidence timing pulse from trigger II was obtained from a coincidence curve for the system. A new curve was obtained experimentally when any significant changes were made in α, β, D2, trigger levels, or PM tube gain.

---

*Full width at half the maximum count rate.

**Plot of counts per unit time versus delay between the timing signals from triggers I and II.

***Time within which two timing signals must reach the coincidence circuit in order for a coincidence logic signal to be generated.

4.3.2.2. D - D Source neutrons

In recoil proton measurements with 2.8 MeV source neutrons the relatively low energy of the scattered neutrons made the low level detection efficiency of detector II critical. The detection efficiency of detector II increased rapidly with decreasing neutron energy in the zero to several MeV range. This variation in efficiency enhanced the coincidence probability for the larger recoil proton energies in scintillator I (lower energy scattered neutrons) relative to the lower recoil energies. Judicious adjustment of the high level amplitude discriminator of trigger II was required to offset this effect and thereby to preserve the symmetry of the recorded pulse height spectra.

PSD could not be employed to reject gamma rays because the system had a negligible detection efficiency for low energy neutrons. However, the flight time of the neutrons scattered from scintillator I to scintillator II was relatively long ($\geq$ 37 nanoseconds) compared to that of gamma rays (2.33 nanoseconds). Therefore, the fast coincidence system with a time resolution of about 30 nanoseconds effectively eliminated by time of flight discrimination any coincidence events resulting from gamma ray scattering from detector I to detector II.

4.3.2.3. D - T Source neutrons

The discrimination requirements were most demanding during recoil carbon ion measurements. Inelastic scattering of the 14.6 MeV neutrons from the carbon nuclei in the anthracene crystal produced undesired but true coincidence events. The energies of the inelastically scattered neutrons reaching detector

II varied between ~8.5 and 7.3 MeV for the scattering angles employed. Amplitude discrimination eliminated such coincidences, but only with a large loss in detection efficiency for the elastically scattered neutrons. A more severe problem was the true coincidences arising from the associated 4.33 MeV deexcitation gamma rays. The directional emission probability and the pulse height spectrum in scintillator II was similar to that of the neutrons elastically scattered from the carbon nuclei. The PSD system provided rejection of the 4.43 MeV and lower energy gamma rays. It was operated at a bias level such that neutrons which produced a scintillation pulse smaller than a 0.35 to 0.4 MeV electron were rejected. This bias level provided a high gamma ray rejection ratio* without an excessive loss in detection efficiency for neutrons with energies greater than a few MeV.

The rejection ratio was determined in direct measurements to be 650 to 1 for the 2.5 MeV and lower energy gamma rays emitted by Th-232 daughter products. The rejection ratio for 4.43 MeV gamma rays was demonstrated to be adequate in an experiment with the 4.43 MeV gamma rays emitted by a Pu-Be neutron source.** The gamma rays emitted by the neutron source arise from the same isomeric state in carbon-12 as that excited by inelastic neutron scattering.

4.3.2.4. Selected spectra

During the preliminary 14.6 MeV source neutron measurements, the linear pulses from detector II were analyzed with the trigger levels, timing, and

---

*The number of gamma rays rejected per gamma ray counted.

**A radioisotope neutron source utilizing the alpha particles emitted by Pu to produce the nuclear reaction $Be^9(\alpha, n\gamma)C^{12}$.

coincidence gating arrangement identical to that used for analysis of the re-coil pulses in detector I. The "companion spectra" so obtained were consistent with the scintillation pulse height spectra expected for neutrons scattering in scintillator II after being elastically scattered from carbon or hydrogen nuclei in scintillator I. Two companion spectra are shown in Figures 14 and 15 for neutron scattering from respectively carbon and hydrogen nuclei. Also shown in the figures are the "singles" spectra obtained with the shadow shield in place and the PSD system in operation. In the carbon recoil case the singles spectra with the shield removed and the PSD system inoperative is included to illustrate the effect of the shield in reducing the count rate in detector II. In one case the minimum pulse height analyzed was determined by the high level of discriminator-trigger II. In the other case the minimum pulse height was determined by the bias level of the trigger employed in the PSD system.

4.3.3. Measurements

All anthracene crystals used in this investigation were grown by the Harshaw Chemical Company. The large 1" high by 1" diameter cylindrical crystal to which the results presented in the subsection 4.4 pertain was selected because of maximum optical clarity and freedom from internal cracks. The orientation of the crystal axes was determined by the "precession" method of x-ray diffraction. The results were confirmed by noting the effects of the optical birefringence which arises because of the monoclinic structure of the crystal.

A scan of the scintillation response was effected as follows. First, the ion recoil energy and recoil direction $\hat{\beta}$ were fixed by the choice of the source
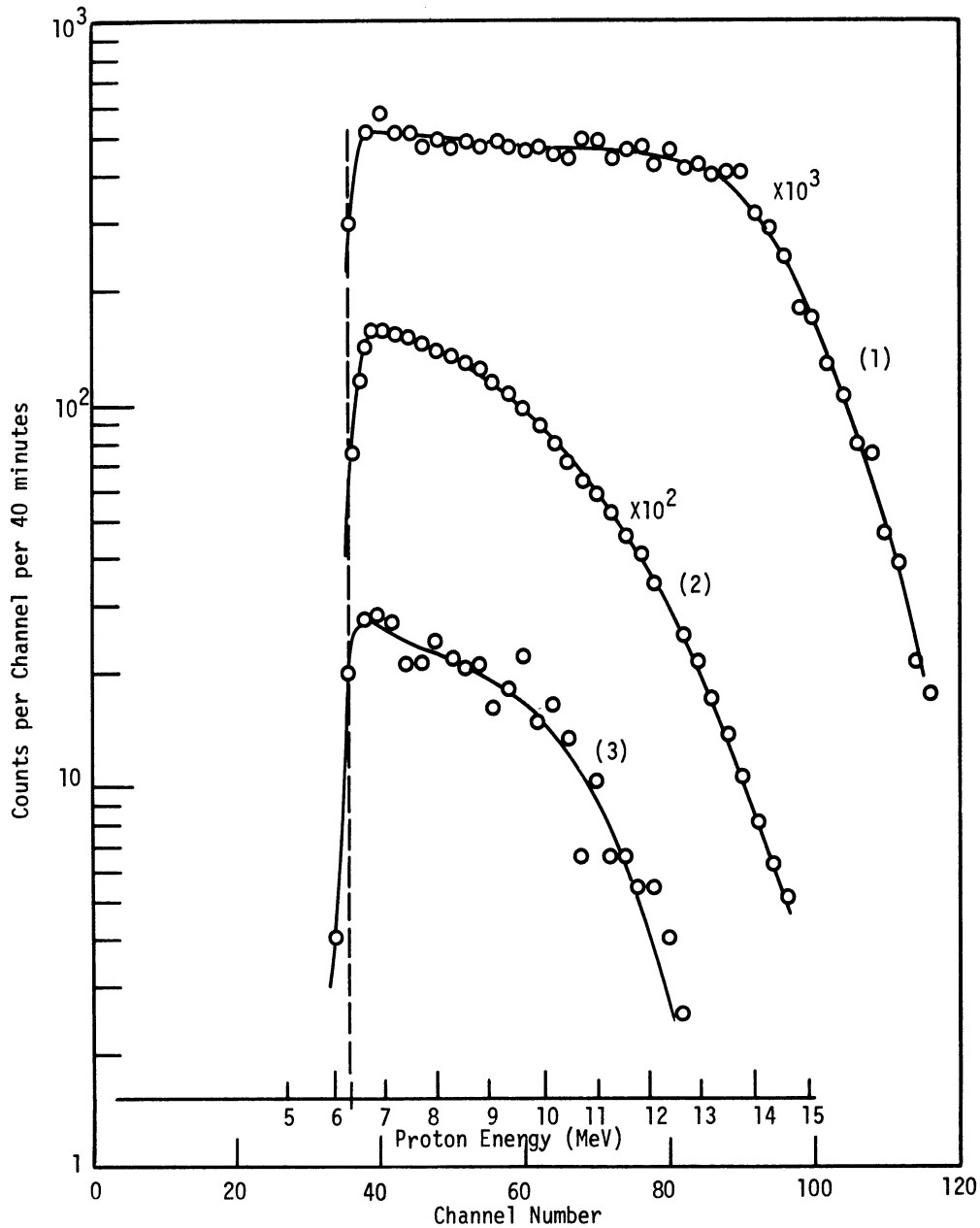
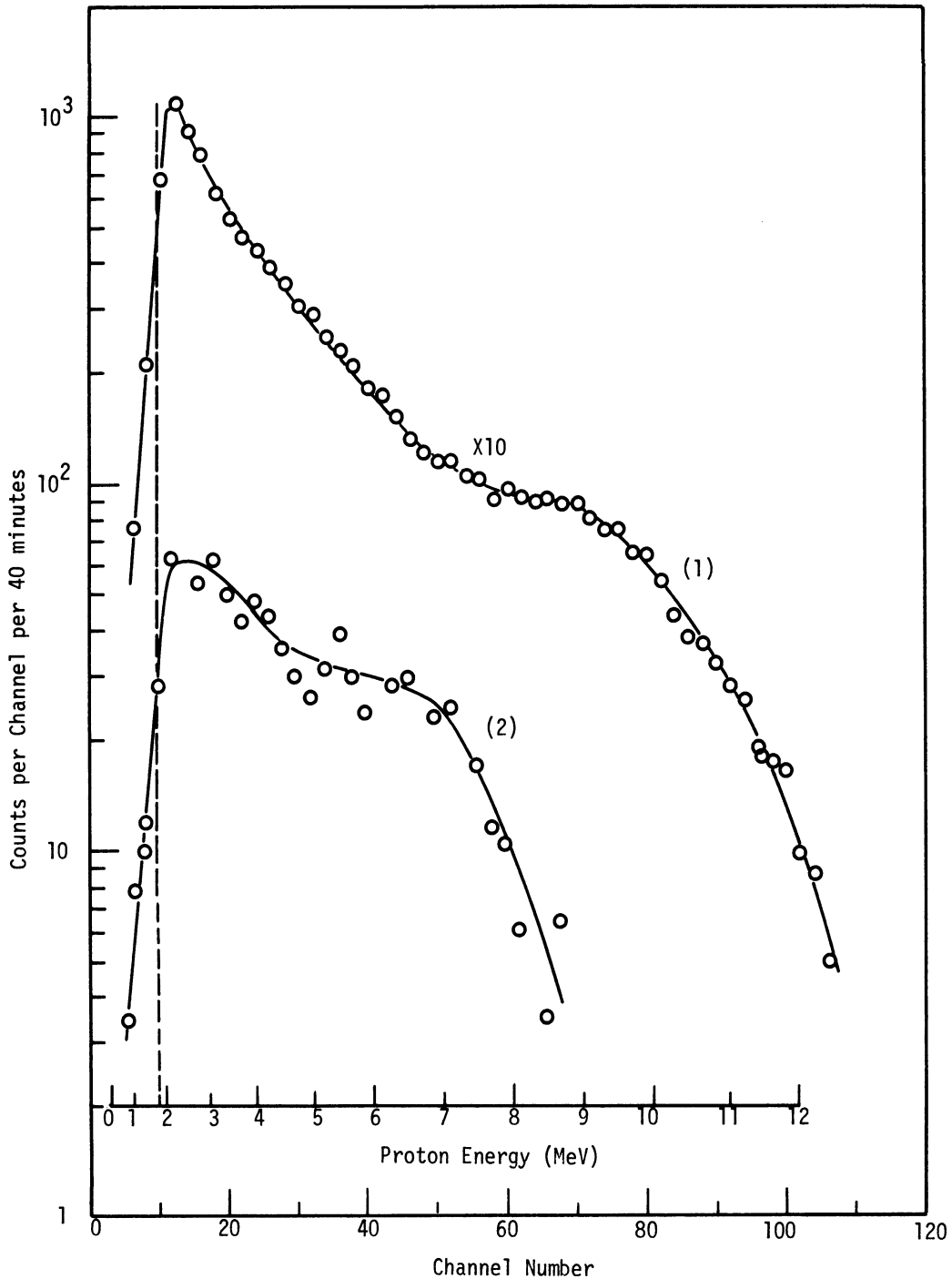(1) is the singles spectrum with no shadow shield or PSD.

(2) is the singles spectrum with the shadow shield and PSD.

(3) is the companion spectrum for selected recoil carbon ions in scintillator I (3 MeV carbon ions, 11.6 MeV scattered neutrons).

— — — is the pulse height corresponding to the high level threshold of discriminator-trigger II.

FIGURE 14

Scintillation pulse height spectra in scintillator II-I.

(1) is the singles spectrum with the shadow shield and PSD.

(2) is the companion spectrum for selected recoil protons in scintillator
   I (7.3 MeV protons, 7.3 MeV scattered neutrons).

— — — is the pulse height corresponding to the PSD bias level.

FIGURE 15

Scintillation pulse height spectra in scintillator II-II.

neutron scattering angle. Then the discriminator settings and coincidence tim-

ing delays were optimized. Finally the scintillation pulse height spectra

were obtained for various orientations of the crystal axis relative to $\hat{\beta}$. Typ-

ically, θ was fixed and then ϕ was varied between $0°$ and $360°$. Usually, θ and

ϕ were changed by $30°$ increments. The centroid of the peak in the pulse height

spectrum was assumed to correspond to the idealized recoil case.

Several low intensity gamma ray sources (Cs-137, Na-22, Co-60 and Th-232

daughters) were used for calibration and linearity check of both detectors and

associated discriminator-triggers as well as the linear signal analyzing sys-

tem. The pulse height corresponding to the half-maximum point in the fall-off

of the "Compton edge" in the recoil electron scintillation pulse height spec-

trum was assumed to represent the maximum energy of the "Compton electrons."

The response of anthracene to electrons is a linear function of energy for

energies greater than 20 KeV. For calibration purposes the low energy non-

linearity was neglected and the response assumed to be linear for all energies.

The error resulting from this assumption was less than 0.5%. Response func-

tions for NE 213 deduced by Bachelor et al.[59] were used to correlate the gamma

ray calibration data and the proton response of detector II.

Detector I and the analyzing system were calibrated before and after each

neutron scattering measurement. Typical variations in the response of the sys-

tem during a measurement were less than 2%. The gain of detector II was rou-

tinely checked and adjusted when necessary during a series of scans to avoid

any significant variation of the detection efficiency for the selected scat-

tering events. The low probability of the occurrence and detection of the

scattering events of interest required high reaction rates in both scintillators for reasonable data acquisition times. However, the rates were limited by the stability and discrimination capabilities of the electronic systems as well as the chance coincidence rate. Neutron source intensities on the order of 10^9 neutrons per second proved to be practical. Typical single rates in detectors I and II were 10^4 and 5×10^3 counts per second (cps) respectively; whereas true coincidence rates varied from 0.1 cps in the recoil carbon ion measurements to 1.0 cps in the recoil proton measurements. A fast gate width (effectively the light collection time) of 0.8 microsecond and a slow gate width of 2 microseconds were employed in the measurements. Chance coincidence rates ranged between 5 and 50% of the true coincidence rates.

Pulse height resolution of the elastic scattering peaks in the scintillation pulse height spectra varied between 35 and 47% for carbon ion recoils and from 20 to 40% for recoil protons. Figures 16 and 17 show peaks for carbon ions and protons. The chance coincidence spectra which are included were obtained by introducing an excessive delay in the timing signal from trigger I. In the recoil proton case a singles spectrum is also shown.

4.4. EXPERIMENTAL RESULTS

The directional scintillation response of the 1" high by 1" diameter anthracene crystal was measured for recoil protons with energies of 0.92, 1.88, 4.8, and 7.3 MeV, and recoil carbon ions with energies of 2, 2.5, 3, and 3.5 MeV. Table 3 provides a summary of the response anisotropy ratios deduced from the results. Ratios are given for all recoil energies. Each value rep-
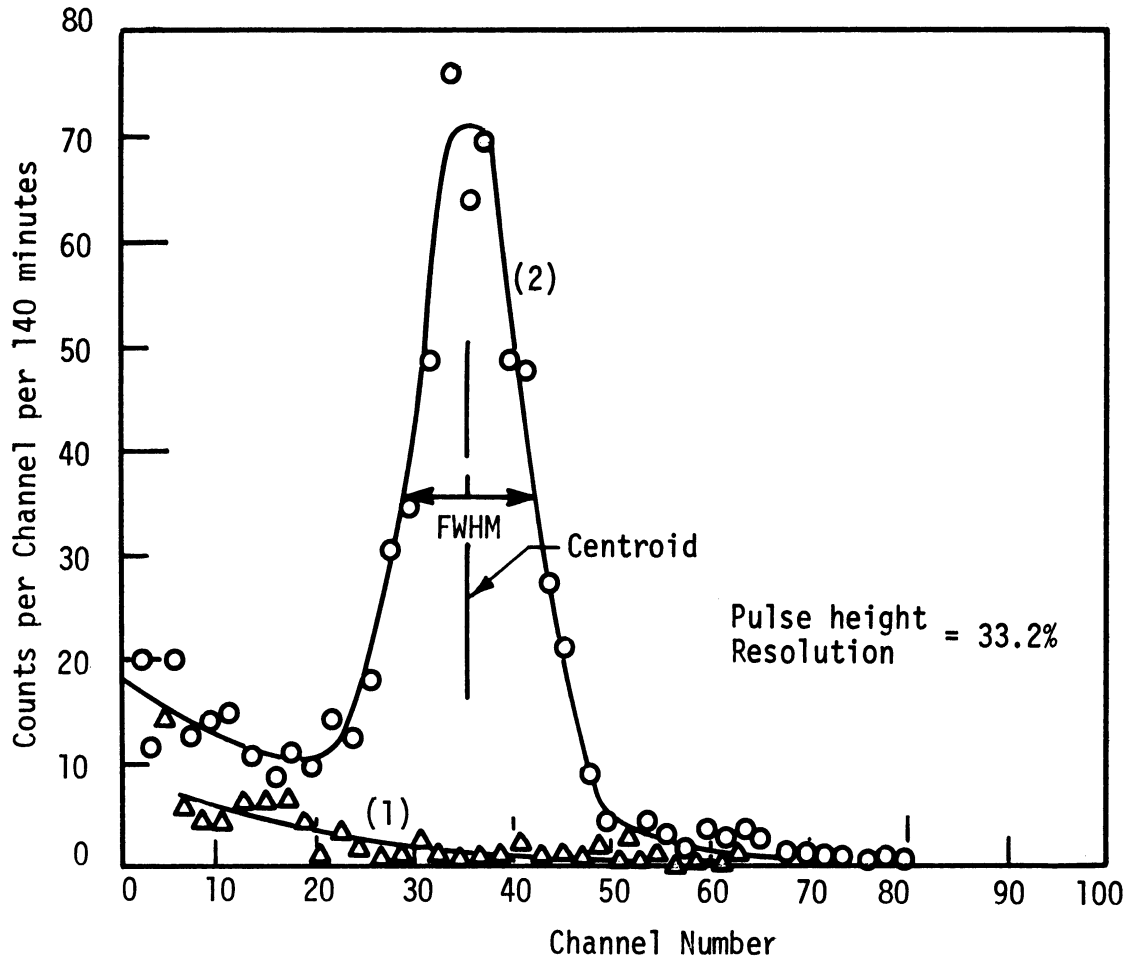
(1) is the chance coincidence spectrum.

(2) is the true coincidence spectrum for 3 MeV recoil carbon ions (α = 111°, β = 32°, θ = 90°, ϕ = 115°).

FIGURE 16

Recoil carbon ion scintillation pulse height spectrum in anthracene crystal.
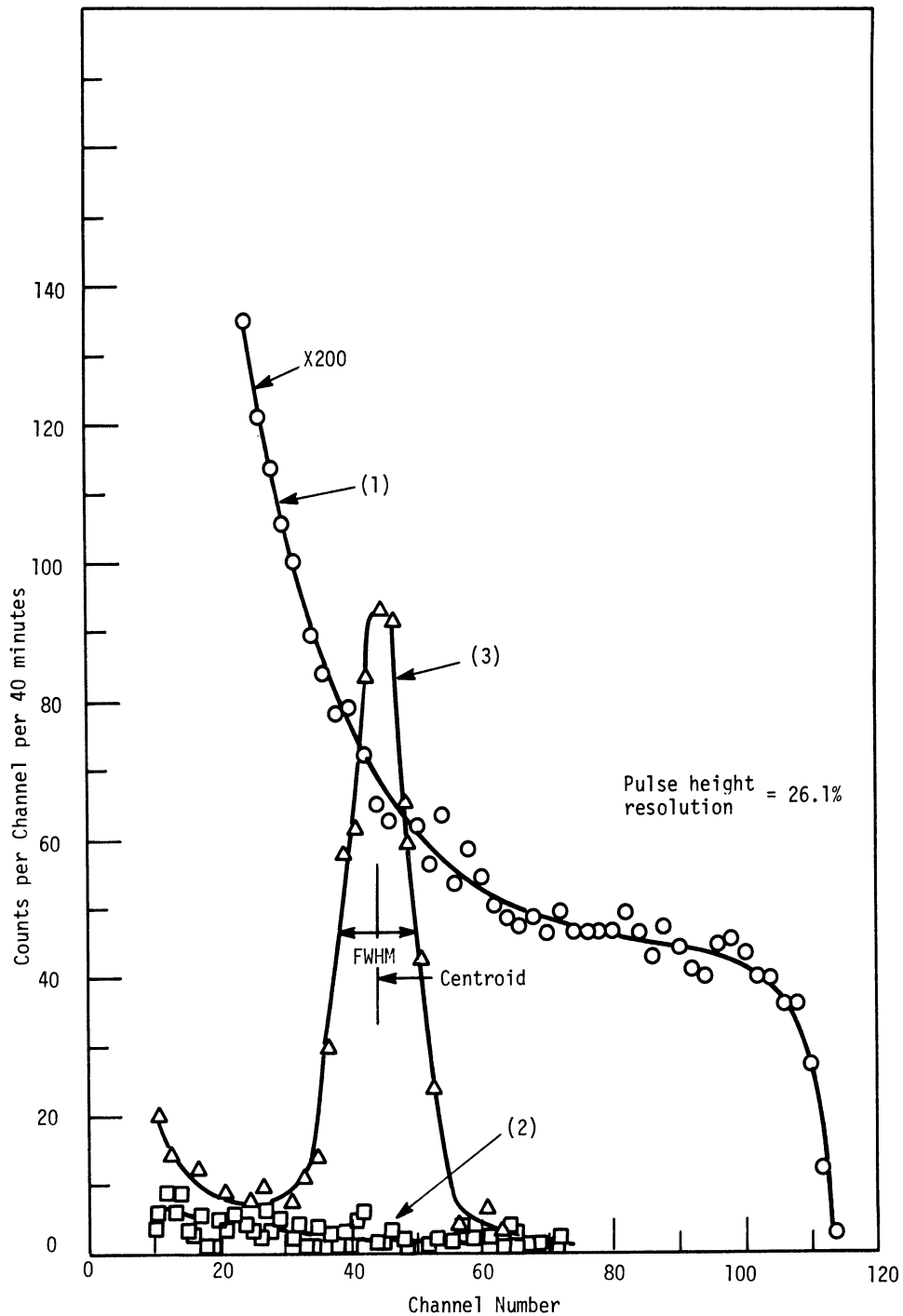
(1) is the singles spectrum.

(2) is the chance coincidence spectrum.

(3) is the true coincidence spectrum for 7.3 MeV recoil protons ($\alpha=\beta=45°$, $\theta=0$).

FIGURE 17

Recoil proton scintillation pulse height spectrum in anthracene crystal.

TABLE 3

RESPONSE ANISOTROPY RATIOS I

Ion Energy and type	Ratio of Maximum Response to that in Direction of:		
	a axis	b axis	c' axis
2 MeV C	1.21	1.68	
2.5 MeV C	1.20	1.62	
3 MeV C	1.22	1.65	1.04
3.5 MeV C	1.22	1.63	
0.92 MeV H	1.16	1.54	1.02
1.88 MeV H	1.12	1.43	1.02
4.8 MeV H	1.06	1.27	1.0
7.3 MeV H	1.03	1.25	1.0

resents the response to protons or carbon ions with recoil directions giving

the maximum response divided by the response for recoil directions parallel to

one of the crystallographic axes (a, b, or c').

4.4.1. Directional Response Scans

Figures 18 and 19 illustrate the results of response scans with 0.92 and

1.88 MeV recoil protons. Results obtained with 3 MeV recoil carbon ions are

shown in Figure 20. Recoil directions relative to the crystallographic axes

are given in terms of the coordinate system shown in Figure 13. The response

is indicated for all azimuthal angles and for polar angles of 30°, 60°, and

90°. The response curves are drawn so as to be symmetric about the ac crystal

plane of symmetry as well as to fit the data points indicated. Incomplete

scans were made with 4.8 and 7.3 MeV protons. Results of azimuthal scans for

a polar angle of 90° are shown in Figure 21. For recoil carbon ion energies
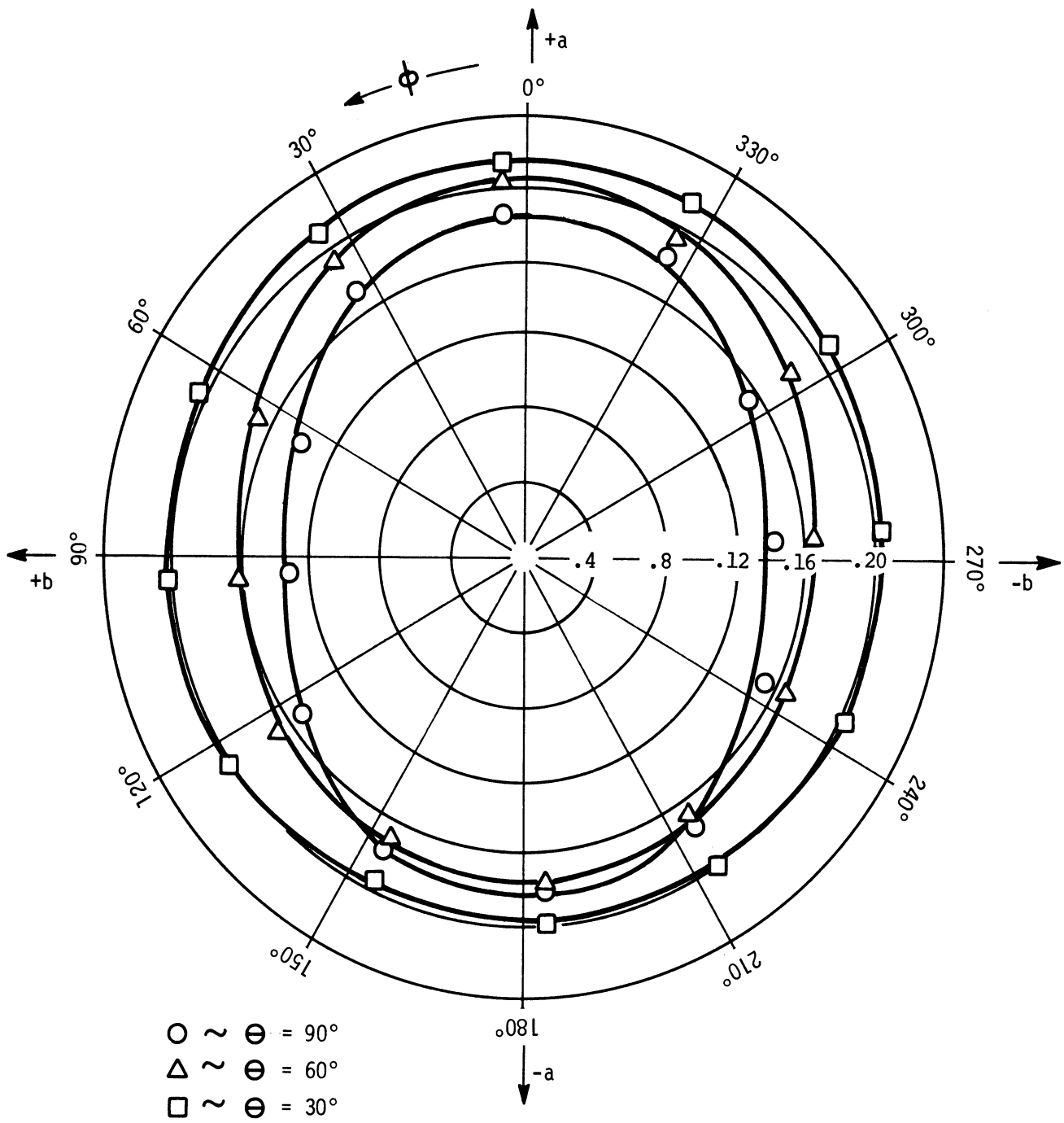
FIGURE 18

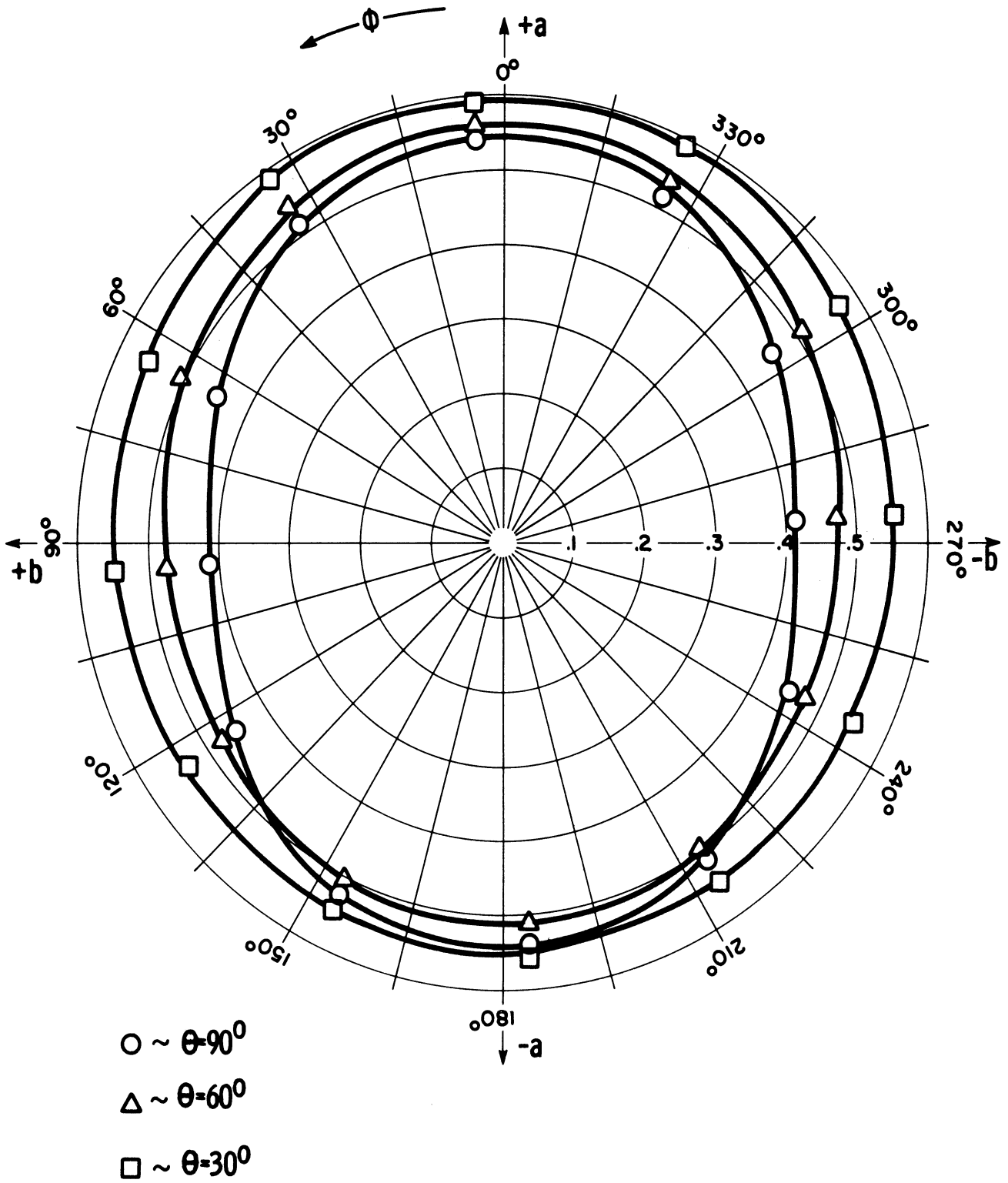Directional response of anthracene crystal to 0.92 MeV protons.

FIGURE 19

Directional response of anthracene crystal to 1.88 MeV protons.
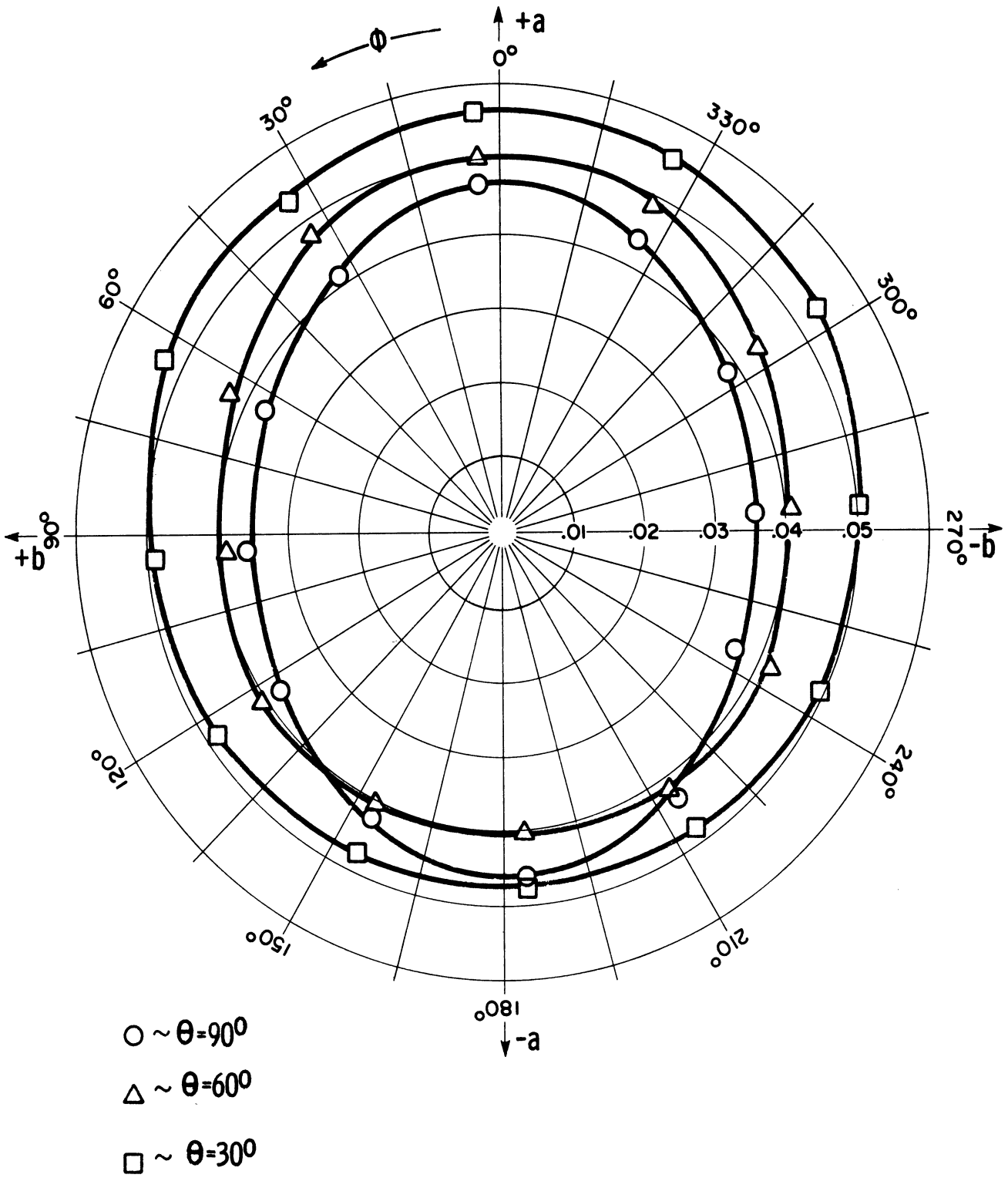
FIGURE 20

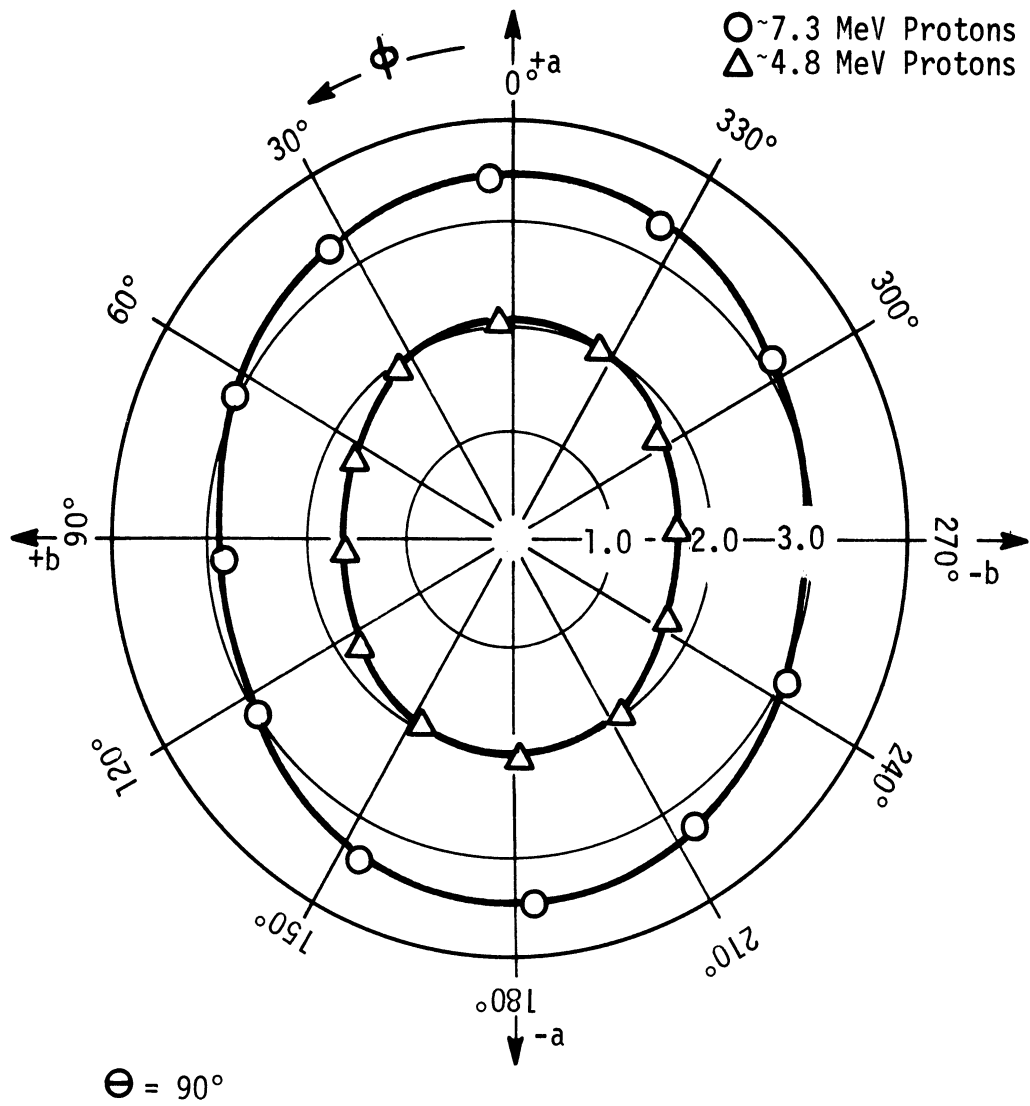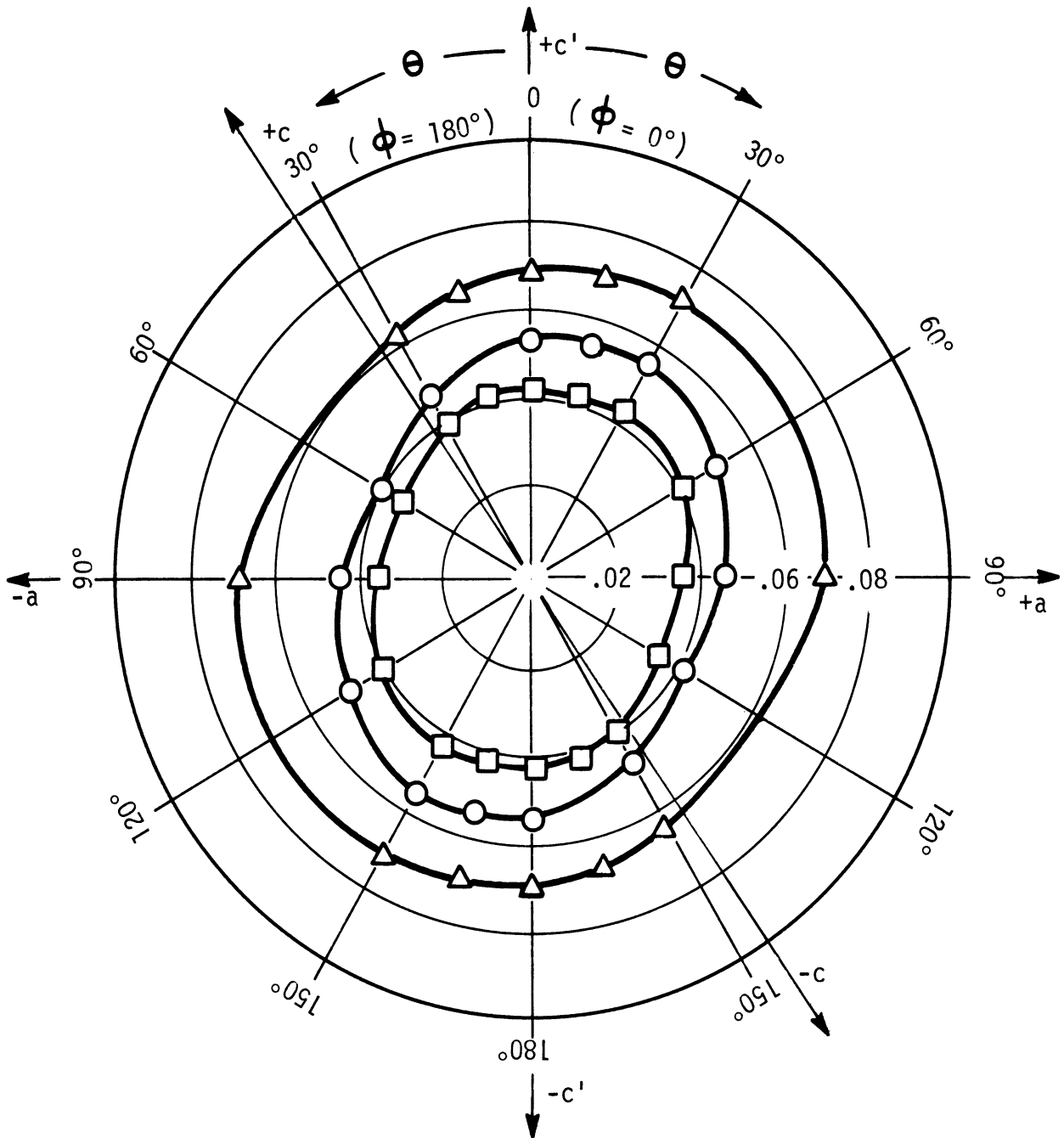Directional response of anthracene crystal to 3 MeV carbon ions.

FIGURE 21

Directional response of anthracene crystal to 4.8 and 7.3 MeV protons.

other than 3 MeV the response was measured only for recoil directions parallel

to the a and b crystal axes and the direction of maximum response as estimated

from the 3 MeV scan.

Figure 22 illustrates the variation of the response in the ac plane for

0.92 and 7.3 MeV recoil protons and 3 MeV recoil carbon ions. The points in-

dicated in the plot for $\theta \leq 90°$ were either measured, or obtained from

the intersection of the ac plane with response curves such as those shown in

Figures 18 through 21. Mechanical limitations restricted θ to $90°$ or less dur-

ing the measurements; therefore, points for $90° < \theta$ are inversions of the points

for $\theta < 90°$. It is difficult to ascertain the exact recoil direction giving

the maximum response in any of the cases. The direction appears to lie in the

ac plane inclined about $30°$ from the c' axis toward the a axis.

All data points represent the estimated centroid of the peak in the re-

coil ion scintillation pulse height spectra. In cases where more than one

measurement was made for a particular set of conditions, the data points are

the averages of the measurements. In several trial measurements corrections

were made in the recorded pulse height spectra to remove the chance coincidence

contributions. These corrections had a negligible effect on the estimated

centroids of the peaks in the spectra. Moreover, it was quite impractical to

take chance coincidence spectra for each recoil direction, and corrections for

subsequent measurements based on one chance spectrum were inaccurate. There-

fore, the centroids of all peaks were estimated without subtracting real or

hypothetical chance coincidence contributions. In all cases the peak pulse

heights were normalized to the pulse height corresponding to a 1 MeV Compton

O ~ Response to 3 MeV Recoil Carbon Ions
△ ~ X 1/20 Response to 7.3 MeV Recoil Protons
□ ~ X 1/20 Response to 0.92 MeV Recoil Protons

Points for θ > 90° are inversions of points for θ < 90°.

FIGURE 22

Directional response of anthracene crystal to 0.92 and 7.3 MeV protons and 3 MeV carbon ions.

recoil electron in the same crystal.

The justification for connecting the experimental points in the plots for relatively widely varying values of ϕ is based on extensive preliminary experiments. Scans of the recoil proton response of a smaller 1/2" high by 1/2" diameter anthracene crystal were conducted with smaller angular increments between recoil directions and better angular resolution. In particular, recoil directions about the b crystal axis and in the ac plane were investigated. No significant structure was noted; hence, more data points than those used in the measurements indicated above seemed unnecessary.

4.4.2. Energy Response

In Figure 23 the normalized response is plotted for proton and carbon ion recoil directions parallel to the a, b c' crystal axes, and the direction which gave the maximum response. The points were deduced from the results obtained with 0.92, 1.88, 4.8, and 7.3 MeV protons and 2, 2.5, 3, and 3.5 MeV carbon ions.

Birks' Formula* with carefully selected quenching parameters was used to generate the curves which seem to describe the proton results. The appropriate values of the quenching parameters are indicated in the figure. To simplify the formula the specific energy loss dE/dx in units of MeV mgm^{-1} cm^2 was assumed to be given by the expression 0.294 $E^{-3/4}$, (E in MeV) which was suggested by Tsukada et al.[6]

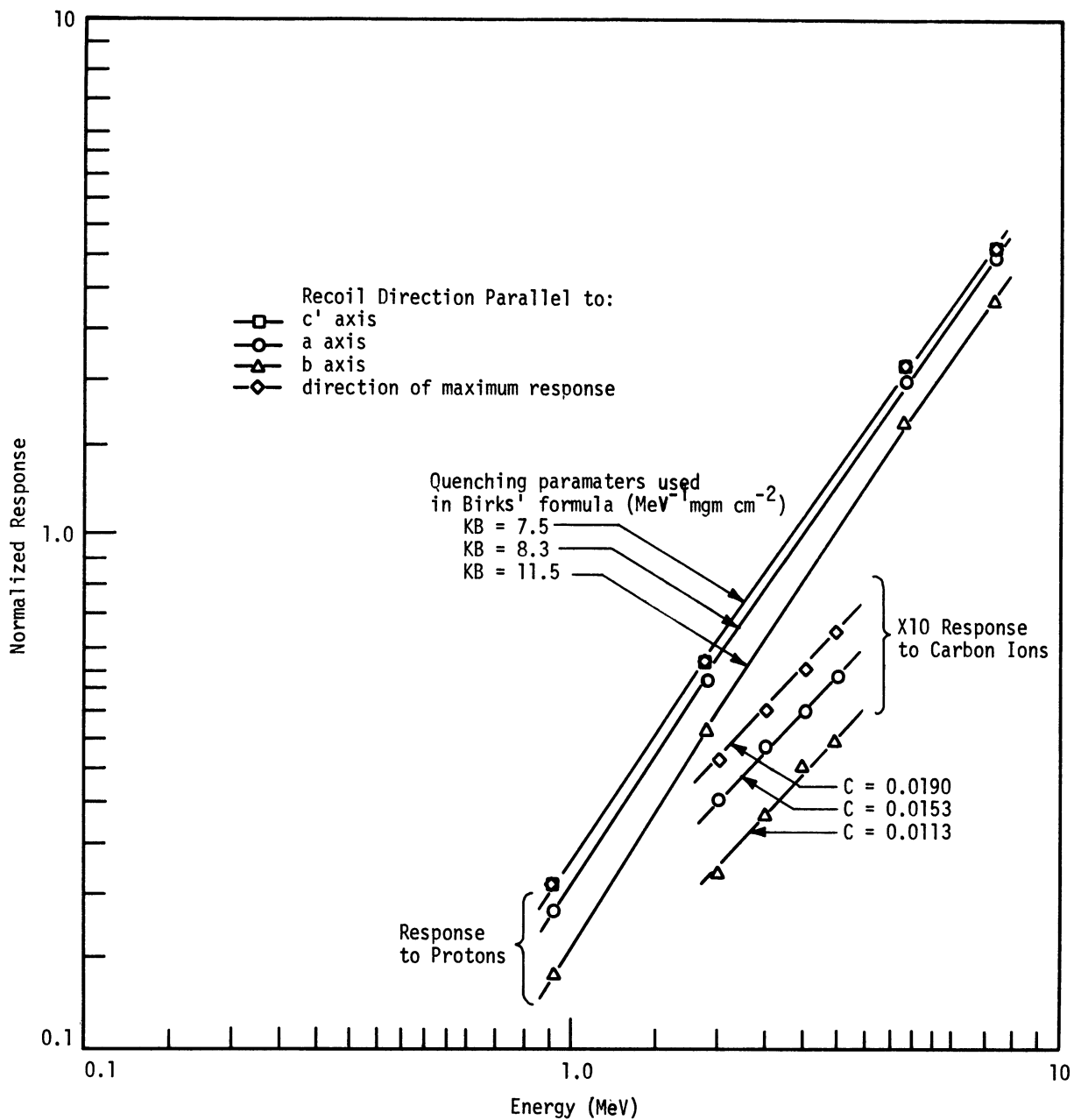$$L(\text{Normalized Response}) = \int_0^{E_\beta} \frac{dE}{1+KBdE/dx}$$

FIGURE 23

Directional response of anthracene crystal as a function of energy.

The carbon ion response points illustrated in Figure 23 may be described by the expression L = CE where L is the normalized response, C in a constant depending on the recoil direction, and E is the recoil energy in MeV. Curves generated with this formula are shown in the figure along with the corresponding values of C.

4.5. DISCUSSION OF RESULTS

The results of this chapter provide an additional basis for the evaluation of the three models of the scintillation process developed in Chapter 3. The static and dynamic cases are considered separately.

4.5.1. Static Quenching

The analysis presented in subsection 3.2.2 is extended by considering the recoil proton and carbon ion results. Figure 24 shows a plot analogous to Figure 7 which includes the curves from Figure 7 and a new curve obtained from a Birks' formula description of the proton data of the present chapter. Results from the recoil carbon ion data are shown also; however, because of the relative uncertainty in dE/dx and F_T in the carbon ion case, only two points are shown. Both correspond to carbon ions in the 2.5 to 3.5 MeV energy range for which the dE/dx values are nearly constant. One point is based on a value of 0.6 for F_T which was indicated by the calculations of subsection 3.2. The other point is for an F_T value of 1, corresponding to the case of no energy loss through delta ray production. It is evident from Figure 24 that the weighted directional difference in specific light yield, as obtained from a wide range of experimental results, cannot be described as a single exponential
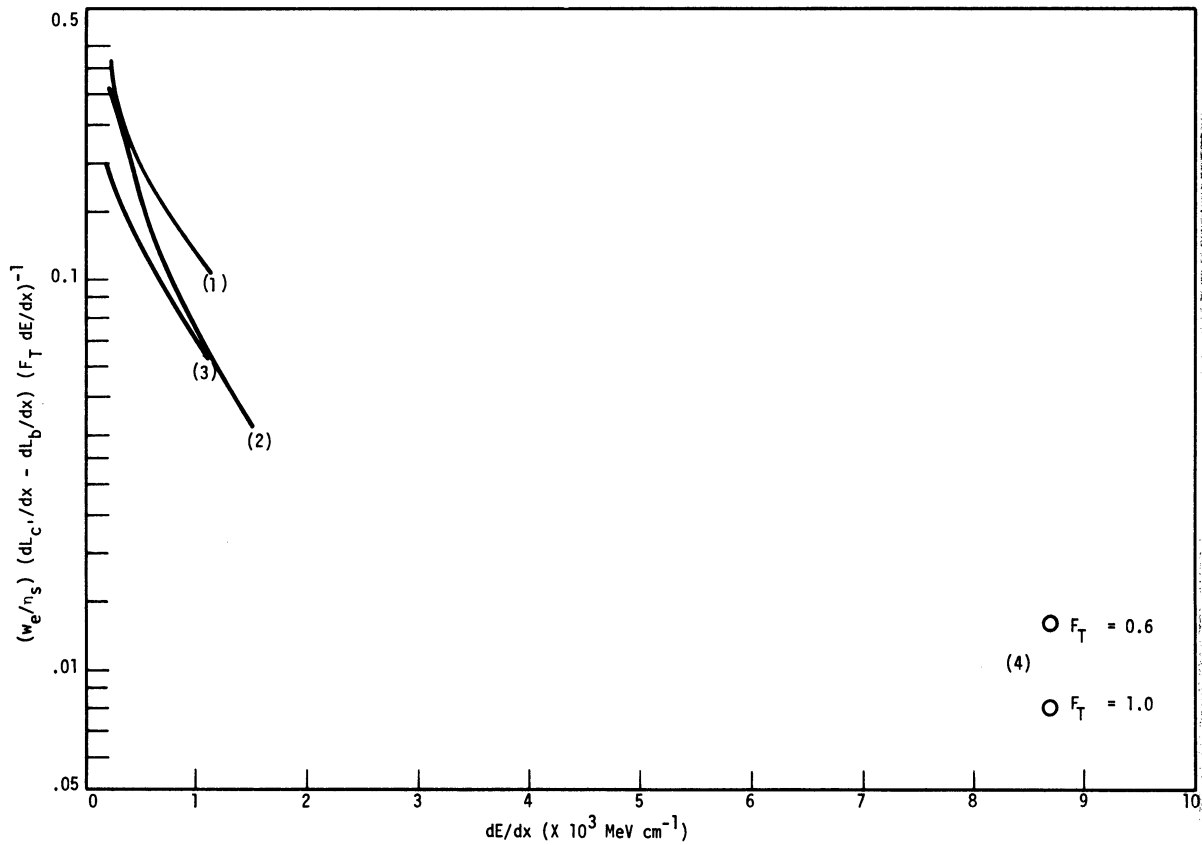
(1) is calculated from the proton results of Tsukada et al.[6]

(2) is calculated from the alpha particle results of Schött.[5]

(3) is calculated from the proton results presented in this chapter.

(4) are calculated from the 2.5 to 3.5 MeV carbon ion results presented in this chapter.

FIGURE 24

Weighted difference in specific light yield as a function of specific energy loss-II.

function of dE/dx, nor as the difference of two such functions. Therefore, an anisotropic yield of excited π-states or anisotropic static quenching, as formulated in Chapter 3, is an inadequate explanation for the experimentally observed directional light yield.

4.5.2. Dynamic Quenching

For the evaluation of the dynamic quenching models it is convenient to consider the plots shown in Figure 25. The specific response for proton recoils parallel to the a, b, and c' axes has been generated from the Birks' formula description of the results of this chapter. Specific response curves for carbon ion recoils in the same three directions were obtained from linear expressions which described the experimentally observed directional yields as a function of recoil energy. Two of the specific response curves obtained from the computer solution of the biexcitonic quenching model equation are also included in Figure 25. Four significant features are noted about the plots in the figure.

(1) A continuation of the Birks' formula description of the proton data describes the magnitude of the 2.5 to 3.5 MeV carbon ion results as well.

(2) Because of the "saturation" nature of the Birks' formula description, the specific response anisotropy ratio for a proper fit of the low energy proton data is about the same for all higher values of dE/dx.

(3) The variation of the specific response of the recoil carbon ions with dE/dx is not described by Birks' formula.

(4) The two curves corresponding to the biexcitonic quenching model have nearly the same shape as those of the Birks' formula description which was shown in 3.3.3 to be analogous to the formulation of the linear quenching model.
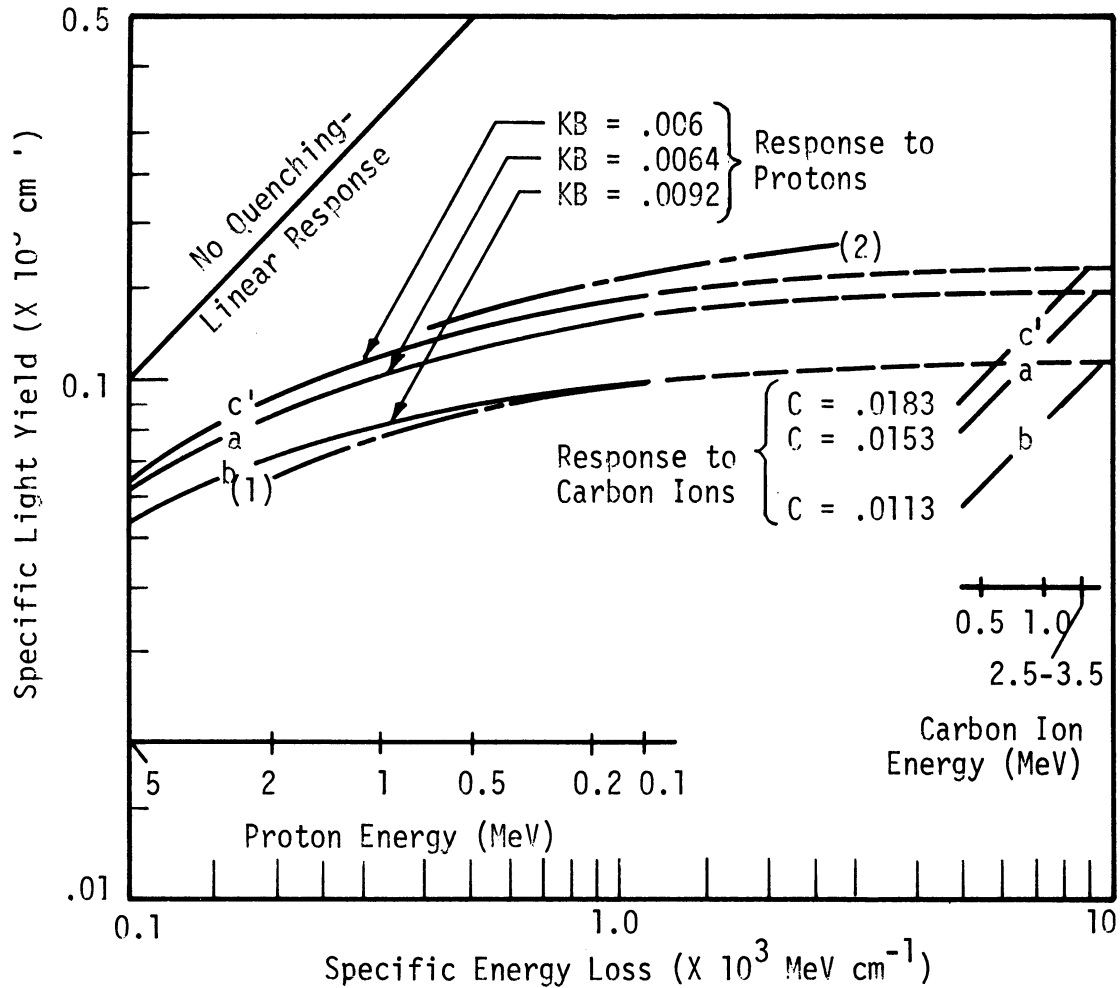
Curve labels (a, b, or c') indicate the crystal axis parallel to the recoil directions of the protons and carbon ions.

The proton response curves were generated from a Birks' formula description of the results of this chapter using the KB values indicated.

The carbon ion response curves were obtained from a linear description of the results of this chapter using the values of C indicated.

(1) is the response generated from the computer solutions (Figure 8) for $B = 4 \times 10^{-4}$ and $E = 3.5 \times 10^{-3}$ cm MeV^{-1} dE/dx.

(2) is the response generated from the computer solutions for $B = 2 \times 10^{-4}$ and $E = 1.75 \times 10^{-3}$ cm MeV^{-1} dE/dx.

FIGURE 25

Scintillation response of anthracene crystals-III.

The basic assumptions of the linear quenching model developed in subsection 3.3.3 are violated if dE/dx is greater than ~1250 MeV cm^{-1}. Qualitatively, this limitation arises because the effective volume of the column of excitation along the track of a heavy charged particle does not get larger as dE/dx increases. For large values of dE/dx, almost all the molecules within the track are damaged and act as quenchers. Hence, in the hopping exciton model of exciton diffusion, the probability of a quenching encounter per hop in the column is close to unity and the diffusion concept is no longer valid. Therefore, the agreement between the continuation of the curves from Birks' formula and the carbon ion results does not demonstrate the success of the linear quenching formulation unless the estimates of column radius or exciton hopping distance are erroneous.

An alternate explanation for the apparent success of Birks' formula is suggested by the similarity between this description and the description provided by the computer solutions for the biexcitonic quenching model. The bases of the biexcitonic model are not as restrictive as those of the linear quenching model. It accomodates both the band and hopping exciton concepts. Because of the absence of serious contradictions or limitations of the model, it is concluded that anisotropic singlet exciton diffusion with the resultant anisotropic biexcitonic quenching rate is the source of the directionally dependent light yield. The fact that a factor of two variation in the diffusion coefficient produces a calculated variation in the yield of more than the maximum observed implies that exciton migration need not be highly anisotropic. The order of the magnitudes of the diffusion coefficients required is:

$D_{ab} > D_{bc'} > D_{ac'}$ where the subscripts indicate the plane perpendicular to the track of the exciting particle. In the specific case of the proton response for dE/dx = 800 MeV cm^{-1} shown in Figure 25, the following relation between the diffusion coefficients may be obtained from the computer solutions presented in Figure 8. D_{ab} = 1.69 $D_{ac'}$ and $D_{bc'}$ = 1.51 $D_{ac'}$ when the solution parameters B and E equal $4x10^{-4}$ and 2.8 respectively for recoils parallel to the b axis.

CHAPTER 5

RADIATION DAMAGE EFFECTS ON THE DIRECTIONAL RESPONSE

5.1. INTRODUCTION

This chapter describes an experimental investigation of the effects of

permanent radiation damage on the directional anisotropy of the prompt and de-

layed scintillation components in an anthracene crystal. A collimated beam of

5.3 MeV alpha particles was used for excitation. The scintillation light emit-

ted during the time intervals 0 to 0.1 microsecond and 1 to 8 microseconds

after the incidence of an alpha particle was measured for a variety of direc-

tions of incidence parallel to the ab crystal plane.

Although the surface condition of the crystal and the efficiency of the

light collection of the detection system required considerable attention, alpha

particle excitation was much superior in these measurements to the neutron scat-

tering technique described in the previous chapter because a low background

was essential.

A 1/4" high by 1/2" diameter cylindrical anthracene crystal was mounted

in a conical reflecting cavity viewed by a single photomultiplier tube. The

crystal could be remotely rotated about the cylindrical c' axis.

Simultaneous analysis of the prompt and a selected portion of the delayed

scintillation yield, as detected by the PM tube, was provided by the electronic

system. Such pulse shape analysis was controlled by an associated discrim-

inator-trigger which after appropriate delays actuated three gate generators

and subsequently the operation of three linear gates. Two of the gates iso-

lated the prompt and delayed part of the scintillation signal from the PM tube, and the third provided both pulse height discrimination and simultaneous analysis of the prompt and delayed signals.

The effects of radiation damage were determined by repeated measurements of the anisotropy of the prompt and delayed emission components as the cumulative Co-60 gamma ray radiation dose was incrementally increased from zero to 1000 kilorads.

5.2. EXPERIMENTAL ARRANGEMENT

5.2.1. Reflecting Chamber

A cross sectional view of the conical cavity in which the crystal was placed is illustrated in Figure 26. The cylindrical crystal was positioned in the apex of the cavity with an ab cleavage face resting on the horizontal end of a vertical coaxial shaft which allowed 360° rotation. All surfaces within the cavity, except the crystal and PM tube face, were covered with five coats of Nuclear Enterprise TiO_2 reflecting paint which provided diffuse reflection. As shown in Figure 26, the small diameter horizontal passage between a Po-210 alpha source and the crystal provided adequate collimation. The angular spread in the directions of the alpha particles incident on the crystal was estimated to be less than 2°. The collimator and the shaft which supported the crystal were designed so that the alpha particles impinged normally on the cylindrical crystal surface at a point equidistant from the ends. The chamber was maintained at a pressure of less than 40 microns of Hg by a mechanical vacuum pump during alpha particle excitation. It was separated from the pump by a
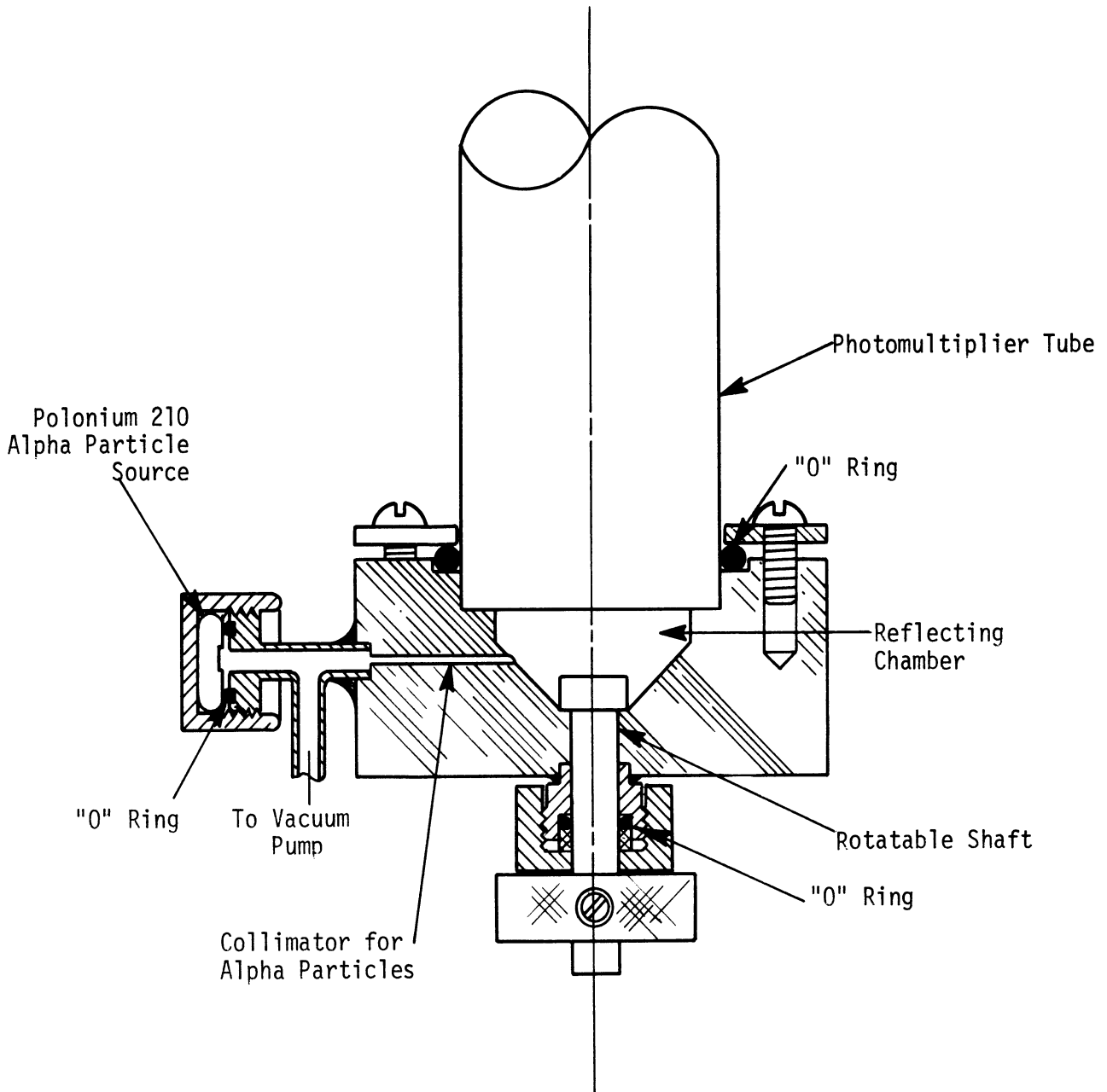
FIGURE 26

Reflecting Chamber.

liquid nitrogen cold trap to protect the crystal and the interior of the chamber from backstreaming vapors.

5.2.2. Detection and Analysis System

The electronic system is illustrated in Figure 27. It consisted mainly of the components used in the experiment described in the previous chapter. However, the 512 channel MCA was replaced with a 1024 channel MCA with two dimensional analysis capabilities. Three signals were obtained from the PM tube. Dynode 11 provided a fast timing pulse, and dynode 9 provided a low level linear signal. A high level signal was obtained from the anode which was linear, at least during the time interval in which the delayed scintillation component was measured.

The timing pulse was analyzed by a discriminator-trigger allowing high and low level leading edge triggering. When the amplitude requirement set by the high level threshold was satisfied, a set of accurately timed logic pulses were generated. Three of these pulses were utilized, after suitable delays to actuate the gate generators controlling the opening of three linear gates. Linear gate I passed only the prompt portion of the low level linear signal; linear gate II passed the delayed portion of the high level signal. The internal gates in the two independent halves of the MCA comprised gate III and allowed simultaneous rejection or analysis of the signals passed by gates I and II.

The electronic system preceding gates I and II produced a minimum amount of pulse shape distortion of the prompt portion of the low level signal and

~*10* µsec

Discriminator-Trigger
EG&G TD101/N

Gate Generator III
E.H. Pulser Model 133

~1 µsec

Gate Generator I
Tektronics Pulser Type 114

Gate Generator II
1/2 EG&G-TR104S/N

Fast Timing Signal

Low Level Linear Signal

High Level Linear Signal

Coincidence Circuit
EG&G-C102A/N

NOR Output

Voltage
Divider

Linear Gate I
EG&G-LG101/N

Fast-Linear Inverting
Amp.   1/2 AN101/N

PM
Tube

Limiter
EG&G-L102/N

Fast Linear Amplifier
EG&G AN101/N

Reflecting
Chamber

Stretcher Amplifier I
EG&G-SA105/N

Linear Gate II-
Stretcher Amplifier II
EG&G-LG102/N

Delay line

Polarity and approximate
pulse shape

Coincidence Inputs
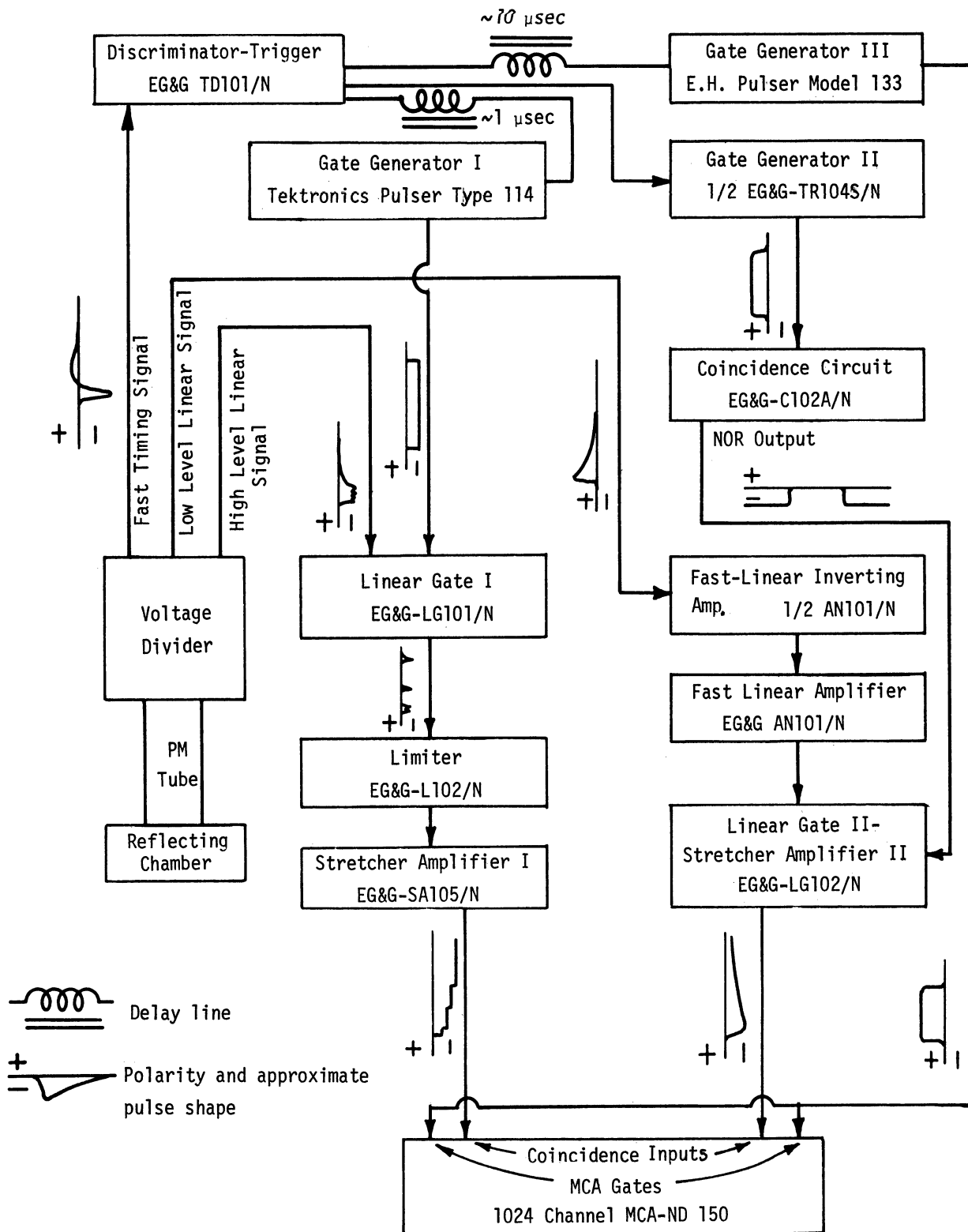MCA Gates
1024 Channel MCA-ND 150

FIGURE 27

Electronic system-II.

the delayed portion of the high level signal. Therefore, subsequent integration of the pulses by stretcher amplifiers I and II provided signals with amplitudes proportional to the total light yield of the prompt and delayed portions of the scintillation yield as defined by the timing and duration of the two gate pulses.

Since a finite time was required for the discriminator-trigger circuit to analyze a timing pulse and initiate the operation of the gate generators, gate I was normally biased open. When the trigger circuit was actuated, after a fixed delay the output of gate generator I closed the gate for the duration of the prompt and delayed signal. Spurious low level pulses below the threshold of the discriminator-trigger passed by gate I because of the normally open condition, were ultimately rejected by the closed gate at the MCA input.

5.3. EXPERIMENTAL TECHNIQUE

5.3.1. Electronic System Parameters

Since the prompt scintillation emission component in anthracene decays rapidly (~30 nanosecond decay constant in a thick crystal), less than 4% of the prompt yield occurs at times greater than 0.1 microsecond after the primary events. Therefore gate I was closed 0.1 microseconds after a timing pulse with the required amplitude arrived at the discriminator-trigger. Subsequently, gate II was set to open 1 microsecond after the activation of the trigger and to remain open for 7 microseconds. Although the delayed emission persists longer than 8 microseconds after a primary event, the method employed for measuring the delayed component was not sensitive enough to improve the accuracy

of the results by longer light collection times.

The RC of stretcher amplifier I was limited by construction to 10 micro-seconds; however, since all the charge accumulation occurred during the 0.1 microsecond gate I was open, negligible charge was lost during the collection time. A value of 300 microseconds was selected for the integrating time constant (RC) of stretcher amplifier II so that an insignificant amount of charge would be lost during the collection time.

Gate III was timed to open for a 2 microsecond interval, 9 microseconds after the actuation of the discriminator-trigger; thereby, the output signals from both stretcher amplifiers were sampled after integration was complete. The resultant coincident pulses were analyzed simultaneously by the MCA in the two dimensional mode of operation or singly as desired.

The timing uncertainty of the trigger-gating combination was observed to be several nanoseconds which was negligible considering the characteristic times of the events enumerated above.

Adequate amplification of the delayed response signal as the fluorescence efficiency of the crystal decreased due to radiation damage required that the PM tube high voltage be increased from 2400 to 2800 volts. When the dose exceeded 500 kilorads, meaningful measurements of the delayed component were no longer possible.

5.3.2. Empirical Investigation of Perturbations

Two potential sources of error in the measurement of the delayed component

were "after-pulsing"* and nonlinear response of the PM tube when operated under high gain conditions. An estimate for the upper limit of the after pulse contribution was obtained by assuming that the magnitude of the after-pulsing is proportional to the magnitude of the prompt pulse. Therefore, when the prompt signals produced by gamma rays and alpha particles were the same, the magnitude of the noticably smaller delayed pulses resulting from the gamma rays was certainly the upper limit for any after pulsing contribution. This information was deduced from the results of a two-dimensional analysis of the prompt and delayed light yields while the crystal was subjected to simultaneous gamma ray and alpha particle excitation. The continuous prompt versus delayed response pulse height spectrum resulting from the gamma rays also gave an indication of the linearity of the delayed pulse height signal regardless of the degree of saturation of the prompt high level output. Figure 28 shows a topographical plot of such a two dimensional analysis. It can be seen that the pulse height of the centroid of the delayed component spectrum for the alpha particles is about ten times as great as that of the gamma rays which produce the same size prompt component. Thus, at least 90% of the alpha particle delayed signal was not due to after pulsing. Also, the centroid of the pulse heights of the delayed gamma ray components appear to be linear over the complete range of corresponding prompt pulse heights which were examined.

Additional proof of the linearity of the delayed response signal was obtained by measuring the delayed response anisotropy over a PM tube high voltage

---

*Large spurious pulses occurring over a period of a few microseconds after a
a true pulse.
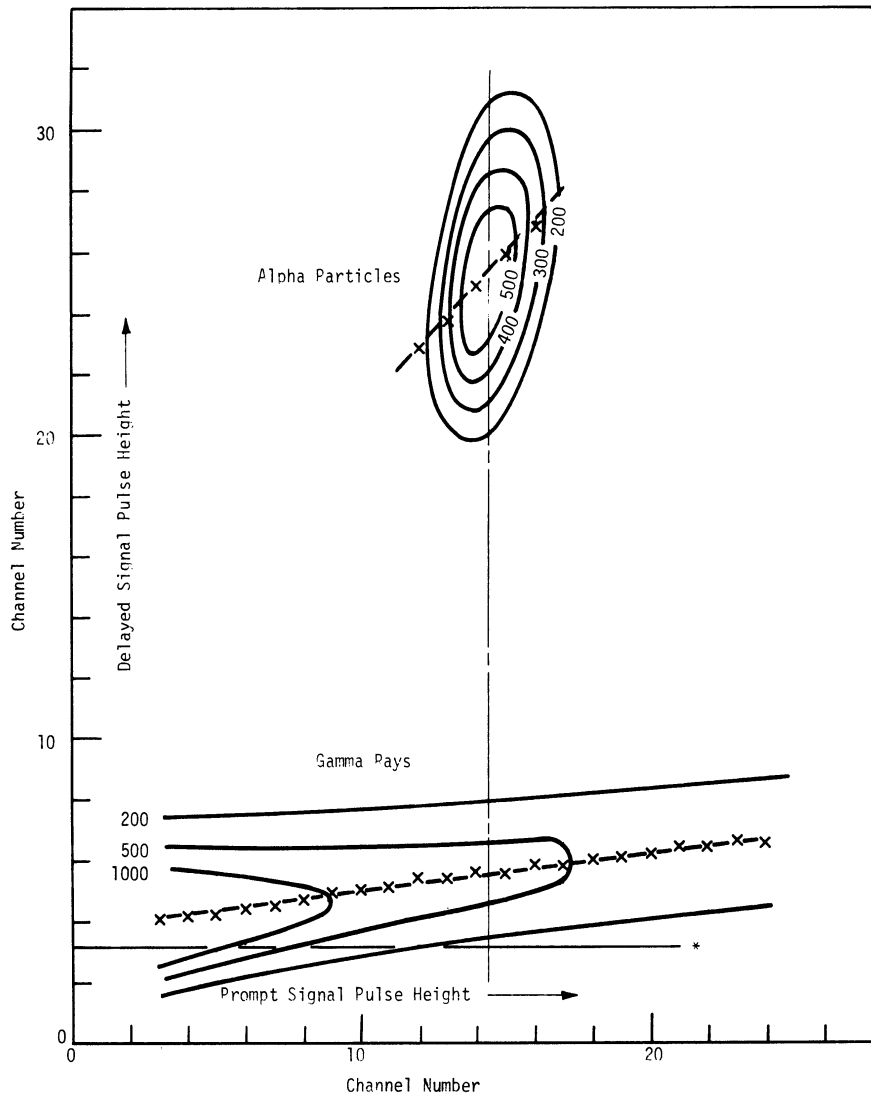
——— are curves through the points with two-dimensional coordinates (channel numbers) for which the numbers of counts indicated would be observed during the two hour counting period.

-x-x- are curves through the centroids of the delayed component spectra corresponding to one channel wide portions of the prompt component spectrum.

— - — indicates the channel number of the centroid of the prompt component spectrum for alpha particle excitation.

* indicates the channel number of zero delayed signal pulse height.

FIGURE 28

Two-dimensional prompt and delayed scintillation component pulse height spectrum for gamma ray and alpha particle excitation.

range of 2400 to 2800 volts. Although the gain and thus the degree of satura-
tion of the prompt high level signal changed considerably with the variation in
high voltage, the anisotropy of the measured delayed response remained essen-
tially constant.

5.3.3. Measurements

The 1/4" high by 1/2" diameter crystal which was investigated in the ex-
periments described in this chapter was obtained from the Harshaw-Chemical
Company. It was optically clear and free from internal cracks. Before a scan
of the directional response, the crystal was etched for two minutes in Benzene.
Initially, the orientation of the a and b crystal axes was estimated by noting
the optical birefringence effects; however, the symmetry of the measured direc-
tional scintillation yield was subsequently used for orientation purposes.

As observed on a Tektronix 585 CRO (~4 nanoseconds rise time), the delayed
scintillation emission as detected by the PM tube and passed by the linear gate
consisted primarily of small intermittent individual spikes probably corres-
ponding to single photons. Because of the size and relative infrequency of
the pulses, the delayed signal after integration was quite sensitive to elec-
tronic drifts, particularly in the DC base line (pedestal) of the fast linear
gate. Calibration before and after a measurement was essential. Likewise,
more reliable values of the prompt response were obtained with frequent cali-
bration. Two dimensional analysis proved to be impractical for a complete re-
sponse scan because of the involved sequence of calibrations which was re-
quired; therefore, this type of analysis was only used in preliminary experi-

ments. All response scans reported in subsection 5.4 were obtained by analyzing the components individually in separate series of measurements. Figures 29 and 30 show corresponding prompt and delayed pulse height spectra obtained by individual measurements. Pulse height resolutions of the prompt component peaks were around 17%. The resolutions of the delayed component peaks were usually about 45%. Count rates of several hundred cps were found to be an optimum compromise between pulse pile-up, system drift and data acquisition time.

5.3.3.1. Calibration techniques

Several gamma ray sources (Cs-137, Na-22, Co-60) were used for absolute calibration and to determine the linearity of the system.

Normalization and constant recalibration of the prompt component pulse height spectra were expedited during an extended series of measurements by making an absolute normalization before and after the series. During the measurements the relative response to alpha particles for various orientations of the crystal was determined by alternating measurements between the initial orientation and other orientations each differing by a fixed angular increment.

The same technique of alternating directional measurements was applied to the delayed component investigation. However, the sensitivity of the system to electronic drifts required additional calibration checks. The following method was utilized. First the crystal was excited with Co-60 gamma rays which resulted in a scintillation pulse height spectrum which was continuous up to the "Compton edge." Next, the fast timing signal was split and sent to both triggers. The original trigger operated as usual; whereas the second trigger
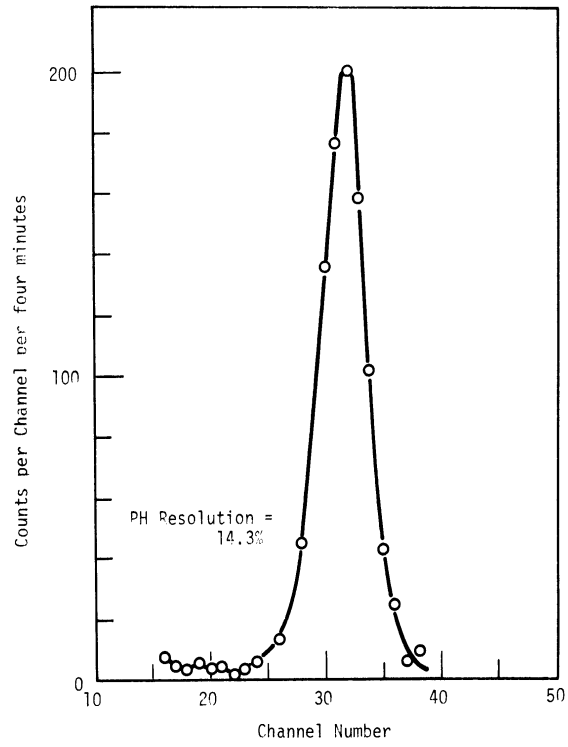
FIGURE 29

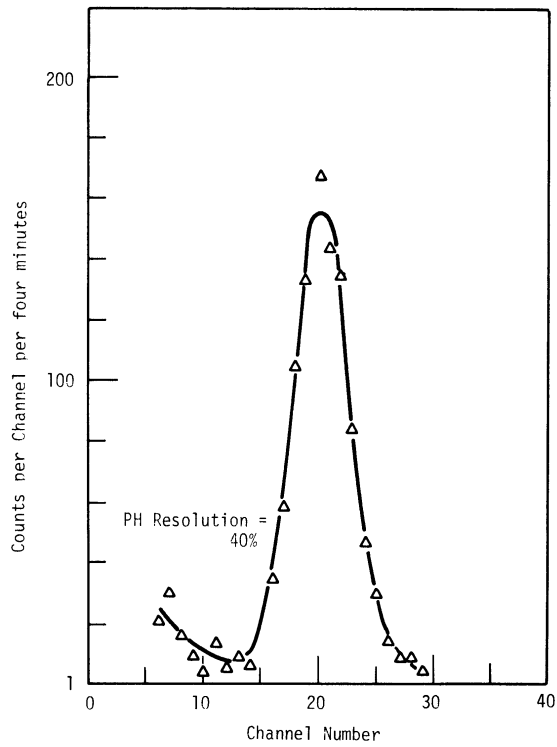Prompt scintillation component pulse height spectrum.

FIGURE 30

Delayed scintillation component pulse height spectrum.

was set to "multiple pulse." Since the number of standard size output logic

pulses in the multiple pulse train was proportional to the time the PM timing

pulse was above the threshold of the trigger, the continuous spectrum of scin-

tillation pulses resulted in an assorted number of logic pulses in each train.

The pulse trains were properly delayed and substituted for the high level (de-

layed signal) PM output and then pulse height analysis conducted as usual. The

resultant pulse height spectra in the MCA consisted of a number of equally

spaced sharp peaks from which any change in the channel number of zero pulse

height or gain was quickly determined.

5.3.3.2. Radiation damage

The 10,000 curie Co-60 gamma ray facility of the Phoenix Memorial Labora-

tory at The University of Michigan was used to produce permanent radiation dam-

age in the anthracene of interest in large increments. During the irradiation,

the crystal was placed 18 cm from the centerline of the cylindrical source.

In this position the measured dose was 70 kilorads per hour.[60] The Co-60 gamma

ray attenuation length in anthracene is ~10 cm;[40] therefore, the damage was

produced uniformly throughout the crystal. The permanent radiation damage was

assumed to increase linearly with the cumulative dose since it has been noted[4]

that at room temperature there is a negligible annealing of the effects of dam-

age on the fluorescence efficiency.

The decrease in the scintillation efficiency of the crystal after an in-

crease in gamma ray dose was determined by comparing the light yield before

and after each irradiation with that of a Pilot B plastic scintillator of the

same size.

5.4. EXPERIMENTAL RESULTS

A scan of the prompt response of the anthracene crystal to 5.3 MeV alpha particles was conducted for directions of incidence parallel to the ab crystal plane as the dose of Co-60 gamma rays absorbed by the crystal was increased incrementally from 0 to 1000 kilorads. The delayed response was correspondingly measured for alpha particles incident in directions parallel to the a and b crystallographic axes. Before the crystal was damaged, both the prompt and the delayed responses were maximum for incident directions parallel to the a crystal axis and minimum for directions parallel to the b axis. Since the directions of maximum and minimum prompt response were noted to be unchanged with radiation damage, it was assumed that the same held true for the delayed component. Table 4 gives a summary of the measured effects of damage on the prompt, delayed, and total anisotropy ratios. The ratios represent the response for alpha particles incident in directions parallel to the a crystal axis divided by the response for directions parallel to the b axis. The abrupt increase in the prompt response ratio when the dose was increased from 215 to 290 kilorads is attributed to a concurrent change in the daily adjustment procedure used with the linear gate-stretcher amplifier component. It is noted that the ratio was essentially constant before and after the change. Moreover, it is seen that the total response anisotropy ratio varied little with dose. However, the 10% increase in the delayed response ratio as the dose was increased from 0 to 500 kilorads is apparently real.

TABLE 4

RESPONSE ANISOTROPY RATIOS II

Response for Alpha Particles with Incident Directions Parallel to the a Axis
Relative to that for Incident Directions Parallel to the b Axis.

Dose (Krad)	Prompt Component	Delayed Component	Total
0	1.35	1.06	1.37
70	1.37	1.06	
145	1.39	1.09	
215	1.36	1.14	
290	1.43	1.12	1.37
355	1.43	1.14	1.36
495	1.46	1.17	1.39
1000	1.46		1.42

5.4.1. Response Scans with no Damage

Figure 31 shows the yield of both the prompt and delayed components as a function of incident direction for the case of no radiation damage. The relation between the incident direction $\hat{\beta}$ and the crystallographic axes is the same as that indicated in Figure 13. In Figure 31 the prompt response data points are the results of a single scan; whereas the points in the delayed response plot were obtained by averaging the results of several partial scans. As in the previous chapter, the curves shown in the figure are based both on the data points and the symmetry of the crystal about the ab plane. In this section the prompt and delayed scintillation response is normalized to the prompt response of the crystal in an undamaged condition to a 1 MeV compton electron.
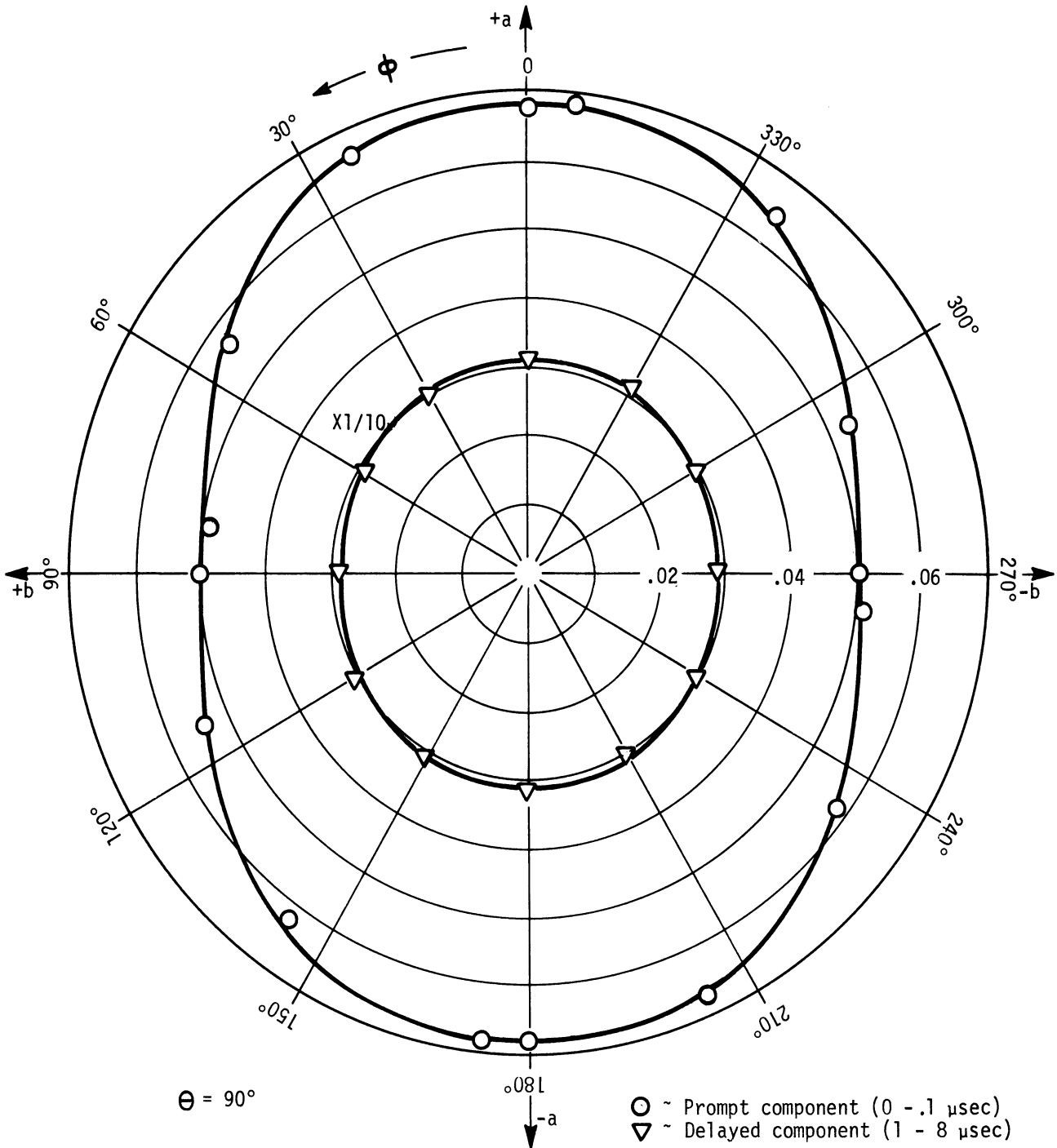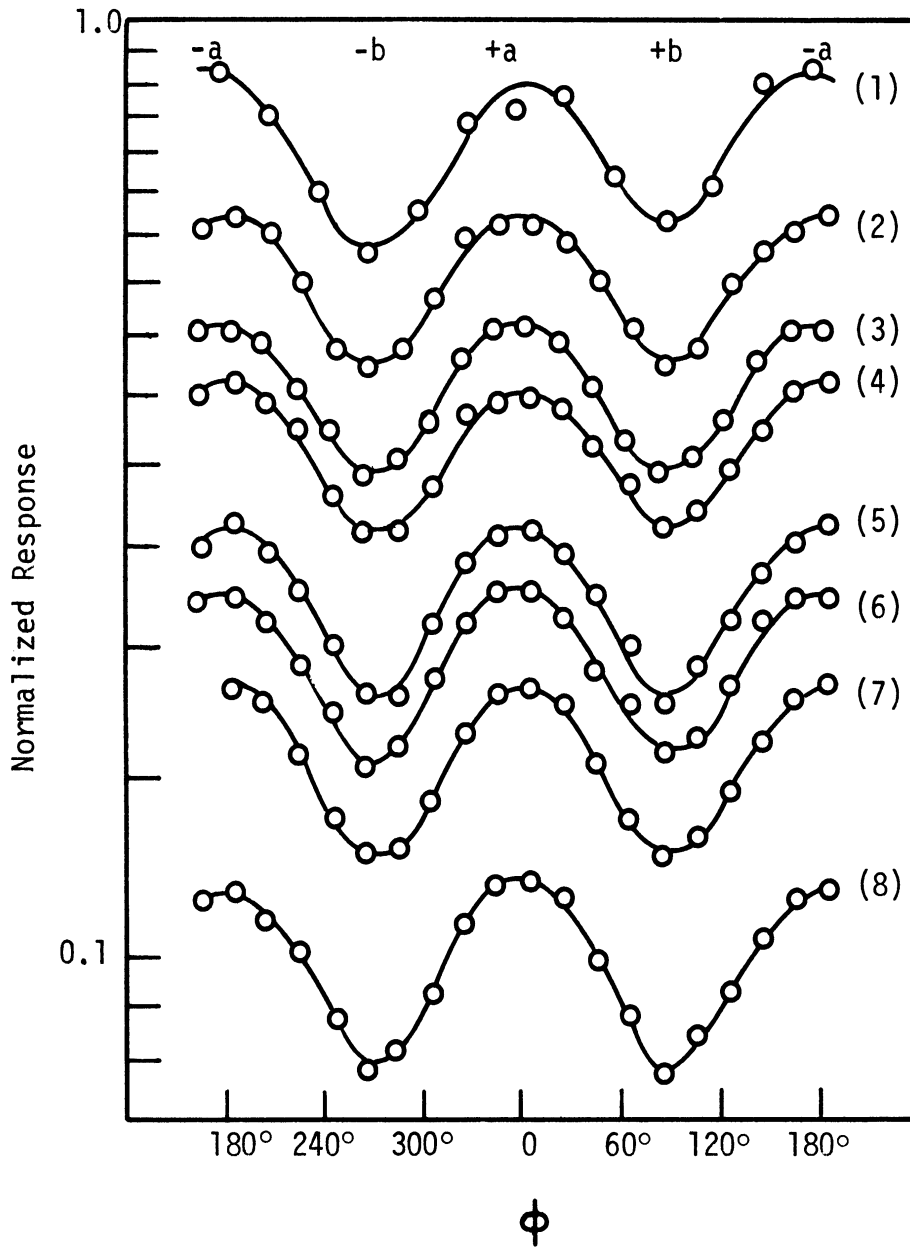
FIGURE 31

Prompt and delayed directional scintillation response of anthracene crystal to 5.3 MeV alpha particles.

5.4.2. Response After Radiation Damage

Figure 32 shows the results of the 360° scans of the prompt response conducted between each irradiation with the high intensity Co-60 gamma ray source. From a polar plot of this data the orientation of the a and b crystal axes was easily estimated. Then, in all cases other than for the undamaged crystal, the delayed component was measured only for directions of incidence parallel to these axes.

The effect of radiation damage on the magnitude of the prompt and delayed scintillation yield is illustrated in Figure 33. The case of alpha particles incident parallel to the a axis is considered. Two quantities are plotted as a function of absorbed dose. One plot corresponds to the prompt scintillation yield with no damage (L°_{p}) divided by the yield for various values of absorbed dose $(L_{p}(D))$. A linear fit of the points generated in this manner from the experimental results is provided by the expression $L^{\circ}_{p}/L_{p}(D) = 1 + AD$ where A is a constant and D is the cumulative dose. As indicated in Figure 33 an appropriate value for A is 4.4×10^{-3} Krads^{-1} when D is measured in kilorads. The second plot shows the variation of the delayed scintillation yield (L_{d}) relative to the prompt as a function of absorbed dose. The ordinate values of the second plot represent the ratio of the delayed scintillation yield to the prompt for the case of no damage $(L^{\circ}_{d}/L_{p}^{\circ})$ divided by the ratio of the delayed yield to the prompt for various amounts of absorbed dose $(L_{d}(D)/L_{p}(D))$.

Response Scan	Dose (Krad)
(1)	0
(2)	70
(3)	145
(4)	215
(5)	290
(6)	355
(7)	495
(8)	1000

FIGURE 32

Effects of radiation damage on the prompt directional scintillation response.
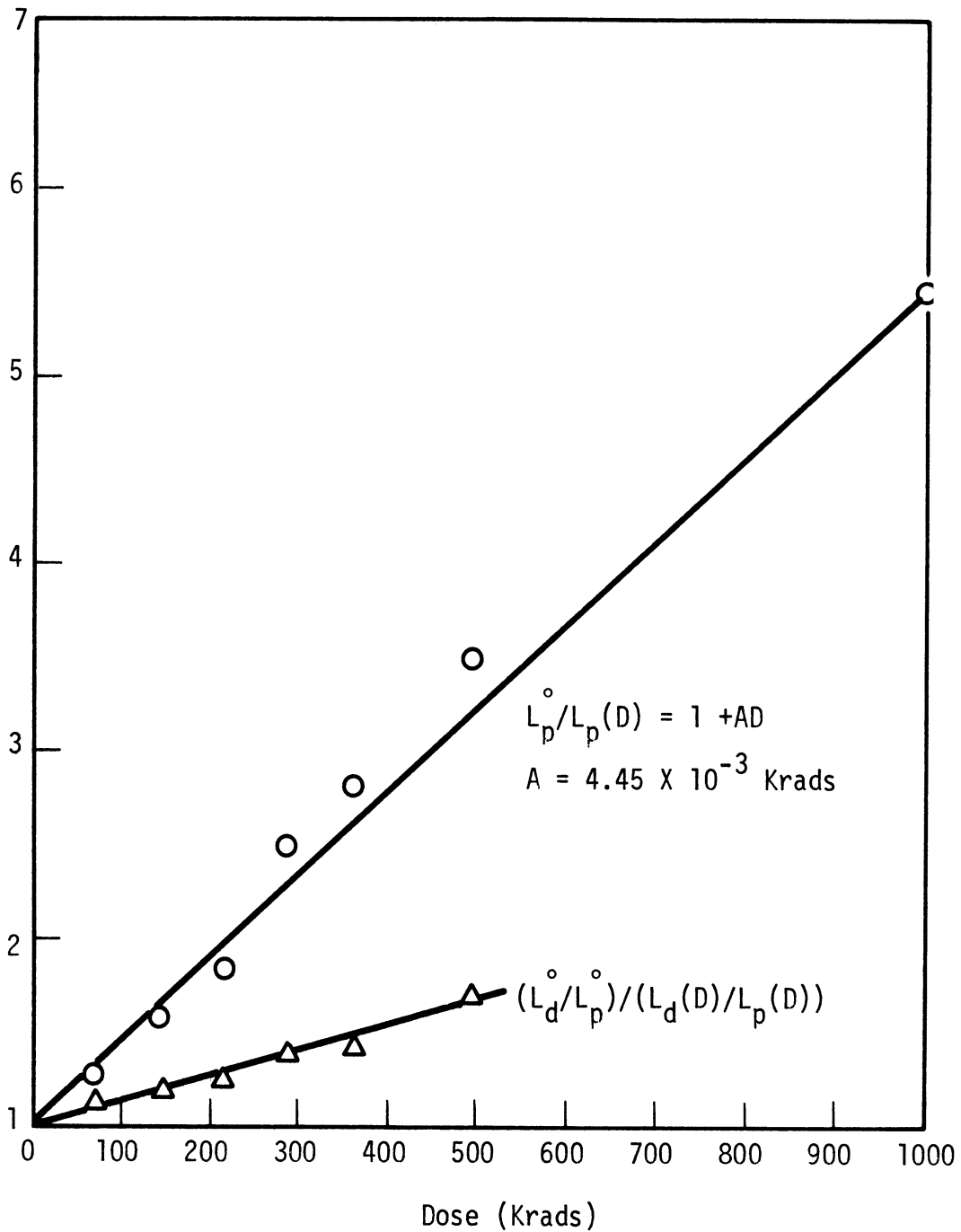
Ratios $L_p^\circ/L_p(D)$ and $(L_d^\circ/L_p^\circ)/(L_d(D)/L_p(D))$ are derived from measurements of the prompt and delayed response of the anthracene crystal to 5.3 MeV alpha particles incident in directions parallel to the a axis. L_p° is the prompt and L_d° the delayed response with no damage. $L_p(D)$ and $L_d(D)$ are the corresponding quantities for various doses D.

FIGURE 33

Variation of prompt and delayed scintillation response with Co-60 gamma ray dose.

5.5. DISCUSSION OF RESULTS

5.5.1. Prompt Component

The 26.4% variation in the prompt response of the undamaged crystal for

5.3 MeV alpha particles incident in directions parallel to the ab plane is in

reasonable agreement with the value of 21.2% Schumacher and Flammersfeld[61] ob-

tained with 8.78 MeV alpha particles.

From Figure 33 it is noted that the dose which reduced the prompt light

yield to one-half the original value is 210 kilorads. Weiss _et al._,[40] deduced

a corresponding value of 500 kilorads using uniform optical photon excitation

throughout the bulk of several crystals. Considering the effects of reabsorp-

tion,[4] the present prompt response results indicate the linear singlet removal

rate $(k_{sf} + k_{sic} + k_{sq}^{D})$ was increased as a result of the 1000 kilorad dose

from 10^{8} sec^{-1} to 2.8×10^{8} sec^{-1}. None of the models in Chapter 3 imply a

change in the measured prompt anisotropy ratio with an increase of this amount,

and none was observed.

5.5.2. Delayed Component

An important feature of the results presented in this chapter is the ap-

parent 10% increase in the directional variation of the delayed scintillation

emission with a 500 kilorad dose. However, such a trend is predicted by the

"forced diffusion" solution of the triplet exciton diffusion-kinetics equation

discussed in the biexcitonic quenching section, 3.3.2. Equation (3.18) was

integrated numerically for a range of values for the characteristic diffusion

time t_{a}, triplet lifetime τ_{t}, and for the parameter E. The parameters t_{a} and

E are inversely proportional to the triplet exciton diffusion coefficient, and τ_t varies inversely with dose. For t_a equal to 60 nanoseconds and E/t_a equal to .06, the numerical solution indicates that a 500 kilorad dose would reduce the delayed scintillation yield by the amount measured if τ_t = 9.9 microseconds. This value of τ_t corresponds to a value for the damage quenching rate k_{tq}^D of .202 sec^{-1} rad^{-1} which is comparable to a corresponding value of .33 sec^{-1} rad^{-1} deduced from the results of Weisz et al.[40] The numerical solutions also show that for k_{tq}^D = .202 sec^{-1} rad^{-1} and E/t_a = .06, a decrease in t_a from 60 to 40 nanoseconds results in a 5.6% decrease in the scintillation yield of an undamaged crystal and a 10% decrease after a 500 kilorad dose. Thus, if t_a (or D_t) is assumed directionally dependent, these caluclations are consistent with the observed increase in the anisotropy ratio of the delayed scintillation component with damage. The relative magnitude of the effective triplet exciton diffusion coefficients necessary to explain the observed directional variation is $D_{ac'} > D_{bc'}$ where the subscripts ac' and bc' indicate the plane perpendicular to the track of the exciting particle.

CHAPTER 6

CONCLUSIONS

6.1. THIS STUDY

The analysis of the scintillation process presented in this dissertation indicates that the directionally dependent scintillation phenomena in crystalline anthracene arises from anisotropic diffusion of singlet and triplet excitons.

Measurements of the prompt response of a large anthracene crystal for 0.92 MeV recoil protons and 2 to 3.5 MeV recoil carbon ions show the percentage variation in the directional response to be nearly the same. Yet, for the recoil carbon ions the average specific energy loss is an order of magnitude greater, and the light yield per MeV an order of magnitude less than the corresponding quantities for 0.92 MeV protons. Anisotropic diffusion of singlet excitons is found to control the rate of biexcitonic annihilation, providing the right magnitude of directionally dependent quenching over a wide range of specific energy loss. By treating the anisotropic diffusion problem with effective isotropic diffusion coefficients, it is found that a variation of two in the value of the diffusion coefficient is more than sufficient to explain the experimental observations. Experimental data indicates that singlet exciton migration is most rapid in a plane nearly parallel to the ab plane and least rapid in the ac crystal plane.

Another result from this investigation is the first measurement of the absolute scintillation yield of anthracene for carbon ions in the 2 to 3.5 MeV

energy range.

A diffusion controlled biexcitonic annihilation rate for triplet excitons explains the measured directional dependence of the delayed scintillation emission as a function of radiation damage. A 33% variation in the effective triplet diffusion coefficient in planes normal to the ab crystallographic plane is adequate to produce the experimentally observed 5.6% directional variation in the response for an undamage crystal. Moreover, the magnitude of the increase in the directional variation of the delayed component as the crystal was progressively damaged by Co-60 gamma radiation is predicted within a factor two.

6.2. SUGGESTED EXPERIMENTS

At least three separate experiments are suggested upon consideration of the study presented here.

First, it would be desirable to determine the diffusion tensor for singlet excitions in anthracene directly. This type of measurement would probably require some unique method involving excitation with optical photons.

Second, a more feasible experiment than that above would be the careful measurement of the directionally dependent delayed scintillation emission in the presence of a strong magnetic field. The role of charge transfer (CT) excitons in the delayed emission process could possibly be clarified. If the CT excitons are intermediate states which are involved between the recombination of electron-hole pairs and the formation of triplet excitons, migration could take place before the formation of the triplets. This mechanism might explain the broad initial triplet exciton distribution implied by the results of King and

Voltz described in subsection 3.3.2.2.

Finally, by use of an accelerator capable of producing a wider range of source neutron energies, the response of anthracene or other organic crystals to energetic carbon ions could be investigated over a wider energy range by the scattering method of Chapter 4. Further knowledge of the variation of the light yield with energy is necessary for a better understanding of the fundamental processes involved in a scintillation event.

REFERENCES

1. C. D. Swartz and G. E. Owen, "Recoil Detection in Scintillators," Fast
   Neutron Physics, Part I (Interscience Publishers, Inc., New York, 1960)
   p. 228.

2. W. F. Kienzle and A. Flammersfeld, "Die Anisotropie der Szintillations-
   lichtausbeute organischer Moleküleinkristalle für α-Strahlen," Z. Phys.,
   165, 1 (1961).

3. J. M. Robertson, "Structure of Naphthalene and Anthracene," Rev. Mod.
   Phys., 30, 155 (1958).

4. J. B. Birks, The Theory and Practice of Scintillation Counting (The
   Macmillan Company, New York, 1964).

5. W. Schött, "Die Szintillationslichtausbeute energiereicher Deuteronen
   und α-Teilchen in organischen Kristallen," Z. Phys., 179, 428 (1964).

6. K. Tsukada, S. Kikuchi and Y. Miyagawa, "Directional Anisotropy in the
   Characteristics of the Organic-Crystal Scintillators, II," Nucl. Instr.
   and Meth., 37, 69 (1965).

7. F. D. Brooks, "Organic Scintillators," Progress in Nuclear Physics, Vol.
   5 (Pergamon Press, London, 1956), Chap. VII.

8. J. Kloppenburg and A. Flammersfeld, "Energieverlustmessungen in Anthrazen,
   Terphenyl und Plastikszintillator für Protonen und Deuteronen im
   Energiebereich von 100 bis 900 KeV.," Z. Phys., 196, 424 (1966).

9. W. Whaling, "The Energy Loss of Charged Particles in Matter," Encyclopedia
   of Physics, Vol. 34 (Springer-Verlag, Berlin, 1958), pp. 193-215.

10. R. Voltz, J. Lopes da Silva, G. Laustriat and A. Coche, "Influence of the Nature of Ionizing Particles on the Specific Luminescence of Organic Scintillators," J. Chem. Phys., 45, 3306 (1966).

11. K. Wick and A. Flammersfeld, "Channelingeffekte bei der Lichtausbeute von Anthrazen bei Beschuss mit α-Teilchen," Z. Phys., 204, 164 (1967).

12. W. Brandt, R. Dobrin, H. Jack Jr., R. Laubert and S. Roth, "Channeling Studies Through Characteristic Radiations," Can. J. Phys., 46, 537 (1968).

13. W. R. Falk and L. Katz, "Fluorescence Decay Time Measurements of Organic Scintillators," Can. J. Phys., 40, 978 (1962).

14. P. G. Sjölin, "The Scintillation Decay of Anthracene Excited by Alpha Particles and Electrons," Nucl. Instr. and Meth., 63, 253 (1968).

15. P. E. Gibbons, D. C. Northrop and O. Simpson, "The Scintillation Phenomenon in Anthracene: II. Scintillation Pulse Shape," Proc. Phys. Soc., 79, 373 (1962).

16. A. Schmillen, "Fluorescence Decay Times of Organic Crystals," Luminescence of Organic and Inorganic Materials (John Wiley and Sons, Inc., New York, 1962), p. 30.

17. K. Tsukada and S. Kikuchi, "Directional Anisotropy in the Characteristics of the Organic-Crystal Scintillators," Nucl. Instr. and Meth., 17, 286 (1962).

18. F. Brinkmeier, "Zeitliches Abklingen des Szintillationslichts von Anthrazen-und p-Terphenyleinkristallen bei Beschuss mit α-Teichen als Funktion der Einschussrichtung," Z. Phys., 190, 316 (1966).

19. R. Hofstadter and J. A. McIntyre, "Measurement of Gamma-Ray Energies with Two Crystals in Coincidence," Phys. Rev., 78, 619 (1950).

20. D. E. Lea, "Physical Properties and Dosimetry of Different Radiations," Actions of Radiations on Living Cells (Cambridge University Press, Cambridge, England, 1955), Chap. I.

21. E. J Hart and R. L. Platzman, "Radiation Chemistry," Mechanisms in Radiobiology, Vol. I (Academic Press, Inc., New York, 1961), Chap. II.

22. F. Hutchinson and E. Pollard, "Physical Principles of Radiation Action," Mechanisms in Radiobiology, Vol. I (Academic Press, Inc., New York, 1961), Chap. I.

23. M. Pope, "Charge-Transfer Exciton and Ionic Levels in Organic Crystals," J. Polymer Sci. Pt. C., Polymer Symposium, (USA), No. 17, 233 (1967).

24. P. Avakian and R. E. Merrifield, "Triplet Excitons in Anthracene Crystals-A Review," Mol. Crystals, 5, 37 (1968).

25. H. A. Bethe and J. Ashkin, "Passage of Radiations Through Matter," Experimental Nuclear Physics, Vol. I (John Wiley and Sons, Inc., New York, 1953), Part. II.

26. W. S. Snyder and J. Neufeld, "On the Passage of Heavy Particles Through Tissue," J. Rad. Res., 6, 67 (1957).

27. J. Linhard and P. V. Thomsen, "Sharing of Energy Dissipation Between Electronic and Atomic Motion," Radiation Damage in Solids, Vol. I (IAEA, Vienna, 1962), p. 65.

28. L. C. Northcliffe, "Passage of Heavy Ions Through Matter," Annual Review of Nuclear Science, Vol. 13 (Annual Reviews, Inc., Palo Alto, California, 1963), p. 81.

29. R. L. Platzman, "On the Primary Processes in Radiation Chemistry and Biology," Symposium on Radiobiology (John Wiley and Sons, Inc., New York, 1952), Chap. VII.

30. J. L. Magee, "Elementary Processes in Action of Ionizing Radiation," Comparative Effects of Radiation (John Wiley and Sons, Inc., New York, 1960), pp. 142, 143.

31. W. Helfrich, "Destruction of Triplet Excitons in Anthracene by Injected Electrons," Phys. Rev. Letters, 16, 401 (1966).

32. E. L. Frankevich and B. M. Rumyantsev, "Charge-Transfer Excitons and Delayed Fluorescence of Anthracene," Phys. Stat. Sol., 30, 329 (1968).

33. R. M. Sternheimer, "The Density Effect for the Ionization Loss in Various Materials," Phys. Rev., 88, 851 (1952).

34. F. A. Black, "The Decay in Fluorescence Efficiency of Organic Materials on Irradiation by Particles and Photons," Phil. Mag., 44, 263 (1953).

35. O. Simpson, "Electronic Properties of Aromatic Hydrocarbons III. Diffusion of Excitons," Proc. Roy. Soc., A238, 402 (1956).

36. J. Jortner, S. A. Rice and J. L. Katz, "Triplet Excitons in Crystals of Aromatic Molecules," J. Chem. Phys., 42, 309 (1965).

37. M. Levine and J. Jortner, "Diffusion of Triplet Excitons in Crystalline Anthracene," J. Chem. Phys., 45, 1951 (1966).

38. S. Z. Weisz, A. B. Zahlan, M. Silver and R. C. Jarnagin, "Radiationless Transition Rate Constant Determination from Delayed Fluorescence," Phys. Rev. Letters, 12, 71 (1964).

39. M. Pope and J. Burgos, "Autoionization and Exciton Annihilation in Anthracene," Mol. Crystals, 3, 215 (1967).

40. S. Z. Weisz, P. Richardson, A. Cobas and R. C. Jarnagin, "Triplet Sampled Radiation Damage," International Symposium on Organic Scintillators, Argonne National Laboratory, 1966.

41. S. Singh, W. J. Jones, W. Siebrand, B. P. Stoicheff and W. G. Schneider, "Laser Generation of Excitons and Fluorescence in Anthracene Crystals," J. Chem. Phys., 42, 330 (1965).

42. A. H. Samuel and J. L. Magee, "Theory of Radiation Chemistry. II. Track Effects in Radiolysis of Water," J. Chem. Phys., 21, 1080 (1953).

43. A. Kuppermann and G. G. Belford, "Diffusion Kinetics in Radiation Chemistry. II. One-Radical-One-Solute Model; Calculations," J. Chem. Phys., 36, 1427 (1962).

44. G. N. Whyte, "Energy Per Ion Pair for Charged Particles in Gases," Rad. Research, 18, 265 (1963).

45. A. Ore and A. Larsen, "Relative Frequencies of Ion Clusters Containing Various Numbers of Ion Pairs," Rad. Research, 21, 331 (1964).

46. A. M. Rauth and F. Hutchinson, "Distribution in Energy of the Primary Energy Loss Events of Electrons in Condensed Media," Biological Effects of Ionizing Radiation at the Molecular Level (IAEA, Vienna, 1962), p. 25.

47. A. S. Newton, "Mechanisms of Chemical Effects of Ionizing Radiation," Radiation Effects on Organic Materials (Academic Press, Inc., New York, 1963), Chap. III.

48. N. Swanson and C. J. Powell, "Excitation of π-Electrons in Polystyrene and Similar Polymers by 20 KeV. Electrons," J. Chem. Phys., 39, 630 (1963).

49. H. Fricke and D. L. Phillips, "High-Speed Computations in Diffusion Kinetics. III. Solute Depletion in the Cylindrical One Radical- One Solute Model," J Chem. Phys., 34, 905 (1961).

50. A. Kuppermann, "Diffusion Kinetics in Radiation Chemistry," The Chemical and Biological Action of Radiations (Academic Press, Inc., London, 1961), Chap. III.

51. G. Jaffé, "Zur Theorie der Ionisation in Kolonnen," Ann. Phys., 42, 303 (1913).

52. D. Blanc, F. Cambou and Y. G. de Lafond, "Cinétique de la composante rapide de la scintillation dans un milieu organique pur. Application au cas de l'anthracène," C. R. Acad. Sci., 254, 3187 (1962).

53. T. A. King and R. Voltz, "The Time Dependence of Scintillation Intensity in Aromatic Materials," Proc. Roy. Soc., A289, 424 (1966).

54. R. Voltz and G. Laustriat, "Radioluminescence Des Milieux Organiques I. Étude Cinétique," J. Physique, 29, 159 (1968).

55. R. Voltz, H. Dupont and G. Laustriat, "Radioluminescence Des Milieux Organiques II. Vérification Experimentale de L'Étude Cinétique," J. Physique, 29, 297 (1968).

56. H. Kallmann and G. J. Brucker, "Decay Times of Fluorescent Substances Ex-

    cited by High-Energy Radiation," Phys. Rev., 108, 1122 (1957).

57. H. B. Rosenstock, "Energy Transfer in Organic Solids," J. Chem. Phys., 48,

    532 (1968).

58. R. B. Owen, "Pulse-Shape Discrimination Identifies Particle Types," Nu-

    cleonics, 17, No. 9, 92 (1959).

59. R. Batchelor, W. B. Gilboy, J. B. Parker and J. H. Towle, "The Response

    of Organic Scintillators to Fast Neutrons," Nucl. Instr. and Meth., 13,

    70 (1961).

60. D. J. Brager, "The Fricke Dosimeter: Dose Rate Calibration of 10,000

    Curie Co-60 Source," (Unpublished Report, The University of Michigan,

    1968).

61. M. Schumacher and A. Flammersfeld, "Szintillationslichtausbeuten

    organischer Molekulkristalle fur α-Strahlen und Elektronen," Z. Phys.,

    178, 11 (1964).